Cardiac $G\alpha_{i2}$ Protein Function and Regulation of High-Voltage-Gated L-type Calcium Channels.

Dissertation

zur

Erlangung des Doktorgrades (Dr. rer. nat.)

der

Mathematisch-Naturwissenschaftlichen Fakultät

der

Rheinischen Friedrich-Wilhelms-Universität Bonn

vorgelegt von

Sara Dizayee

aus

Bagdad/Irak

Bonn 2011

Angefertigt mit Genehmigung der Mathematisch-Naturwissenschaftlichen Fakultät der Rheinischen Friedrich-Wilhelms-Universität Bonn

1. Gutachter: Professor Dr. S. Herzig
2. Gutachter: Professor Dr. K. Mohr

Tag der mündlichen Prüfung: 30.03.2012

Erscheinungsjahr: 2012

Meinen Eltern.

Danksagung

Mit der Beendigung meiner Arbeit möchte ich all jenen danken, die am Gelingen dieser Arbeit maßgeblich beteiligt waren:

- Herrn Professor Dr. S. Herzig für die Bereitstellung des Themas und des Arbeitplatzes, die intensive Betreuung und die zahlreichen wissenschaftlichen Diskussionen.

- Herrn Professor Dr. K. Mohr am Pharmazeutischen Institut, Pharmakologie und Toxikologie der Universität Bonn für die Annahme einer externen Doktorarbeit und die Bereitschaft den persönlichen Kontakt über die gesamte Zeit aufrechtzuerhalten.

- Herrn Professor Dr. Dr. B. Nürnberg am Institut für Pharmakologie und experimentelle Therapie der Uniklinik Tübingen und Dr. R. P. Piekorz am Institut für Biochemie und Molekularbiologie II an der Uniklinik Düsseldorf für die Kooperation und die konstruktive Diskussion meiner wissenschaftlichen Arbeit.
  Dem Arbeitskreis von Dr. R. P. Piekorz für die nette Aufnahme und Unterstützung, insbesondere Herrn F. Kuck für die sehr gute Zusammenarbeit.

- Herrn PD. Dr. M. Schubert und seinem Arbeitskreis an der ZMMK der Uniklinik Köln für die Bereitstellung ihres Labors für die letzten relevanten Versuche meiner Doktorarbeit.
  Herrn Dr. A. Markl und Herrn O. Stöhr aus dem Arbeitskreis PD. Dr. M. Schubert für die gute Beratung und die sehr erfrischenden Unterhaltungen.

- Herrn Dr. Dr. P. Hein für seine wertvollen Ratschläge in allen Belangen, seine ermunternden Worte und seiner Freundschaft.

- Herrn PD. Dr. J. Matthes für seine unermessliche Unterstützung, seine Geduld mit einem und sein Glaube an einen.

- Frau Dr. E. Kuzmenkina und Herrn Dr. J. Mezaros für die Beratung bei der Anwendung und Auswertung der Patch-Clamp Methode, sowie Herrn Dr. Klein für die Einführung in die Myozytenisolation.

- Frau S. Kästner und Frau Dr. M. Hübner für die fruchtbare wissenschaftliche und freundschaftliche Zusammenarbeit.

- Allen Mitgliedern des Arbeitskreises für die gute Stimmung und das herzliche Arbeitsklima, besonders Frau S. Kirchmann-Hecht für Ihre Unterstützung in der Laborarbeit und Herrn J. Reifenrath für seine Zusammenarbeit in der Tierhaltung.

Zu guter Letzt, möchte ich mich bei meinen Freunden für Ihr Verständnis und Ihre Hilfsbereitschaft bedanken. Theresa danke ich für die schöne gemeinsame Promotionszeit in Köln und den unermüdlichen Zusammenhalt, sowie Maximilian für seine Freundschaft, Unterstützung, und dass er immer für mich da ist.
Ein besonderer Dank gilt meinen Eltern, die mich in Allem unterstützt, mir den Rücken gestärkt und immer an mich geglaubt haben.

Für die finanzielle Unterstützung danke ich der DFG (He 1578/13 1,2).

Erklärung:

An Eides statt versichere ich, dass ich die von mir vorgelegte Dissertation selbst und ohne jede unerlaubte Hilfe angefertigt habe, dass diese oder eine ähnliche Arbeit noch keiner anderen Stelle als Dissertation eingereicht worden ist dass sie an der nachstehend aufgeführten Stelle auszugsweise veröffentlicht worden ist. Ich habe früher noch keinen Promotionsversuch unternommen.

Sara Dizayee Köln, den 23.10.2011

CONTENTS

Abbreviations **10**

1 INTRODUCTION **13**

1.1 Cardiovascular disease **13**

1.2 Principles of cardiac function **13**

1.3 Voltage-dependent calcium channels **17**

1.4 Heterotrimeric G proteins **20**

1.5 Animal models **23**

1.6 Aims of this thesis **25**

2 MATERIALS AND METHODS **27**

2.1 Materials **27**

2.1.1 Chemicals/enzymes 27

2.1.2 Equipments/consumables 29

2.1.3 Computer software 30

2.2 Animals **31**

2.2.1 Mouse models 31

2.2.2 Breeding 31

2.3 Genotyping **32**

2.3.1 Genomic deoxyribonucleic acid (gDNA) purification 32

2.3.2 Polymerase chain reaction (PCR) 32

2.3.3 Gel electrophoresis 34

2.3.4 Mendelian inheritance 35

2.4 Messenger ribonucleic acid (mRNA) analysis 36

2.4.1 mRNA isolation 36

2.4.2 Complementary DNA (cDNA) synthesis 37

2.4.3 Quantitative Real-Time PCR (RT-PCR) 37

2.5 Protein analysis 39

2.5.1 Cardiac cell membrane preparation 39

2.5.2 Cardiac tissue preparation 40

2.5.3 Sodium dodecyl sulfate-polyacrylamide gel electrophoresis (SDS-PAGE) 42

2.5.4 Western Blot 44

2.5.5 Adenosine diphosphate (ADP)-ribosylation 46

2.6 Electrophysiology 48

2.6.1 Cardiac myocytes isolation 48

2.6.2 Pertussis toxin experiments 50

2.6.3 Patch-clamp technique 50

2.6.4 Electrodes 53

2.6.5 Patch pipettes 54

2.6.6 Whole-cell recordings 54

2.7 Statistical analysis 58

3 RESULTS 59

3.1 Genotyping 59

3.2 Animals 61

3.2.1 Offspring statistics 61

3.2.2 Phenotype 63

3.3 Cardiac $G\alpha_{i/o}$ isoforms 65

3.3.1 mRNA expression levels 65

3.3.2 $G\alpha_{i2}$ and $G\alpha_{i3}$ protein expression levels 67

3.3.3 Specificity of the detected $G\alpha_{i2}$ and $G\alpha_{i3}$ protein bands 70

3.3.4 $G\beta\gamma$ protein expression levels 70

3.3 Cardiac L-type calcium currents of $G\alpha_{i2}$-/- and $G\alpha_{i3}$-/- mice 71

3.3.1 Basal whole-cell calcium current 71

3.3.2 Time- and voltage-dependent inactivation 73

3.3.3 Recovery from inactivation 75

3.3.4 Acute inactivation of remaining $G\alpha_i$ proteins by PTX incubation 76

3.4 Cardiac L-type calcium channel subunits 79

3.4.1 mRNA expression levels 79

3.4.2 $Ca_v\alpha_1$ protein expression level 81

3.5 G_i posttranslational effects induced by carbachol stimulation 82

3.5.1 Akt and Gsk3β phosphorylation levels 82

3.5.2 ERK1/2 phosphorylation level 84

4 DISCUSSION 86

4.1 G_i structural and functional modification mediated by $G\alpha_{i2}$ deletion 86

4.2 Alterations of L-type calcium channel regulation by $G\alpha_{i2}$ deletion 87

4.3 Structural aspects and mechanisms underlying $G\alpha_{i2}$ requirement 90

4.4 Conclusion and outlook 93

5 SUMMARY 95

6 ZUSAMMENFASSUNG 97

7 BIBLIOGRAPHY.....99

8 PUBLICATIONS.....115

Abbreviations

ABP	α binding pocket
ACh	acetylcholine
ADP	adenosine diphosphate
AID	α interaction domain
AKAP	α kinase anchoring protein
AP	action potential
APS	ammoniumpersulfate
AR	adrenergic receptor
ATP	adenosine triphosphate
AV	atrioventricular
bp	base pair
BSA	bovine serum albumine
BW	bodyweight
C-	carboxyl-
CaM	calmodulin
CaMK	calcium calmodulin dependent protein kinase
cAMP	cyclic adenosine monophosphate
CCh	carbachol
CDF	calcium dependent facilitation
CDI	calcium dependent inactivation
cDNA	complementary DNA
$C_{12}E_{10}$	polyoxyethylene 10 dodecyl ether
CT	cycle threshold
CTX	cholera toxin
DNA	deoxyribonucleic acid
dsDNA	double stranded DNA
DTT	dithiothreitol
ECL	enhanced chemiluminescence
EDTA	ethylenediaminetetraacetic acid
EGTA	ethylene glycol-bis (2-aminoethylether)- tetraacetic acid
ERK1/2	extracellular regulated kinase subtype 1 and 2
$G\alpha_i+/+$	wt control

$G\alpha_i$+/-	heterozygote
$G\alpha_i$-/-	homozygote
GAP	GTPase activating protein
GAPDH	glyceraldehydes 3-phosphate dehydrogenase
gDNA	genomic DNA
GDP	guanosine diphosphate
GK	guanylate kinase
G protein	guanine nucleotide binding protein
GPCR	G protein-coupled receptor
GPI	Glycosylphosphatidylinositol
GRK	G protein-coupled receptor kinase
GSK3α/β	glycogensynthase kinase 3 α and β
GTP	guanosine triphosphate
HEPES	4-(2-hyrdoxyethyl)-1-piperazinethanesulfonic acid
HF	heart failure
HW	heartweight
i.p.	intraperitoneal
IV	current voltage
MAPK	mitogen activated protein kinase
mRNA	messenger RNA
mut	mutant
N-	amino-
NAD^+	nicotinamide adenine dinucleotide
$NADP^+$	NAD^+ phosphate
NCX	sodium calcium exchanger
NKA	sodium potassium pump
PAGE	polyacrylamide gel electrophoresis
PBS	phosphate buffered saline
PCR	polymerase chain reaction
PIKfyve	phosphatidylinositol 3-phosphate 5-kinase
PKA	protein kinase A
PKB/Akt	protein kinase B
PKC	protein kinase C
PTX	pertussis toxin

RasGAP	RasGTP activating protein
RGS	regulators of G protein signaling
RLT	RNeasy lysis
RNA	ribonucleic acid
RT PCR	real time PCR
RyR	ryanodine receptor
SA	sinusaterial
SDS	sodium dodecylsulfate
SEM	standard error of mean
SERCA	sarcoplasmic reticulum calcium-ATPase
SR	sarcoplasmic reticulum
STIM1	stromal interaction molecule 1
TAE	tris acetate EDTA
TBS	tris buffer saline
TBST	TBS and Tween 20
TEMED	N, N, N′, N′-tetramethylethylenediamine
tg	transgenic
Tris	trishydroxymethylaminomethane
UV	ultraviolet
VDF	voltage dependent facilitation
wt	wild type

1 INTRODUCTION

1.1 Cardiovascular disease

Cardiovascular disease includes all diseases relating to the heart and blood vessels. It is the worldwide leading disease and the most common cause of death [1]. For example, about 10 million Europeans including 1.3 million Germans suffer from heart failure (HF) [2]. 40 % of the HF patients die within the first year after initial diagnosis and patients younger than 65 years have an overall survival rate of 8 years [3]. Death rate caused by cardiovascular disease for females and males are similar [4]. Patients with HF have 6-9 times higher risk for sudden cardiac death than the general population [5]. In Germany, the event of sudden cardiac death per year is estimated to occur in 0.1-0.2 % of the total population [6]. In addition to the burden for the individual patient, this disease has tremendous negative economic and clinical impact on public health [7].

The mortality rates have been declining or rather the survival rate has been increasing over the last decade due to the therapeutic improvement, the improved prevention and better guidelines [8]. However, with the rise of other risk factors such as advanced age and diabetes [9], cardiovascular disease remains one of the major issues in health care. Nowadays, cardiovascular function is well investigated. However, there are still many unknown processes such as pathway mechanisms and ion channel functions. Elucidating these processes might be crucial for new therapeutic targets.

1.2 Principles of cardiac function

The heart is a muscular organ divided into four chambers (two atria and two ventricles) for receiving and ejecting the blood. Right atrium and ventricle comprise the right side of the heart, which transports the deoxygenated venous blood to the pulmonary circulation. The oxygenated blood returns to the left side of the heart, composed of left atrium and ventricle,

and pumps it out through the aorta. The heart relaxes in the period of receiving blood (diastole), while it ejects blood by contracting (systole). The heart distributes the blood throughout the body by contracting rhythmically enabled by its electrical pacemaking and conduction system, a muscular contraction system and many signaling pathways.

The action potential (AP) is generated normally in the fastest pacemaker cells, the sinoatrial (SA) node [10] in the right atrium. The generated pulse migrates from the SA node through the atrium to the atrioventricular (AV) node and passes rapidly along the AV bundle, which is divided into right and left bundle branches. The action potential is mediated to the ventricular walls by the His-purkinje system ([11], Figure 1.2:1).

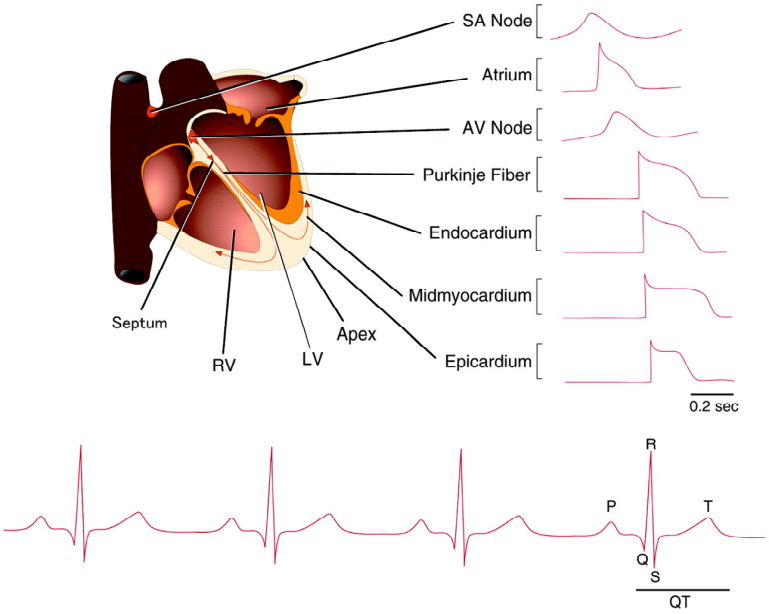

Figure. 1.2:1. Diagram illustrating the conduction system and corresponding waveforms in different heart regions (top). The effects on action potential are dependent on the differences in ion channel expressions in each region. Bottom diagram shows electrical functioning of the heart detected by a typical electrocardiogram (Nerbonne and Kass, Physiological Reviews 2005).

In SA node the upstroke of the AP is slow. It initiates the AP by opening hyperpolarization activated cyclic nucleotide-gated (HCN) channels carrying nonselective inward current [12], and involves T-type and L-type calcium channels. The ion influx depolarizes the membrane from a potential of approximately -50 mV to 0 mV. Voltage-dependent potassium channels

open and potassium efflux takes place for repolarization [13]. Inward rectifier potassium channels expressed at rather low levels are responsible for the more positive resting potential. Furthermore, a coupled-clock system composed of a surface “membrane clock” and an intracellular “calcium clock” determines the normal cardiac pacemaker cell automaticity and flexibility by stimulation [14]. The AV node transduces similar to the SA node. Purkinje fibers operate more like cardiac muscle cells in atrium and ventricle, where the upstroke is rapid and followed by a plateau. The height and duration of the plateau is influenced by transient repolarization and calcium channel activation. For the AP repolarization, there are multiple types of potassium currents with distinct properties. Variation in potassium channel expression in different regions contribute to modifications in AP [13].

Gap junctions connect single cardiac muscle cells and are responsible for the electrical pulse to travel [15]. Therefore, initial ion influx in the pacemaker cells causes a depolarization in cardiomyocytes from a resting potential of -80 mV rapidly to higher membrane potentials using voltage-gated sodium channels [16, 17]. Once these channels close at positive potentials, potassium ions leave the cell through the delayed rectifier potassium channels. Counteracting, L-type calcium channels open and calcium ions enter the cell generating an inward current [18]. Calcium influx induces calcium release from sarcoplasmic reticulum (SR) by binding to intracellular calcium release channels called ryanodine receptors (RyR). Consecutive calcium release from the SR via RyR (so called calcium-induced calcium-release) causes a sufficiently high cytoplasmic calcium concentration to induce contraction [19, 20]: the increased calcium concentration leads to the binding of calcium to thin filament protein troponin C causing muscle contraction and discharging blood from the left ventricle to the body. For relaxation, sarcoplasmic reticulum calcium-ATPase (SERCA) pumps calcium ions from the cytoplasm back into the SR to lower cytosolic calcium concentration [21]. Calcium ions also leave the cell using sodium/calcium exchanger (NCX) [22]. Rapid delayed rectifying and inward rectifying potassium channels open for a fast

repolarization. In addition, sodium ions are transported out of the cell by the sodium/potassium pump (NKA) to keep the resting potential constant (Figure 1.2:2). In the whole excitation contraction coupling process, calcium/calmodulin-dependent protein kinase (CaMKII in the heart) play a relevant role in the phosphorylation of several calcium handling proteins [23, 24].

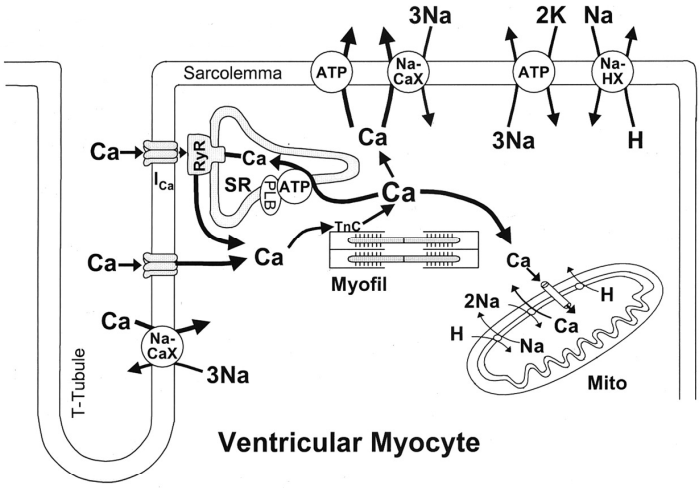

Figure 1.2:2. Schematic diagram describing calcium transport and homeostasis in cardiac muscle cells (Bers, Circulation Research 2000).

Heart rhythm is altered by the autonomic nervous system, which is divided into parasympathetic and sympathetic nervous systems [25]. The parasympathetic nervous system uses acetylcholine as its only neurotransmitter. Concerning the heart, it binds to the G protein-coupled muscarinic (M_2)-receptor in the plasma membrane, causing inhibitory effects. Potassium efflux increases by the opening of acetylcholine-gated potassium channels leading to a decreased membrane potential. Hence, the depolarization is slowed and the excitation frequency (chronotropy) of the SA node and the excitation velocity (dromotropy) via the AV node are reduced. However, the parasympathetic nervous system has no primary effects on ventricular muscles [26, 27]. In contrast to the parasympathetic nervous system, the sympathetic nervous system innervates both the excitation and the contraction system. The

neurotransmitter catecholamines bind to the G protein-coupled adrenergic receptors (AR) [28]. Increased sympathetic tone causes a higher firing frequency (positive chronotropy) in pacemaker cells and the membrane potential accelerates faster. In cardiomyocytes the calcium influx is increased and the calcium clearing from cytoplasm into SR proceeds much quicker (positive lusitropy), generating a stronger contraction (positive inotropy) with a shorter duration [29].

Heart diseases are often accompanied by electrical remodeling and a prolonged AP. Alteration in calcium homeostasis and potassium channel function lead to a reduced repolarization and an increased depolarization phase [30]. As mentioned in Chapter 1.1, up to 50 % of HF patients die by sudden cardiac death, in particular by lethal ventricular tachyarrhythmias, occurring mostly as a result of electrical remodeling, [31, 32]. Although interventional cardiology is well established, the understanding of arrhythmia mechanisms and treatment strategies are still limited [33].

1.3 Voltage-dependent calcium channels

As described above, calcium channels play an essential role in cell excitability and in coupling excitation to contraction [34]. Calcium ions regulate many complex processes by entering the cell. Voltage-dependent calcium channels are classified into two main types due to their electrophysiological and pharmacological properties [35]. Low voltage-gated calcium channels, the T-type calcium channels, activate at low membrane potentials, build a small conductance and their current lasts short [36]. As mentioned in Chapter 1.2 T-type calcium channels play an important role in pacemaker activity, but they are almost absent in cardiomyocytes. However, it was previously reported that T-type calcium channel blockade prevents ventricular arrhythmias and sudden cardiac death in mice with heart failure [37]. In this context, the role of its subunits remains controversial [38, 39]. In contrast to low

voltage-gated calcium channels, high voltage-gated calcium channels require higher membrane potentials for activation, and they provide large and long lasting currents. The class of high voltage-gated calcium channel consists of L-type and non-L-type (N-, P-, Q- and R-type) channels. The non-L-type calcium channels are predominantly located in the brain and in peripheral nervous system [40]. In the heart, the main calcium channel is the L-type calcium channel [41]. In the cell calcium ions interact with several effectors (Figure 1.2:2.), which play a central role in cardiac excitation-contraction coupling [42, 43].

Cardiac L-type calcium channels are hetero-multimeric proteins composed of three different subunits: the pore forming $Ca_v\alpha_{1c}$ (also $Ca_v1.2$) subunit, the $Ca_v\beta$ subunit and the $Ca_v\alpha_2\delta$ subunit. The $Ca_v\alpha_{1c}$ subunit is composed of four homologous motifs, each with six putative transmembrane segments. Its molecular weight is about 240 kDa and both the amino- (N-) and the carboxyl- (C-) terminus are located in the cytoplasm. The $Ca_v\alpha_{1c}$ subunit is an ion selective pore, contains the voltage sensor and gating apparatus, and is regulated by a variety of molecules. The calcium-binding protein calmodulin (CaM) is responsible for calcium-dependent inactivation (CDI) and calcium-dependent facilitation (CDF) by binding the "IQ-like" motif in the C-terminal tail of $Ca_v\alpha_{1c}$ subunit [44]. Recently, a CaM bridge between the N- and the C-terminus of the channel was described, transforming from global (required for general signaling) to local, spatially confined, calcium selectivity and producing a distinct channel modulation [45]. The CaMKII interacts as well with the C-terminus and is essential for modulation of CDF and voltage-dependent facilitation (VDF) [46]. The $Ca_v\alpha_{1c}$ subunit is phosphorylated by PKA and balanced by A-kinase anchoring proteins (AKAPS) and protein phosphatases [47, 48]. Many different models have been proposed – involving different parts of the pore forming subunit –, but the exact regulation mechanisms remains unclear [49]. However, for L-type calcium channel inhibition the $Ca_v\alpha_{1c}$ subunit provides specific binding sites for channel antagonists including dihydropyridines, phenylalkylamines

and benzothiazepines [50]. Nevertheless, dihydropyridines in therapeutical doses have no myocardial effects and are selective for calcium channel inhibition in smooth muscles.

The two auxiliary subunits, the intracellularly located $Ca_v\beta$ and extracellularly located $Ca_v\alpha_2\delta$ are associated with the $Ca_v\alpha_{1c}$ subunit [51]. There are four $Ca_v\beta$ subunits in the heart, encoded by different genes [52-54]. The $Ca_v\beta$ core, containing a Src homology 3 domain and a guanylate kinase-like (GK) domain, binds the $Ca_v\alpha_{1c}$ subunit with high affinity at the α interaction domain (AID) of the α binding pocket (ABP), building a complex [55, 56]. They differentially modify the functional properties of the pore forming subunit [57-59], for instance the $Ca_v\alpha_{1c}$ subunit plasma membrane trafficking and regulating gating kinetics of the channels [60-62].

Although different genes encode four different isoforms, the $Ca_v\alpha_2$ and $Ca_v\delta$ are generated by a single gene [52, 63] and are bound by a disulfide bridge. The $Ca_v\alpha_2\delta$ subunits also regulate the gating properties of the channel [64] and are important for pharmacological properties [65]. Recently and different to general assumptions, $\alpha_2\delta$ were proposed to be associated with plasma membrane through a glycosylphosphatidylinositol (GPI) anchor instead of having a transmembrane topology [66].

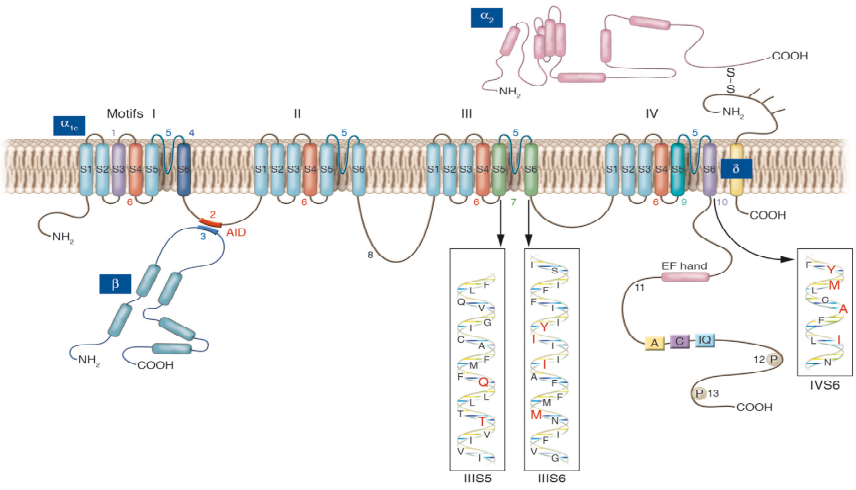

Figure 1.3:1. Structural organization of cardiac L-type calcium channel. Interaction sites are indicated (Bodi et al., The Journal of Clinical Investigation 2005).

L-type calcium channel are regulated as described in the previous Chapter (1.2). Schroder *et al.* observed changes in L-type calcium channel activity of failing hearts [67]. However, abnormal calcium handling leads to electrical and mechanical dysfunction, thus to arrhythmic risk and HF [68]. Concomitantly, the loss of cardiac calcium channel function in patients with inherited cardiac arrhythmia is associated with channel genetic mutations. Notably, the majority of the mutated sites are located in highly conserved regions of all three subunits [69].

1.4 Heterotrimeric G proteins

The heterotrimeric guanine nucleotide binding proteins (G proteins) are located at the inside surface of the cell membrane. They are activated by G protein-coupled receptors (GPCR) that are stimulated on the plasma membrane. Among other effects, G protein activation leads to activation of phosphorylation cascades. One major regulatory pathway is the activation of G_s protein by the predominant β_1-AR leading to enhanced stimulation of L-type calcium channels via adenylyl cyclase-mediated enhanced cyclic adenosine monophosphate (cAMP) levels and successively increased protein kinase A (PKA) activity [25, 70, 71]. The lesser-present β_2-AR subtypes generate more local than global effects, since they reside predominantly in compartments organized by caveolins of the plasma membrane [72, 73]. However, they also bind to G_s proteins increasing intracellular cAMP, but this does not lead to accelerate relaxation kinetics in cardiomyocytes of many mammalian species (except human and canine). This phenomenon is attributed to β_2-AR's ability to G_i- coupling counterbalancing the stimulating properties [74, 75].

G proteins consist of three subunits, Gα, Gβ, and Gγ. Their α-subunits are classified into four main families ($G\alpha_s$, $G\alpha_{i/o}$, $G\alpha_q$ and $G\alpha_{12/13}$, Table 3.1.1) based on their structural and functional homologies [76]. The Gα subunits are myristoylated or palmitolyted at their

N-termini and therefore responsible for protein and membrane interactions. They also bind the guanosine triphosphate (GTP) in the core domain [77], are linked to the united βγ-subunit [78]. The GPCRs contain seven transmembrane segments, of which the third intracellular loop seems to interact with the core domain of Gα proteins optionally by collision coupling [79, 80]. Hence, ligand activated GPCR promotes dissociation of guanosine diphosphate (GDP) from and binding of GTP to the G protein α-subunit [81]. The GTP-bound α-subunit induces a conformational change, thus leading to dissociation from βγ-complex (Figure 1.4:1). Activated Gα and Gβγ subunits interact with a plethora of effectors, including enzymes and ion channels, mediating downstream processes and regulating cell-signaling pathways [82, 83]. The desensitization of GPCR process is initiated by receptor phosphorylation through G protein-coupled receptor kinases (GRK), followed by β-arrestin binding leading to receptor internalization [84]. Accordingly, the GTPase-activating protein (GAP) enhances hydrolysis of GTP to GDP on the Gα subunit. Thus, the exchange induces re-association of the heterotrimeric G-protein and its functional inactivation [81]. In addition, regulators of G protein signaling (RGS) proteins are able to accelerate the GTPase activity [85]. However, the majority of the identified RGS proteins interact mainly with members of $G_{i/o}$ and G_q families [86].

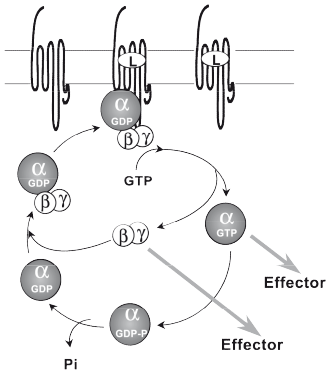

Figure 1.4:1. The G proteins undergo activation-inactivation cycle. Agonist binds preferably to the active receptor conformation leading to interaction of the receptors and the G proteins. GDP bound α-subunit is released and replaced by GTP. The dissociated and activated α- and βγ-subunits are restricted by re-association (Zolk et al., Canadian Journal of Physiology and Pharmacology 2000).

For G protein βγ-complex, there are five β- and twelve γ- gene products known so far (Table 1.4:1). The complex is a result of a coiled-coil interaction between their N-termini [78]. However, the C-terminus of the γ-subunit is modified by isoprenylation for membrane association of the complex. Gβγ protein-complex was identified as a direct or indirect modulator of diverse cell functions, for instance the regulation of inwardly rectifying potassium channels induced by acetylcholine (ACh) activation and second messenger-dependent mechanisms on ion channels [78]. Effects on voltage-dependent calcium channels were also described [87-89].

Different subunit combinations of the G proteins are decisive for the variety of their effects. The exact subunit combination and the expression profile in cell or tissue are essential for the outcome of receptor signaling.

In the heart, most of the known G proteins are expressed, but it was shown that their expression vary in cardiac tissue specific manner on mRNA levels [90, 91]. Stimulatory cholera-toxin (CTX) sensitive $G\alpha_s$ and inhibitory pertussis-toxin (PTX) sensitive $G\alpha_i$ protein isoforms mediate signaling pathways and play a central role in cardiac function [74]. Their PKA mediated signaling mechanisms are well studied [70]. Moreover activation of $G_{i/o}$ protein subfamily modifies cell and channel function *via* diverse signal cascades [92]. $G\alpha_{i2}$ and $G\alpha_{i3}$ are present in cardiomyocytes, whereas $G\alpha_{i1}$ and $G\alpha_o$ are likely transcribed in non-cardiomyocyte cells [93]. The $G\alpha_{i2}$ and $G\alpha_{i3}$ isoforms are highly homologous, with $G\alpha_{i3}$ protein being clearly less abundant in cardiomyocytes. Inactivation of G_i proteins in general and specific mutations in the GTP binding domain of the $G\alpha_{i2}$ protein correlate with arrhythmic effects [94]. Additionally, alterations of $G\alpha_{i2}$ and $G\alpha_{i3}$ expression levels are found in heart disease [95]. Furthermore, elevated levels of $G\alpha_{i2}$ and $G\alpha_{i3}$ isoforms were found in heart failure patients [96-99], but the reason for the upregulation of $G\alpha_{i2}$ and $G\alpha_{i3}$ in cardiomyocytes remains unexplained.

Table 1.4:1. Heterotrimeric G protein subunits and subtypes and their expression pattern (Offermanns S., Progress in Biophysics & Molecular Biology 2003).

Name	Gene	Expression
α-Subunits		
$G\alpha_s$ class		
$G\alpha_s$	*Gnas*	Ubiquitous
$G\alpha_{sXL}$	*Gnasxl*	Neuroendocrine
$G\alpha_{olf}$	*Gnal*	Olfact. epithelium, brain
$G\alpha_{i/o}$ class		
$G\alpha_{i1}$	*Gnai1*	Widely distributed
$G\alpha_{i2}$	*Gnai2*	Ubiquitous
$G\alpha_{i3}$	*Gnai3*	Widely distributed
$G\alpha_o$	*Gnao*	Neuronal, neuroendocrine
$G\alpha_z$	*Gnaz*	Neuronal, platelets
$G\alpha_{gust}$	*Gnag*	Taste cells, brush cells
$G\alpha_{t-r}$	*Gnat1*	Retinal rods, taste cells
$G\alpha_{t-c}$	*Gnat2*	Retinal cones
$G\alpha_{q/11}$ class		
$G\alpha_q$	*Gnaq*	Ubiquitous
$G\alpha_{11}$	*Gna11*	Almost ubiquitous
$G\alpha_{14}$	*Gna14*	Kidney, lung, spleen
$G\alpha_{15/16}$	*Gna15*	Hematopoietic cells
$G\alpha_{12/13}$ class		
$G\alpha_{12}$	*Gna12*	Ubiquitous
$G\alpha_{13}$	*Gna13*	Ubiquitous
β-Subunits		
β_1	*Gnb1*	Widely, retinal rods
β_2	*Gnb2*	Widely distributed
β_3	*Gnb3*	Widely, retinal cones
β_4	(*Gnb4*)	Widely distributed
β_5	*Gmb5*	Mainly brain
γ-Subunits		
γ_1, γ_{rod}	*Gngt1*	Retinal rods, brain,
γ_{14}, γ_{cone}	*Gngt2*	Retinal cones, brain
γ_2, γ_6	*Gng2*	Widely
γ_3	*Gng3*	Brain, blood
γ_4	*Gng4*	Brain and other tissues
γ_5	*Gng5*	Widely
γ_7	*Gng7*	Widely
γ_8, γ_9	*Gng8*	
γ_{10}	*Gng10*	Widely
γ_{11}	*Gng11*	Widely
γ_{12}	*Gng12*	Widely
γ_{13}	*Gng13*	Taste buds

1.5 Animal models

Animal studies have been improved over the last decades and play a fundamental role in research. For the last years, mouse models contributed significantly to the understanding of the function of ion channels in the cardiovascular system. However, mouse hearts differ from human hearts. They have a more rapid heart rate (600-700 beats per minute) and thus the AP duration in mouse cardiomyocytes is much shorter. Hence, the plateau phase is absent and

accordingly the repolarization is much quicker [100]. Consequently, voltage-gated potassium channels exhibit the highest structural and functional diversity [101], but overall similar types of channels are found in human and mouse hearts.

Mouse models used in this study (β_2-AR transgenic, $G\alpha_{i2}$- deficient and $G\alpha_{i3}$- deficient mice) have been well established. Cardiac-specific β_2-AR overexpression was induced using cDNA ligation of human β_2-AR with the α-myosin heavy chain promoter [102, 103]. Their cardiac phenotype is dependent on the level of overexpression [104]. Mice develop cardiac hypertrophy and fibrosis at a total receptor expression level over a hundred-fold leading to HF and higher mortality.

Global $G\alpha_{i2}$- or $G\alpha_{i3}$- deficient ($G\alpha_{i2}$-/- or $G\alpha_{i3}$-/-) mice were generated by gene targeting. Detailed methods were described previously [105, 106]. $G\alpha_{i2}$-/- mice developed inflammatory disease due to defect in the regulation of immune responses [107, 108], whereas $G\alpha_{i2}$+/- did not reveal any clinical signs of disease. Furthermore, $G\alpha_{i2}$-/- mice suffer from gastrointestinal symptoms, such as ulcerative colitis and adenocarcinoma of the colon [106, 107], but this phenotype vanished by backcrossing. However, their survival time was significantly shortened [109, 110]. Recently, electrical abnormalities inducing ventricular arrhythmia resulting in prolonged ventricular AP was associated with $G\alpha_{i2}$ gene deletion [111]. Interestingly, in mice with cardiac overexpression of human β_2-AR, gene deletion of $G\alpha_{i2}$ - but not $G\alpha_{i3}$ - leads to hypertrophy and excess mortality [109].

In contrast to $G\alpha_{i2}$ deficient mice, mice lacking $G\alpha_{i3}$ do not seem to have obvious phenotypic changes [110]. However, $G\alpha_{i3}$ is required as a specific regulator of autophagy in the liver [110, 112].

1.6 Aims of this thesis

The excessive catecholamine activation in cardiac cells leads to signal transduction desensitization, β-AR down regulation, receptor internalization [70, 113, 114] and ion channel remodeling [30].

So far, specific modulation of basal L-type calcium current in the heart by $G\alpha_i$ protein remained unclear and controversial. In human HF, single channel studies demonstrated a significant increased L-type calcium channel open probability [67]. On the other hand and different to β_1-AR, chronically selective increased β_2-AR tone in the mouse suppresses basal L-type calcium channel density [115, 116]. This phenomenon was attributed to its additional G_i coupling, forming dual signaling effects [74, 75]. Since the highly homologous $G\alpha_{i2}$ and $G\alpha_{i3}$ are upregulated in heart failure [95-99] and the predominant $G\alpha_{i2}$ protein protects β_2-AR tg cardiomyocytes from apoptosis [109], activation of G_i signaling pathways seems to be crucial in balancing cardiomyocyte function. It was previously demonstrated that a reduction of single L-type calcium channel activity is caused by β_2-AR overexpression [117]. This effect was aggravated by additional $G\alpha_{i2}$ gene deletion and reversed by PTX treatment [109]. On the other hand, $G\alpha_{i2}$ protein has been considered to be exclusively responsible for the cholinergic inhibition of the cardiac L-type calcium current [118]. Therefore, this study is significant from a number of perspectives.

First, it assesses the phenotypic effects by $G\alpha_{i2}$ protein deletion and differentiates the impact of the mouse models on expression levels of G_i isoforms and L-type calcium channel subunits in the heart. Second, it determines $G\alpha_{i2}$ protein effects on cardiac L-type calcium channel regulation. Third, it further elucidates specific signaling pathways implicated in cardiac L-type calcium channel modulation by $G\alpha_i$ proteins. Finally, it explores the role of $G\alpha_{i2}$ protein in cardioprotection.

To address these questions mice lacking global $G\alpha_{i2}$ are used and compared to mice lacking global $G\alpha_{i3}$, mice overexpressing cardiac human β_2-AR and wt control mice. Their effects are explored at the following levels: mRNA expression, protein expression, electrophysiological whole-cell, and relevant pathway enzyme phosphorylation.

This study examines the mouse models by generating and comparing the genetic distribution, and the cardiac phenotypic consequences by $G\alpha_{i2}$ gene deletion. Furthermore, the influence and extent to which specific gene deletion of $G\alpha_{i2}$ or $G\alpha_{i3}$ isoform or β_2-AR overexpression affect cardiac expression levels of G_i isoforms and L-type calcium channel subunits using quantitative real-time PCR, immunoblot and ADP-ribosylation is determined.

On electrophysiological level, the aim is to measure whole-cell L-type calcium currents and gating properties in cardiomyocytes, to assess channel chronic effects following $G\alpha_{i2}$ and $G\alpha_{i3}$ selective deletion and to bring them into relation to the existing single channel data. Since double-deficient ($G\alpha_{i2}$-/- / $G\alpha_{i3}$-/-) mice are not viable [110], electrophysiological experiments in acute $G_{i/o}$ inactivated cardiomyocytes mediated by PTX-treatment were performed.

Finally, signaling pathways known to be involved in G_i protein-mediated action and L-type calcium channel functions are investigated. Here, the focus is on protein kinase B (PKB/Akt) and extracellular regulated kinase subtype 1 and 2 (ERK1/2) activations [115, 119, 120], and characterization of cardiac G_i effects towards their phosphorylation on protein levels.

2 MATERIALS AND METHODS

2.1 Materials

2.1.1 Chemicals/enzymes

Glycerol 87 % (v/v)	Applichem
Agarose powder	Bio-Rad
Kaleidoscope prestained protein standard ($Ca_v\alpha_1$)	Bio-Rad
Tween 20	Bio-Rad
Saline 0.9 %	Braun
Prestaied protein molecular weight marker	Fermentas
Page Ruler prestained protein ladder (Akt and ERK1/2)	Fermentas
Bromphenol blue	Merck
$CaCl_2$ x 2 H_2O	Merck
D(+)-glucose	Merck
Glycin	Merck
$MgCl_2$	Merck
$MgSO_4$ x 7 H_2O	Merck
NaCl	Merck
NaF	Merck
NaH_2PO_4 x H_2O	Merck
SDS	Merck
^{32}P-NAD^+	PerkinElmer
APS	Promega
Heparin, Liquemin®5000 IU/ml	Roche
TBS, Western Blocking Reagent	Roche
AcOH ≥ 99 %	Roth
Acrylamide 30 % (m/v), Rotiphorese	Roth
n-Butanol	Roth
CsCl	Roth
Formaldahyde	Roth

Milk powder	Roth
KCl	Roth
Methanol	Roth
NaOH	Roth
TEMED	Roth
Tris	Roth
ATP-Na_2 x H_2O	Sigma-Aldrich
ATP-Mg	Sigma-Aldrich
β-Mercaptoethanol	Sigma-Aldrich
BSA	Sigma-Aldrich
CCH	Sigma-Aldrich
$C_{12}E_{10}$	Sigma-Aldrich
CsOH	Sigma-Aldrich
DNase	Sigma-Aldrich
DTT	Sigma-Aldrich
EDTA	Sigma-Aldrich
EGTA	Sigma-Aldrich
Fluka urea	Sigma-Aldrich
GTP	Sigma-Aldrich
MES	Sigma-Aldrich
NAD+	Sigma-Aldrich
NADP+ x H_2O	Sigma-Aldrich
Na_3VO_4	Sigma-Aldrich
PBS	Sigma-Aldrich
Ponceau	Sigma-Aldrich
PTX	Sigma-Aldrich
Thymidine	Sigma-Aldrich
Triton x-100	Sigma-Aldrich
HEPES	USB

2.1.2 Equipments/consumables

Allegra 64R-High-Speed Centrifuge	Beckman Coulter
DB Microlance injection needles (21, 22, and 27G)	Becton Dickinson
Insulin syringe (1 ml, sterile)	Becton Dickinson
Comb (10 wells, 1.0 mm thick)	Biometra
Fastblot B33/B34	Biometra
Glass plates 10x10 cm with spacer	Biometra
Power Pac P25T Power Supply	Biometra
Silicone rubber seal (1.0 mm)	Biometra
Power Pac 3000 Power Supply	Bio-Rad
Intrafix®air infusionset	Braun
Single-use syringe (2, 5, 10 and 20 ml, sterile)	Braun
Sterifix Injection and Aspiration Filter	Braun
Pipette references (2, 10, 20, 100, 200, 1000 µl)	Eppendorf
Themomicter compact	Eppendorf
35 x 10 mm Petri dish	Falcon
UV quartz cuvette (100 µl)	GE-Healthcare
F423 heated circulating bath	Haake
MR3001 heating plate and stirrer	Heidolph Instruments
Biofuge Fresco Microlitre Centrifuge	Heraeus Instruments
Sterilizing oven	Heraeus Instruments
Comb (15 wells, 1.5 mm thick)	Hoefer
Glass plates 16x18 cm	Hoefer
SE 400 Sturdier Vertical Electrophoresis Unit	Hoefer
Spacer (2 cm x 24 cm x 1.5 mm)	Hoefer
Heating plate RET control IKAMAG	IKA
T20 basic Ultra-Turrax	IKA
Pipetboy acu	Integra Biosciences
Microfuge Fire Polisher	Narishige
Disposable transfer pipettes (2 ml)	Sarstedt
Falcon tubes (15 and 50 ml)	Sarstedt
Micro tubes (1.2 and 2 ml)	Sarstedt
Pipette tips (10, 100 and 1000 µl)	Sarstedt

Serological pipettes (1, 5, 10 and 25 ml, sterile)	Sarstedt
Vortex Genie 2	Scientific Industries
Orion Research Expandable ion Analyzer EA940	Thermo Fisher Scientific
Finn pipettes (2, 10, 20, 100, 200, 1000 μl)	Thermo Scientific
Varioklav 1355	Thermo Scientific
Microcentrifuge Galaxy MiniStar	VWR International

2.1.3 Computer software

GraphPad Prism4	GraphPad
Microsoft Office XP	Microsoft
MicrocalOrigin6	OriginLab

2.2 Animals

2.2.1 Mouse models

Existing mouse models were used [102, 103, 105, 106]:

- mice overexpressing the human β_2-AR (β_2-AR tg, "transgenic")

- mice deficient for $G\alpha_{i2}$ ($G\alpha_{i2}$-/-, "knockout")

- and mice deficient for $G\alpha_{i3}$ ($G\alpha_{i3}$-/-, "knockout").

Adult mice (3-9 months of age) analyzed in this study were of both sexes and weighted 20-40 g.

2.2.2 Breeding

Transgenic mice and knockout mice were backcrossed onto a C57Bl6 background for at least 10 generations. Littermates served as the wild-type (wt) controls. Sufficient offspring was achieved by strict breeding control of cross breeding schemes shown in Figure 2.2.2:1.

C57Bl6	x	C57Bl6
β_2-AR tg	x	C57Bl6
$G\alpha_{i2}$+/+	x	$G\alpha_{i2}$+/-
$G\alpha_{i2}$+/-	x	$G\alpha_{i2}$+/-
$G\alpha_{i2}$+/-	x	$G\alpha_{i2}$-/-
$G\alpha_{i3}$+/+	x	$G\alpha_{i3}$+/-
$G\alpha_{i3}$+/-	x	$G\alpha_{i3}$+/-
$G\alpha_{i3}$+/-	x	$G\alpha_{i3}$-/-

Figure 2.2.2:1. Following eight breeding schemes were used at the animal facilities of Institute of Pharmacology at the University of Cologne to raise β_2-AR tg and $G\alpha_i$ knockout mice.

All mouse models were maintained at the animal facilities of the Heinrich-Heine University of Düsseldorf and of the Institute of Pharmacology at the University of Cologne. All animal procedures are complied with respective laws and regulations and conform to the *Guide for the Care and Use of Laboratory Animals* (US National Institutes of Health, NIH Publication No. 85-23, revised 1996).

2.3 Genotyping

2.3.1 Genomic deoxyribonucleic acid (gDNA) purification

Tail-clip (about 4 mm) analysis was performed on 3-4 weeks old mice. NucleoSpin®96 Tissue Kit and NucleoVac®96 Vacuum Manifold (Macherey-Nagel, Düren, Germany) were used for the isolation of gDNA from mice tails. Samples were processed according to manufacturer's protocol (NucleoSpin®96 Tissue, Macherey-Nagel). Contaminations were removed by washing steps with washing buffer. Pure gDNA of each sample was finally eluted in 150-300 µl buffer (pH 8.5) and stored at -20 °C.

2.3.2 Polymerase chain reaction (PCR)

PCR was carried out to multiply and identify isolated DNA fragments of each genotype. Primer pairs (Table 2.3.2:1) were purchased from Metabion GmbH (Martinsried, Germany) and used to detect wt and $G\alpha_i$ mutant (mut, which stands for $G\alpha_i$ allelic deficiency) and for human β_2-AR tg mice to verify their existence.

PCR reaction volume was 25 µL. PCR was carried out in thermal cycler (Mastercycler Family, Eppendorf, Hamburg, Germany). PCR conditions (DreamTaq™ Green DNA Polymerase, Fermentas, Burlington, Canada) for each genotype are listed in Table 2.3.2:2.

$G\alpha_{i2}$ wt and mutant (mut) cycler programs are show in Table 2.3.2:3. PCR were run separately, because of divergent melting temperature. In contrast, same conditions were used for $G\alpha_{i3}$ wt and mut (Table 2.3.2:3). The conditions for β_2-AR are also listed in 2.3.2:2-3. Here, PCR products were further digested by insert restriction enzyme to separate human β_2-AR DNA fragments from murine β_2-AR.

Table 2.3.2:1. Following primer pairs were used to detect mouse models analyzed in this project.

Primer name	**Sequence**
$G\alpha_{i2}$ wt forward:	5'- GAT CAT CCA TGA AGA TGG CTA CTC AGA AG -3'
$G\alpha_{i2}$ wt reverse:	5'- CCC CTC TCA CTC TTG ATT TCC TAC TGA CAC -3'
$G\alpha_{i2}$ mut forward:	5'- CAG GAT CAT CCA TGA AGA TGG CTA C -3'
$G\alpha_{i2}$ mut reverse:	5'- GCA CTC AAA CCG AGG ACT TAC AGA AC -3'
$G\alpha_{i3}$ wt forward:	5'- GTG GCC AAA GAT CCG AAC GA -3'
$G\alpha_{i3}$ wt reverse:	5'- TTC ATG CTT TCA TGC ATT CGG TTC -3'
$G\alpha_{i3}$ mut forward:	5'- TGC CGA GAA AGT ATC CAT CAT G -3'
$G\alpha_{i3}$ mut reverse:	5'- TTC ATG CTT TCA TGC ATT CGG TTC -3'
human β_2-AR forward:	5'- ACA TTG TGC ATG TGA TCC -3'
human β_2-AR reverse:	5'- ATT CTT CCC TTG TGA ATC -3'

Table 2.3.2:2. Selected PCR conditions needed for genotyping the mouse models.

	$G\alpha_{i2}$ sample	**$G\alpha_{i3}$ sample**	**β_2-AR sample**
	Final concentration	**Final concentration**	**Final concentration**
Primer forward	0.50 µM	1.00 µM	0.50 µM
Primer reverse	0.50 µM	1.00 µM	0.50 µM
dNTPs	0.20 mM	0.20 mM	0.20 mM
10x buffer green	1x	1x	1x
Dream taq green	0.04 U/µl	1.25 U/µl	0.04 U/µl
gDNA	(1 µl)	(1 µl)	(1 µl)

Table 2.3.2:3. Each genotype specified cycler programs for PCR runs. Step 3. denaturation until step 5. elongation were repeated 35x for $G\alpha_{i2}$ wt and mut and for β_2-AR tg before starting the final elongation. 37 cycles were set for $G\alpha_{i3}$ wt/mut.

	Cycler program	**$G\alpha_{i2}$ wt**	**$G\alpha_{i2}$ mut**	**$G\alpha_{i3}$ wt/mut**	**Human β_2-AR tg**
1.	Hotstart	94°C	94°C	94°C	94°C
2.	Initial denaturation	94°C 0:05:00 min	94°C 0:05:00 min	94°C 0:05:00 min	94°C 0:0:45 min
3.	Denaturation	94°C 0:00:30 min	94°C 0:00:30 min	94°C 0:00:30 min	94°C 0:00:45 min
4.	Annealing	62°C 0:00:30 min	57.5°C 0:00:30 min	60°C 0:01:00 min	57.5°C 0:01:00 min
5.	Elongation	72°C 0:01:00	72°C 0:00:45 min	72°C 0:01:00 min	72°C 0:01:00 min
6.	Final elongation	72°C 0:05:00 min	72°C 0:05:00 min	72°C 0:10:00 min	72°C 0:05:00 min
7.	Cooling	16°C hold	16°C hold	16°C hold	16°C hold

2.3.3 Gel electrophoresis

Agarose powder was mixed with trishydroxymethylaminomethane (Tris) acetat ethylenediaminetetraacetic (EDTA) -buffer (TAE buffer) to 1.5 % for $G\alpha_{i2}$-/-, to 1.6 % for $G\alpha_{i3}$-/- and to 2.0 % for β_2-AR tg separation and heated until completely melted. Ethidium bromide was added to the gel (1 μM). Ethidium bromide is a fluorescent dye and intercalates between double strands of DNA and therefore facilitates the visualization of DNA after electrophoresis. After solidification at room temperature, the gel was inserted horizontally into the electrophoresis chamber (Horizon® 11.14, Biometra, Göttingen, Germany) and covered with TAE-buffer. PCR products (wt or mutant of $G\alpha_i$ isoform) were pipetted into the respective sample well. A DNA ladder (GeneRuler 1 kb DNA-Ladder, Fermentas) was used for comparative discrimination of amplicon length. Finally, a current of 100 mA was applied. During electrophoresis, PCR products migrated towards anode at different rates, determined

by their size of the DNA fragments. For visualization, the gel was placed on an ultraviolet transilluminator and an image was taken (3UV-Transilluminator Model LMS-20E, UVP, Cambrigde, UK; Digital Camera DC290, Kodak, Stuttgart, Germany).

2.3.4 Mendelian inheritance

Mendelian inheritance is based on the transmission of hereditary genes from parents to their offspring. The theoretical distribution according to our breeding schemes is shown in Figure 2.2.4:1 (except pure C57Bl6 breeding). This distribution was compared to each $G\alpha_{i2}$, $G\alpha_{i3}$ and β_2-AR breeding scheme (illustrated in Figure 2.2.2:1) in a period of 2.5 years in our own animal facility.

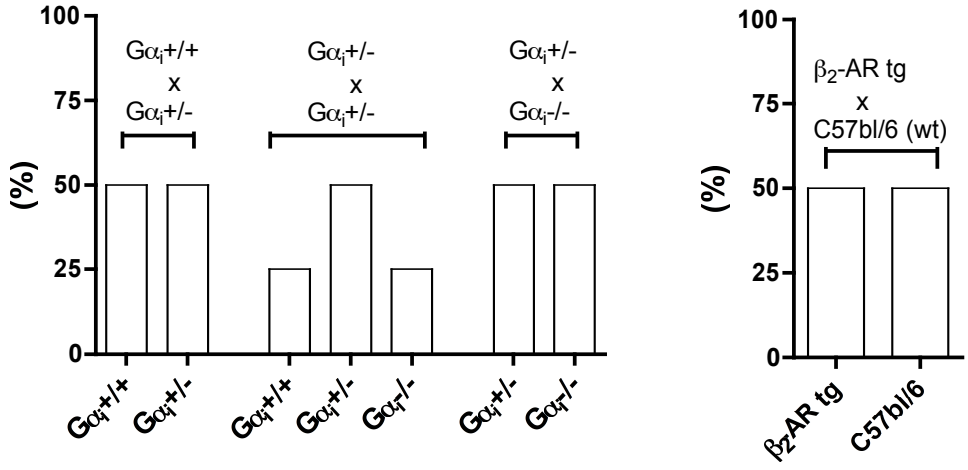

Figure 2.3.4:1. Expected genotype distribution according to Mendelian inheritance $G\alpha_i$+/- paired either with $G\alpha_i$+/+ or $G\alpha_i$-/- revealed 50 % of each genotype combined together. $G\alpha_i$+/- x $G\alpha_i$+/- breeding presented three offspring genotype possibilities: $G\alpha_i$+/+, $G\alpha_i$+/- and $G\alpha_i$-/-, which were distributed 25 %, 50 % and 25 %, respectively. β_2-AR tg mice bred with C57Bl6 wt control indicate 50 % distribution for each genotype.

2.4 Messenger ribonucleic acid (mRNA) analysis

2.4.1 mRNA isolation

For RNA stabilization, dissected heart tissues from $G\alpha_{i2}$-/-, $G\alpha_{i3}$-/-, β_2-AR tg and wt animals were dropped into RNAlater®Solution (invitrogen, Carlsbad, CA, USA) at room temperature. Samples were then stored at 4 °C or further processed. Tissue samples were disrupted and homogenized in RNeasy lysis (RLT) -buffer (Qiagen, Hilden, Germany) using a rotor-stator homogenizer. Cellular nucleic acids were extracted from murine atrium and ventricle according to the standard manufacturer's protocol (Qiagen QIAshredder and RNeasy Mini Kit, Qiagen). DNA was removed with on-column DNAse digestion (RNAse Free DNAse Set, Qiagen). RNA concentration was determined by measuring the absorbance at 260 nm and the contamination absorbance at 280 nm using a DU 800 UV/Visible Spectrophotometer (Beckman Coulter, Brea, CA, USA). Using a 100 µl UV quartz cuvette, 1 µl of RNA sample was diluted in 99 µl RNAse-free solution (Qiagen). The ratio between the absorbance values estimated the RNA purity and should fall between 1.8 and 2.0. To ensure that samples were comparable and of similar integrity, qualitative analysis of RNA integrity was performed. On a 1 % formaldehyde denaturating agarose gel, 2 µg of total RNA was separated by electrophoresis as described in 2.3.3 (Figure 2.4.1:1).

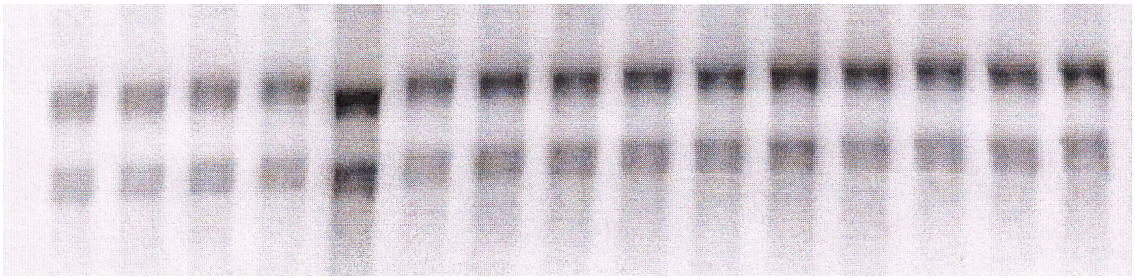

Figure 2.4.1:1 Validation of purified RNA from heart tissue to ensure accurate measurement of intact total RNA. In the intact RNA sample 18S and 28S ribosomal RNA bands are clearly visible in a ratio of 2:1.

2.4.2 Complementary DNA (cDNA) synthesis

Total RNA served as a template to synthesize cDNA by ImProm-II Reverse Transcription Kit (Promega, Madison, WI, USA). In brief, up to 1 μg RNA was reverse transcribed to cDNA in a final volume of 20 μl using Oligo $(dT)_{15}$ primers (0.5 μg/reaction) and 3.75 mM $MgCl_2$. Reverese transcription was performed in a PCR thermal cycler (Eppendorf) using the following conditions: incubation at 25 °C for 10 min, incubation at 37 °C for 120 min, and incubation at 85 °C for 5 min. The resulting cDNA was stored at -20 °C.

2.4.3 Quantitative Real-Time PCR (RT-PCR)

Primers for $G\alpha_{i1}$, $G\alpha_{i2}$, $G\alpha_{i3}$ isoforms and $Ca_v\alpha_1$ and $Ca_v\beta$ subunits (isoform $Ca_v\beta_1$ and $Ca_v\beta_3$) were described previously [121, 122]. Gnao ($G\alpha_o$) and Cacnb2 ($Ca_v\beta_2$) sequences were downloaded from NCBI's RefSeq database. Consensus sequence for $Ca_v\beta_2$ isoforms was formed. Specific primers for the $G\alpha_o$ (amplicon size 80 bp) and $Ca_v\beta_2$ subunit (59 bp) were designed using Primer Express Software v 3.0 (Applied Biosystems, Foster City, CA, USA). Primer sequences (Table 2.4.3:1) were confirmed using NCBI's Basic Local Alignment Search Tool (BLAST).

Each sample was analyzed using SYBR Green (Applied Biosystems) as fluorescent detector, glyceraldehydes 3-phosphate dehydrogenase (GAPDH) as endogenous control and 200 nM PCR primers in 96-well plates (Applied Biosystms). After preparing, a brief centrifugation of 1500 g for 2 min with a 96-well plate adapter was performed. The mixture was initially incubated at 95 °C for 10 min, followed by 40 cycles of 95 °C for 15 sec and 60 °C for 60 sec. PCR reaction was carried out using the 7500 RT-PCR system (Applied Biosystems) in triplets. The fluorescent detector binds to the minor groove of double-stranded DNA (dsDNA) and fluoresces when bound to dsDNA is excited by a light source. Graphs were generated for

each probe in each sample. The graphs have three phases: no detectable fluorescence, exponential phase, and plateau phase (Figure 2.4.3:1).

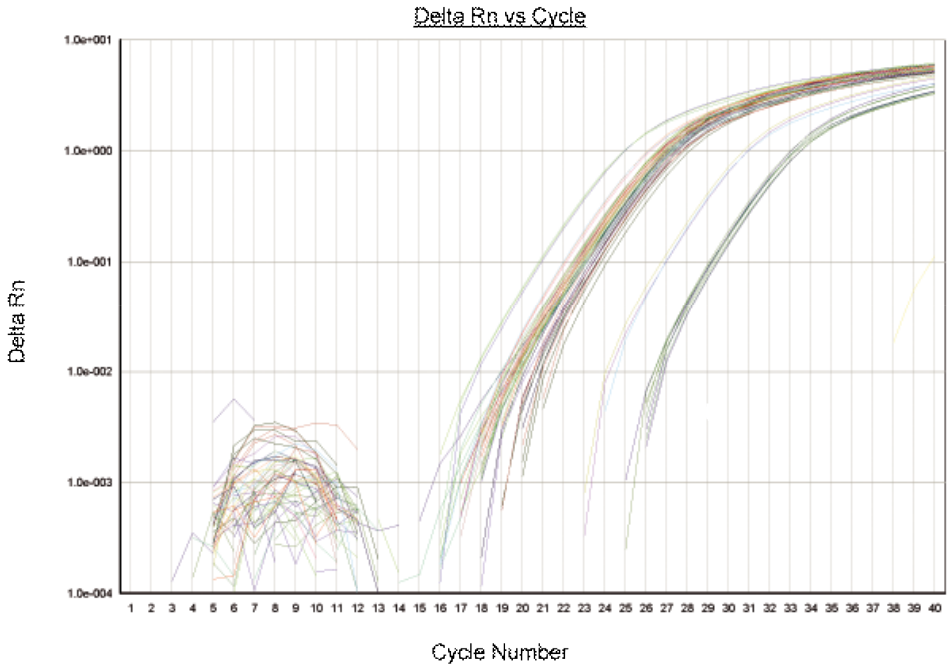

Figure 2.4.3:1. Representative RT-PCR run for 40 cycles of $G\alpha_{i2}$-/- cardiac samples with endogenous control GAPDH. The CT was the quantitative endpoint.

The comparative cycle threshold (CT) method for quantitative gene expression was used [123, 124]. It is defined as the number of cycles required for the fluorescent signal to cross the threshold. CT levels are inversely proportional to the amount of target cDNA in the sample. The mean of the PCR replicates was taken to analyze the individual samples. Data were normalized to GAPDH to ΔCT (CT gene of interest - CT endogenous control). Wt samples were chosen as the internal calibrator and expressions are expressed in relation to them. The calibrator has an expression of 1. Then ΔCT of the internal calibrator was subtracted from the ΔCT of the test sample ΔΔCT. Each cycle represented a tow fold increase of cDNA molecule. The amount of target, normalized to an endogenous control and relative to calibrator, was given by: $2^{-\Delta\Delta CT}$.

Table 2.4.3:1. Specific primer pairs were designed for $G\alpha_o$ and for all $Cav\beta_2$ isoforms.

Primer name	**Sequence**
$G\alpha_o$ forward:	5'-TGGCATCGTAGAAACCCACTT-3'
$G\alpha_o$ reverse:	5'-CGACGTCAAACAGCCTGAAG-3'
$Ca_v\beta_2$ forward:	5'-GGGAGGCAGTACGTAGAGAAGCT-3'
$Ca_v\beta_2$ reverse:	5'-TGCAAATGCAACAGGTTTT GTC-3'

2.5 Protein analysis

2.5.1 Cardiac cell membrane preparation

Single murine cardiac ventricles from $G\alpha_{i2}$-/-, $G\alpha_{i3}$-/-, β_2-AR tg and wt animals were disrupted and washed in ice-cold phosphate buffered saline (PBS). Cardiac tissues were homogenized in lysis buffer containing an EDTA-free protease inhibitor cocktail (Table 2.5.1:1, Roche, Mannheim, Germany) using an ultra-turrax blender.

Cellular membranes were isolated by two steps of centrifugation, first at 450 g and 4 °C for 10 min to eliminate the nuclei. The supernatants were transferred into new tubes and used for the second step of centrifugation at 30000 g and 4 °C for 30 min. Membrane pellets were subsequently resuspended in a buffer consisting of freezing supplement and lysis buffer in a ratio of 1:6 in order to stabilize membrane-associated proteins and kept at -80 °C (Table 2.5.1:2). Membrane protein concentrations were determined by modified Lowry protein assay (Peterson's method [125, 126]). This method is based on the reaction of Cu^{2+}, which built complexes with protein under alkaline condition. Through the conversion of Cu^{2+} to Cu^{+} in the protein complex, the aromatic amino acid of the protein sample reduces Folin Reagent and changes color from yellow to blue. The amount of protein in the sample can be estimated via reading the absorbance at 750 nm of the end product of the Folin reaction against a standard curve using linear equation. The assay was carried out according to

manufacturer's instruction manual (Bio-Rad, Hercules, CA, USA) and DC Protein Assay Kit (Bio-Rad). The visible change was detected by spectrophotometer (DU 800 UV/Visible Spectrophotometer, Beckman Coulter).

Table 2.5.1:1. Composition of the cell lysis buffer added to the EDTA-free protease inhibitor cocktail and used for cardiac membrane tissue isolation.

Lysis buffer	**Final concentration**
Tris-HCl (pH 7.4)	10 mM
EDTA	1.0 mM
DTT	0.5 mM

Table 2.5.1:2. Composition of freezing buffer stabilized membrane-associated proteins.

Freezing buffer	**Final concentration**
Tris-HCl (pH 7.4)	70 mM
$MgCl_2$	12 mM
Glycerol (v/v)	60 %
DNase	240 μg/ml

2.5.2 Cardiac tissue preparation

To examine functional $G\alpha_i$-dependent activation *in vivo*, $G\alpha_{i2}$-/-, $G\alpha_{i3}$-/- and wt animals were injected i.p. with 0.5 mg carbachol (CCh) per kg body weight diluted in 0.9 % normal saline [127]. CCh stimulates parasympathomimetic signaling pathways, which include the G protein-coupled muscarinic receptors (see Figure 2.5.2:1). Sham injections were performed with 400 μl 0.9 % saline per 30 g weight.

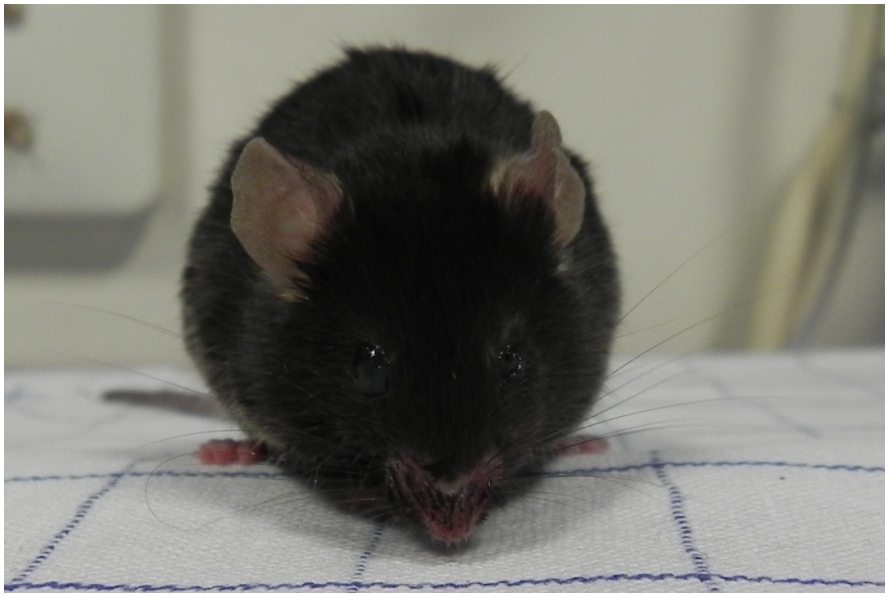

Figure 2.5.2:1. Mouse showing typical parasympathetic side effects (increased lacrymal fluid and salivation) after CCh i.p. injection.

After 15 min, animals were sacrificed by cervical dislocation. Ventricular tissue was harvested and lysed by homogenization in ice-cold buffer containing an EDTA-free protease inhibitor cocktail (Table 2.5.2:1, Roche). To ensure complete cell lysis, the mixture was incubated for 30 min at 4 °C.

Total cell lysates were extracted from the supernatant by centrifugation at 13500 g and 4 °C for 20 min. Protein concentrations were determined by Bradford method [128], which is based on an absorbance shift of the dye Coomassie Brilliant Blue G-250 from 470 nm (red) to 595 nm (blue) by hydrophobic and ionic interactions with the protein under acid condition. The increase of absorbance at 595 nm is proportional to the amount of bound dye. The amount of protein in the sample can then be estimated against a standard curve using linear equation. The Bradford assay is linear over a short range therefore dilutions of the sample are often necessary before analysis. The assay was carried out according to manufacturer's protocol (Bio-Rad) and Quick Start Bradford Protein Assay Kit (Bio-Rad). The visible change was detected by spectrophotometer (Mithras LB 940, Berthold Technologies, Bad Wildbad, Germany).

Table 2.5.2:1. Composition of the cell lysis buffer used for cardiac tissue preparation.

Lysis buffer	Final concentration
HEPES	50 mM
Triton X-100 (v/v)	1.0 %
NaCl	50 mM
Na_3VO_4	10 mM
SDS (w/v)	0.1 %
NaF (w/v)	0.1 %
EDTA	10 mM

2.5.3 Sodium dodecyl sulfate-polyacrylamide gel electrophoresis (SDS-PAGE)

Protein samples were prepared by adding Laemmli buffer ([129]; Table 2.5.3:1). This buffer contains SDS, which denatures and reduces proteins to their primary structure and coats them with uniform negative charges. This property allows protein separation on an electric field due to their size. The buffer also contains β-mercaptoethanol to break the disulfide bridges and bromphenol blue to label the progress of the protein solution through the gel during the electrophoretic run. The pore-size of the PAGE-gels can be altered by varying the acrylamide concentrations, leading to different protein movement properties. Generally, smaller proteins migrate faster than larger proteins through the gel. For gel formation ammoniumpersulfate (APS) as a radical initiator and N,N,N´,N´-tetramethylethylenediamine (TEMED) as a catalysator are used. Two parts of gel can be distinguished in a stacking and a separating gel. After polymerization of the separating gel solution, injected n-butanol layer for an even surface above was removed completely. Then the stacking gel solution was cast over the polymerized separating gel and the comb was inserted. The stacking gel allows the protein samples to be evenly stacked before they enter the separating gel during electrophoresis.

G_i proteins in cell membrane preparations were prepared with 4x Laemmli and separated on 6 M urea / 9 % SDS-PAGE maxi gels (Table 2.5.3:2). Protein content of 90 μg per lane was

loaded into the stacking gel. $Ca_v\alpha_1$ proteins in cell membrane preparations and Akt as well as ERK1/2 in total cell lysates were separated on 8 % and on 10 % SDS-PAGE mini gels, respectively (Table 2.5.3:3). Samples were pretreated with 4x Lämmli and only total cell lysates were preheated at 95 °C for 20 min. For all proteins, 100 µg were injected into each well of stacking gel.

Table 2.5.3:1. Composition of 4x Laemmli buffer mixed with protein samples for denaturation and preparation.

Sample buffer (4x)	**Final concentration**
Tris-HCl (pH 6.8)	62.5 mM
Glycerol (v/v)	10 %
SDS (w/v)	2 %
β-mercaptoethanol (v/v)	5 %
Bromphenolblue (w/v)	0.001 %

Table 2.5.3:2. Maxi gel conditions and quantities used for separation of membrane G_i proteins.

Separating gel buffer	**Final concentration**
Tris-HCl (pH 8.8)	3 M
SDS (w/v)	0.8 %
9 % separating gel solution	**Volume**
6 M Urea Tris-HCl (pH 7.4)	25.75 ml
Acrylamide 40 %	9.0 ml
Separating gel buffer	5.0 ml
APS 12.5 %	80 µl
TEMED	10 µl
Stacking gel buffer	**Final concentration**
Tris-HCl (pH 6.8)	0.25 M
SDS (w/v)	2 %
5 % stacking gel solution	**Volume**
Acrylamide 30 %	1.0 ml
Stacking gel buffer	9.0 ml
APS 12.5 %	70 µl
TEMED	10 µl

2.5.3:3. Mini gel conditions and quantities used for separation of membrane $Ca_v\alpha_1$ protein and Akt and ERK1/2 proteins in total cell lysates.

8 % separating gel solution	**Volume**
Tris-HCl (pH 8.8)	1.5 ml
Acrylamide 30 %	3.2 ml
SDS 10 %	120 µl
H_2O	7.14 ml
APS 10 %	160 µl
TEMED	12 µl
10 % separating gel solution	**Volume**
Tris-HCl (pH 8.8)	1.5 ml
Acrylamide 30 %	4.0 ml
SDS	120 µl
H_2O	6.34 ml
APS 10 %	160 µl
TEMED	12 µl
10 % stacking gel solution	**Volume**
Tris-HCl (pH 6.8)	500 µl
Acrylamide 30 %	680 µl
SDS	40 µl
H_2O	2.74 ml
APS 10 %	80 µl
TEMED	4 µl

2.5.3:4. Composition of running buffer poured in the electrophoretic chamber for starting the electrophoretic run and supporting the protein separation.

Running buffer	**Final concentration**
Tris-HCl	25 mM
SDS (w/v)	0.1 %
Glycin	200 mM

2.5.4 Western Blot

After gel electrophoris, all separated proteins were blotted onto nitrocellulose membranes (Amersham Hybond C extra, GE Healthcare) using a tank blotting system for maxi gels and a rapid semi-dry blotting system (Fastblot B33/B34, Biometra) for mini gels. Membranes were

placed on the gel between Whatman filter papers saturated with transfer buffer (Table 2.5.4:1). Overall transfer effectiveness and equal loading on blotting membrane for maxi gels were controlled by a non-specific protein staining using Ponceau S (Table 2.5.4:2). Only blots with equal loading were analyzed. After blotting, membranes were washed (> 1 h at room temperature, $Ca_v\alpha_1$ over night at 4 °C) with a blocking solution to block unspecific bindings of antibody, thus leading to a reduced background signals. For maxi gels 5 % blocking solution diluted in tris-buffered saline and tween 20 (TBST) and for mini gels 1 % blocking solution diluted in TBS were used. After blocking, membranes were incubated in primary antibody of each gene of interest (diluted in blocking solution) over night at 4 °C, except for $Ca_v\alpha_1$, which was gently agitated for an hour at room temperature. $G\alpha_i$ proteins were detected with a $G\alpha_{common}$ antibody [108], $G\beta\gamma$ complex with $G\beta_{common}$ antibody (1:2000; [130, 131]) and $Ca_v\alpha_1$ with $Ca_v\alpha_1$ antibody (1:200; Sigma Aldrich, St. Louis, MO, USA). The Ras-GTP-activating protein antibody (RasGAP 1:1000;[132]) was used as a loading control for $Ca_v\alpha_1$. For detection of phosphorylation, membranes were incubated with phospho-Akt (Ser473), phospho-glycogensynthase kinase 3 α and β (GSK3α/β; Ser21/9) and phospho-ERK1/2 (Thr202/Try204) antibodies (each 1:1000; Cell Signaling, Danvers, MA, USA). To normalize the phosphorylation data to total amount, membranes were reprobed with Akt and ERK1/2 antibodies (each 1:1000; Cell Signaling) after stripping. Further, membranes were washed by repeated steps of TBST and with TBS to remove unbound primary antibodies and included with the secondary antibody Anti-Rabbit IgG (1:1000; Sigma Aldrich). Enhanced chemiluminescence (ECL) was used for visualization of bound proteins. It is based on the emission of light during the horse-radish peroxides and hydrogen peroxide-catalyzed oxidation of luminal. Membranes were stained with two component of Amersham ECL Western blotting detection reagents and analysis system (GE Healtcare) mixed in equal volumes before using. The emitted light was captured on Amersham hyperfilm^{TM} ECL

(GE Healthcare) using an X ray film cassette and the film was developed in different exposition times using Agfa Curix 60 processor (Agfa Health Care, Mortsel, Belgium). Scanned films were analyzed and protein densities calculated using Aida Image Analyzer (Raytest, Straubenhardt, Germany) software.

Table 2.5.4:1. Composition of buffer used to transfer on the gel separated proteins to nitrocellulose membranes.

Transfer buffer	**Final concentration**
Tris-HCl	25 mM
Glycin	192 mM
Methanol (v/v)	20 %

Table 2.5.4:2 Ponceau S is a reversible staining dye and allows the detection of protein bands on nitrocellulose membranes.

Ponceau S	**Final concentration**
Ponceau (w/v)	0.1 %
Acetic acid	5.0 %

2.5.5 Adenosine diphosphate (ADP)-ribosylation

ADP ribosylation was performed as previously described [105, 133, 134]. ADP-ribose moiety of radioactively labeled substrate [^{32}P] nicotinamide-adenine-dinucleotide (NAD^+) was transferred to the cysteine residue of α subunit of G_i proteins, catalyzed by PTX. 100 µg ventricular membrane protein were centrifuged at 13000 g (Beckman Coulter) and 4 °C for 10 min. The membrane pellet was resuspended in 20 µl buffer per sample containing 25 mM Tris/HCl (pH 7.4) and 1 mM EDTA and kept on ice. 0.2 µl PTX (1 mg/ml) was incubated with 0.1 µl adenosine triphosphate (ATP; 10 mM), 25 µl dithiotreitol (DTT; 40 mM) and 0.3 µl H_2O per sample at 37 °C for the preactivation. After 30 min preactivated PTX was diluted 1:9 with a stop buffer (Table 2.5.5:1). Each sample was mixed with 10 µl of the diluted PTX solution. The ADP ribosylation reaction was started after adding 30 µl of

reaction buffer (Table 2.5.5:2). The samples were incubated with PTX and its substrate [^{32}P] NAD^+ over night at 4 °C in a steel tube rack. Thereafter, proteins were separated on a 6 M urea / 9 % SDS/PAGE gel, blotted onto nitrocellulose as described in Chapter 2.5.3 and 2.5.4 for maxi gels above. After staining with Ponceau S, nitrocellulose membranes were inserted with phosphor imaging plates (GE Measurement & Control Solution, Billerica, MA, USA) into a cassette for further detection and kept in safe over night. Incorporated [^{32}P] on imaging plate was visualized with an FLA 5000 Fuji Phosphoimager (3.0, Raytest).

Table 2.5.5:1. Composition of stop buffer mixed with preactivated PTX solution.

Stopp buffer	**Final concentration**
Tris-HCl (pH 7.4)	30 mM
BSA (w/v)	0.25 %
DTT	25 mM
EDTA	1.2 mM

Table 2.5.5:2. Reaction buffer was added to each sample. Samples were incubated over night for ADP ribosylation reaction.

Reaction buffer	**Final concentration**
Tris-HCl (pH 7.4)	200 mM
ATP	10 mM
GTP	2 mM
EDTA	2 mM
$C_{12}E_{10}$	0.6 %
Thymidine	20 mM
DNase	0.04 mg/ml
NAD^+	0.02 mM
$NADP^+$	0.2 mM
^{32}P-NAD^+	0.5 μCi

2.6 Electrophysiology

2.6.1 Cardiac myocytes isolation

Single ventricular myocytes were isolated from hearts of 3-9 months old mice by enzymatic dissociation. The heart was perfused through the coronary arteries using Langendorff column and organ bath. To prevent thrombus formation in the aorta, mice were injected i.p. with 15 µl/g heparin (500 IU/ml). Six solutions (A-F) were used for isolation (Table 2.6.1:1). The substances of solution A were diluted in aqua bidestillata and the pH was adjusted to 7.4 using 1.0 M NaOH. Solution B contains bovine serum albumine (BSA) diluted in solution A to 0.1 %. For solution C, two Collagenases (Collagenases Type I & II, Worthington, CellSystems, St. Katharinen, Germany) were mixed in a ratio of 1:1 and diluted in solution B to an final concentration of 75 U/ml. Solutions D-F contain increasing calcium chloride concentrations mixed with solution B.

The double-walled Langendorff column and bath organ were filled with solution B, heated to 37-40 °C using a water bath and supplied with oxygen. The height of the column defined the perfusion pressure. After 30 min of heparin injection, the mouse was sacrificed by cervical dislocation and the heart was dissected immediately and placed in a dish with cold solution A. Fatty and connective tissues were removed and the aorta ascendens was prepared, cannulated on a blunt injection needle, fixed with a binder yarn and connected to the Langendorff column. The heart was plunged into the bath organ and perfused with solution B. After 5 min of perfusion the drop frequency was determined and solution B was replaced by solution C (pre-heated in a water bath to 37 °C). The dropping rate was checked again after 4 min of perfusion and every minute afterwards. The digestion was stopped after maximum 15 min of perfusion or when the drop frequency had doubled compared to the first value obtained with solution C or according to the heart shape. The heart was taken from the cannula and placed in a dish with 10 ml of the lowest calcium concentration solution D. Atrial and remaining

connective tissues were removed and ventricular tissue was cut into small pieces using sharp scalpels. The tissue pieces were gently agitated by a transfer pipette to separate single cells from the tissue and then poured through a nylon cheese-cloth of 250 μm pore diameter into a falcon tube. Cells were left for 20 min at room temperature to settle. The supernatant was extracted carefully and replaced by the next calcium concentration step solution E and left for another 20 min. The procedure was repeated until the final solution F (highest calcium concentration) was reached. For the electrophysiological experiments only rod shaped cardiomyocytes were used (Figure 2.6.1:2). Cells were maintained at room temperature and subjected to patch-clamp analysis for up to 6 h.

Figure 2.6.1:2. A rod shaped intact murine ventricular myocyte to ensure accurate measurement.

Table 2.6.1:1. Following solutions were necessary for the isolation.

Solution A	**Final concentration**
NaCl	133 mM
KCl	4 mM
NaH_2PO_4 x H_2O	1.2 mM
$MgSO_4$ x 7 H_2O	1.2 mM
HEPES	10 mM
Glucose	12.1 mM
Solution B (g/mol)	**Final concentration**
BSA	1 mg/ml

Solution C	**Final concentration**
Collagenase Type I (191 U/mg)	37.5 U/ml
Collagenase Type II (200 U/mg)	37.5 U/ml
Solution D	**Final concentration**
$CaCl_2$	100 μM
Solution E	**Final concentration**
$CaCl_2$	200 μM
Solution F	**Final concentration**
$CaCl_2$	500 μM

2.6.2 Pertussis toxin experiments

PTX lyophillized powder (Sigma Aldrich, St. Louis, USA) was dissolved in H_2O to a concentration of 0.2 mg/ml. The PTX solution was diluted in solution A (Table 2.6.1:1) to a final concentration of 0.1 mg/ml. For acute G_i inactivation, a fraction of isolated ventricular myocytes in solution F (Table 2.6.1:1) was incubated with 1.5 μg/ml of PTX for 3 h at 37 °C in a water bath. Fractions incubated without PTX served as controls for heating and time effects. Afterwards, cells were maintained and examined at room temperature. It has been shown that this protocol completely ablates G_i-mediated signaling from adenosine receptors [135].

2.6.3 Patch-clamp technique

The patch-clamp technique was developed by Erwin Neher and Bert Sackmann in 1979 and accomplished in 1981 [136]. The technique is based on attaching cell membranes to micropipettes under a microscope. A micropipette is pressed against a cell membrane by gentle suction. A high resistance seal (gigaohm seal) is induced between glass and cell membrane, which is needed for complete electrical isolation of the membrane patch and for reduction of current noises. The seal resistance (GΩ range) is inversely proportional to

leakage current. The lower the leakage current, the higher the quality of the measured electronically isolated currents.

The following variations of basic patch-clamp techniques can be applied (Figure 2.6.3:1): A) Cell-attached recordings: cell membrane remains intact after gigaohm seal. Small size of the patched area allows current recordings through a single ion channel in the patch. B) Inside-out patch: the micropipette is quickly withdrawn from the cell after gigaohm seal, pulling the membrane patch off the cell into the external solution. C) Whole-cell recordings: after the cell-attached configuration, more suction destroys the membrane patch and connects pipette solution with cytoplasm, which leads to current recordings through multiple channels at once over the entire cell membrane. D) Outside-out patch: after whole-cell configuration is formed, the pipette is pulled away from the cell isolating the piece of membrane patch and building a convex membrane on the end of the pipette. The intracellular surface of ion channels is in contact with the pipette solution.

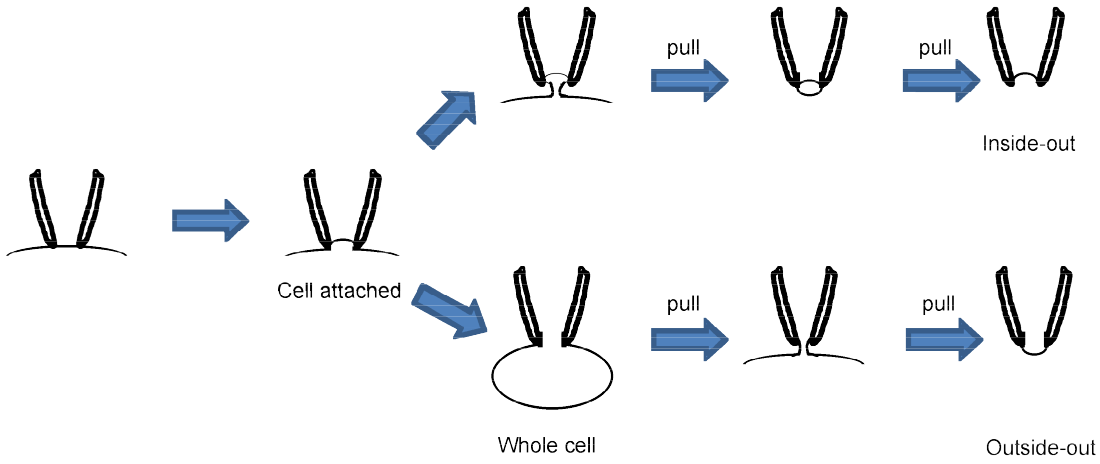

Figure 2.6.3:1. Diagram illustrating the variety of configuration techniques.

Patch-clamp techniques are based on the voltage-clamp method, which was described in the early 1950s by Alan Hodgkin and Andrew Huxley [137]. It allows the membrane potential of a cell to be clamped at a constant value and the current that flows through the membrane at any particular potential can then be measured. Patch-clamp technique employs a single

electrode voltage-clamping approach. The technique can be applied to small cells and *in vivo* measurements (Figure 2.6.3:2). Because currents detected in the experiments are at a range of pA and nA, specialized amplifiers (operating amplifier) are used for high-resolution current recordings (The Axon Guide).

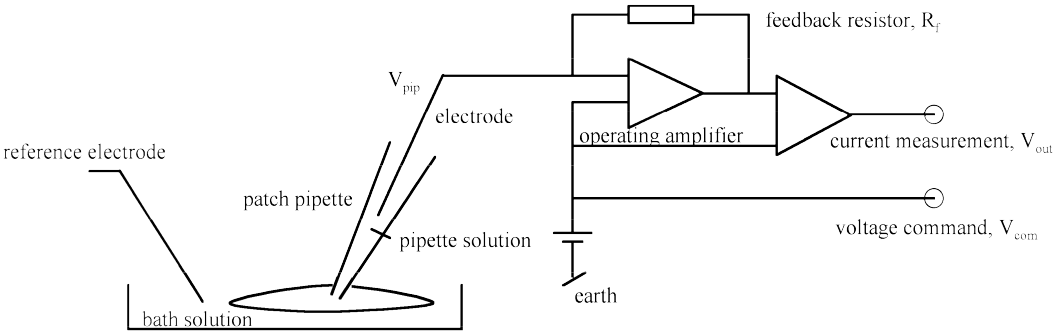

Figure 2.6.3:2. Simplified circuit of a patch clamp amplifier:
R_f: Feedback-resistance, V_{com},: voltage command, V_{pip},: Pipette-potential, V_{out},: Exit-potential proportionally to the current.

Due to a negative feedback mechanism, the operating amplifier sets the pipette voltage, *Vpip*, to the command potential, *Vcom* (Figure 2.6.3:2). In the simplified scheme in Figure 2.6.3:2, the membrane current, *I*, flows through the feedback resistor, *Rf*, which makes the difference between inputs of the second differential amplifier to be *I*Rf*. Thus, the output voltage, *Vout*, is proportional to the current to be measured.

Our patch clamp setup (Figure 2.6.3:3 left) is constructed in a Faraday cage for shielding to minimize noises. The apparatus further requires an inverted microscope (Nikon Diaphot, Nikon, Japan) for visualizing the cells and controlling the experiments, an automotive battery as a power source, a hydraulic three-directional movable micromanipulator (Narishige, Tokyo, Japan) for stable positioning of the electrodes, and a headstage preamplifier CV201A/CV203BU (Axon Instruments, Sunnyvale, CA, U.S.A.) which is connected on one side to the electrode and on the other side to the main amplifier through a shielded cable. The setup is installed on a vibration-cushioned table.

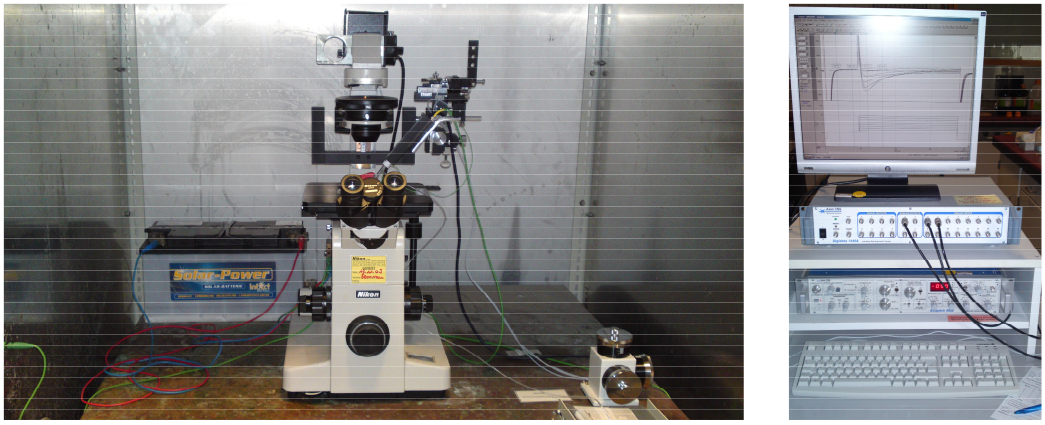

Figure 2.6.3:3. The patch clamp apparatus (Axopatch 200B) used for this study in the Institute of Pharmacology at the University of Cologne.

Data were sampled using Axopatch 200A/B amplifier (Axon Instruments) and were converted by analog-digital 1200/1440A Digitizer (Axon Instruments) data acquisition systems for further storage and analysis by the computer. The main amplifier and the analog-digital converter were positioned outside the Faraday cage (Figure 2.6.3:3 right).

2.6.4 Electrodes

Silver (Ag) wires coated with AgCl served as bath and measuring electrodes. The current was carried by chloride ions in the solution and converted into electrons, according to the following reversible reaction: $Cl^- + Ag \Leftrightarrow AgCl + e^-$. Coating of Ag wire was repeated whenever the AgCl was scraped from the wire. Cleaned wire by polishing was immersed into a 3 M KCl solution and connected to an anode of a direct current voltage source. A current of 1 mA was applied until the wire was uniformly blackened.

2.6.5 Patch pipettes

Borosilicate glass capillaries of 1 m length (OD/ID: 1.7/1.42 mm, Hilgenberg, Malsfeld, Germany) were cut up to 80 mm by a glass-cutter. A conventional pull technique P-97 Flaming/Brown Horizontal Pipette Puller (Sutter Instrument, Novato, CA, USA) was used to fabricate two symmetrical micropipettes with each pull. For an accurate patch clamping of myocytes, pipettes were prepared on the day of measurement and fire polished using Narishige Microforge. The pipette resistance was 1.8 – 3.2 MΩ for whole-cell recordings.

2.6.6 Whole-cell recordings

Conventional whole-cell patch clamp recordings were performed as described in Chapter 2.6.3 with cells maintained at room temperature. Cells (300 µl in solution F) were placed in a 35x10 mm disposable petri-dish, superfused with freshly prepared external bath solution (Table 2.6.6:1) of 3 ml final volume and left for 10 min to settle. A reference electrode connected to the preamplifier was placed into the bath solution. The pipette solution (Table 2.6.6:2) was prepared at the day of experiment and filtered via a 0.2 µm injection and aspiration filter and a 10 ml syringe. Glass pipettes were filled with pipette solution to 2/3 by two filling steps (tip and back filling) and bubbles were removed by gentle rapping. Pipettes were imposed over the measuring electrode and an overpressure was applied with a connected syringe. Before beginning the experiment, liquid junction potential were corrected and the pipette was placed next to cardiomyocyte. A gigaohm seal (resistance 2-5 GΩ) was formed by gentle suction. Stable gigaohm seal was crucial before penetrating the membrane for whole-cell calcium channel measurement. Further suction disrupts the small membrane patch building whole-cell configuration. If necessary, leak currents were removed by leak subtraction to study the current of interest.

Measured currents were low-pass filtered at 2 kHz (4-pole Bessel filter). Membrane capacitance was measured after holding at -80 mV for 15 ms by fast hyperpolarising ramp pulses from -80 to -85 mV over 25 ms. During the first 2.5 ms of the ramp, the current achieved its plateau level. The current plateau level was divided by the speed of the voltage ramp, yielding the cell membrane capacitance (in pF). To reduce the error, the means of 5 test pulses in series was calculated and the pulse repetition frequency was 3 sec. Alternatively, the membrane capacitance was automatically displayed after membrane rupture in the newer pClamp 10.2 software (Axon Instruments). Then, the cell membrane capacitive properties were compensated by the main amplifier.

For whole-cell calcium current measurement, cells were depolarized from the holding potential -80 mV to the first level -40 mV. The level was held for 50 ms in order to inactivate sodium channels. Then, test pulse voltages in 10 mV steps ranging from -40 to +50 mV were applied for 150 ms (Figure 2.6.6:1). Time between single pulses was 3 sec. To determine current-voltage curve, the peak current amplitude of each test pulse was measured by assessing the difference between the maximal current and the current at the end of the pulse of every trace. The peak current was divided by the respective cell capacitance to build the current density-voltage relationship.

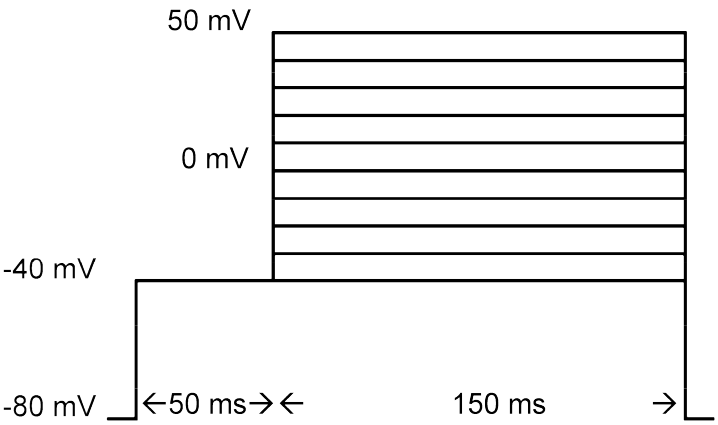

Figure 2.6.6:1. Cells were depolarized from holding potential -80 mV to a 50 ms long prepulse of -40 mV to inactivate contaminating currents. Calcium channel currents were obtained by test pulses of voltages ranging from -40 to +50 mV in 10 mV steps (pulse duration 150 ms).

The time-dependent inactivation was obtained from the declining phase of raw calcium current traces. The declining phase was fitted by a double-exponential function, yielding a fast time constant for the first quick inactivation phase and a slow time constant for the second plateau inactivation phase.

For further investigation of gating kinetics, a standard two-pulse protocol was used for voltage-dependent steady-state inactivation. For this protocol cells were hold at -45 mV. Cells were inactivated by conditional prepulses ranged from -70 to 0 mV in 5 mV steps and lasting for 150 ms. Thereafter, channels were tested for 100 ms at 0 mV (Figure 2.6.6:2). The stimulation frequency was 0.3 Hz. The steady-state inactivation curve, assessed by the peak currents obtained at 0 mV after variable conditional prepulses was normalized to the maximum peak current. The midpoint-voltage $V_{0.5}$ and the slope-factor of steady-state inactivation were determined by fitting a Boltzmann function to the data.

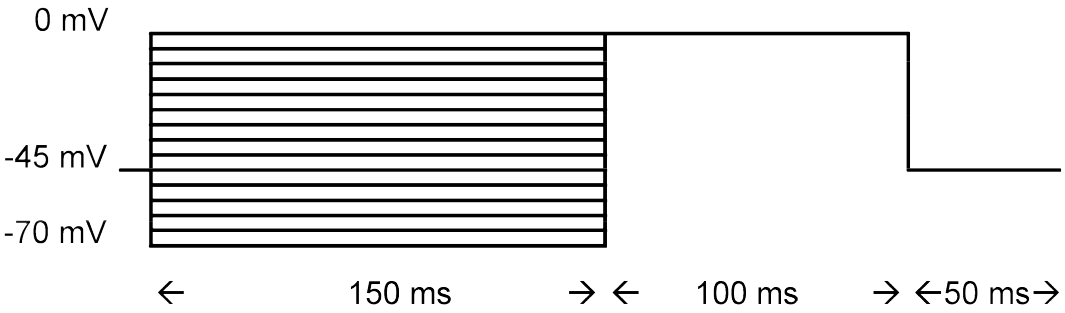

Figure 2.6.6:2. Voltage-dependent inactivation was determined by a standard two test pulse protocols. A prepulse from -45 mV to voltages varying from -70 to 0 mV was followed by a fixed test pulse at 0 mV (pulse duration 100 ms).

The recovery from inactivation was determined by a double-pulse protocol. An inactivating prepulse from -45 mV to 0 mV was applied and held for 100 ms. Varying interpulse intervals from 50 to 375 ms in 25 ms steps at -45 mV holding potential were followed by test pulses to 0 mV (Figure 2.6.6:3). The recovery from inactivation curve was determined by calculating the current at the test pulse and normalized it to the respective current amplitude measured

during the prepulse. Data were quantified by mono-exponential fits, yielding the recovery time constant τ.

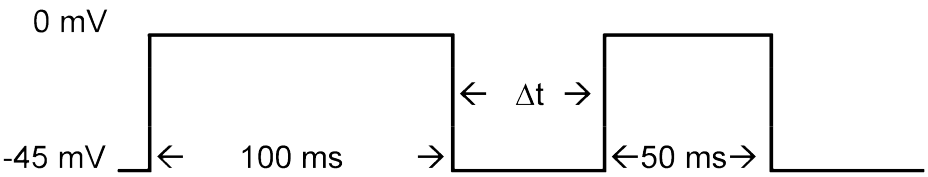

Figure 2.6.6:3 Recovery from inactivation was determined by a prepulse from -45 to 0 mV for 100 ms and varying recovery intervals.

Table 2.6.6:1. Physiological conditions were used for the bath solution.

Bath solution	**Final concentration**
NaCl	137 mM
CsCl	5.4 mM
$CaCl_2$	2.0 mM
$MgCl_2$	1.0 mM
Glucose	10 mM
HEPES	10 mM
NaOH (pH 7.4)	1.0 M

Table 2.6.6:2. Cesium ions were used as internal cations to block potassium channels. EGTA served as calcium chelator. ATP was added to prevent rapid calcium current rundown.

Pipette solution	**Final concentration**
CsCl	120 mM
Mg-ATP	4.0 mM
$MgCl_2$	1.0 mM
EGTA	10 mM
HEPES	5.0 mM
CsOH (pH 7.2)	50 wt. % in H_2O

2.7 Statistical analysis

Data are presented as mean values and statistical dispersion as standard error of the mean (SEM). Analysis of patch-clamp data was performed using pClamp software (CLAMPEX 6, CLAMPEX 10.2 and FETCHAN, Axon Instruments) and calcium channel kinetics were analyzed as described before [138]. GraphPad Prism 4 and MicrocalOrigin 6 were used for data analysis and statistics. A one-sample t-test was applied for normally distributed data. Differences between groups were demonstrated using one-way ANOVA followed by Dunnett's (comparing means to control) or Tukey's (comparing all possible pairs of means) post-test. Differences between treatments within one group were given by unpaired two-sample t-tests. Statistics were expressed using n=number of cardiomyocytes for electrophysiological experiments and n = number of animals for molecular biology experiments. P values < 0.05 were considered statistically significant.

3 RESULTS

3.1 Genotyping

All mice used for this study were genotyped successfully and pieces of their tail clips were stored at -20 °C for repeating the genotyping, if necessary. Figures 3.1:1 and 3.1:2 show an exemplary genotyping results for $G\alpha_{i2}$ and $G\alpha_{i3}$, respectively. β_2-AR genotypes are demonstrated in Figure 3.1:3.

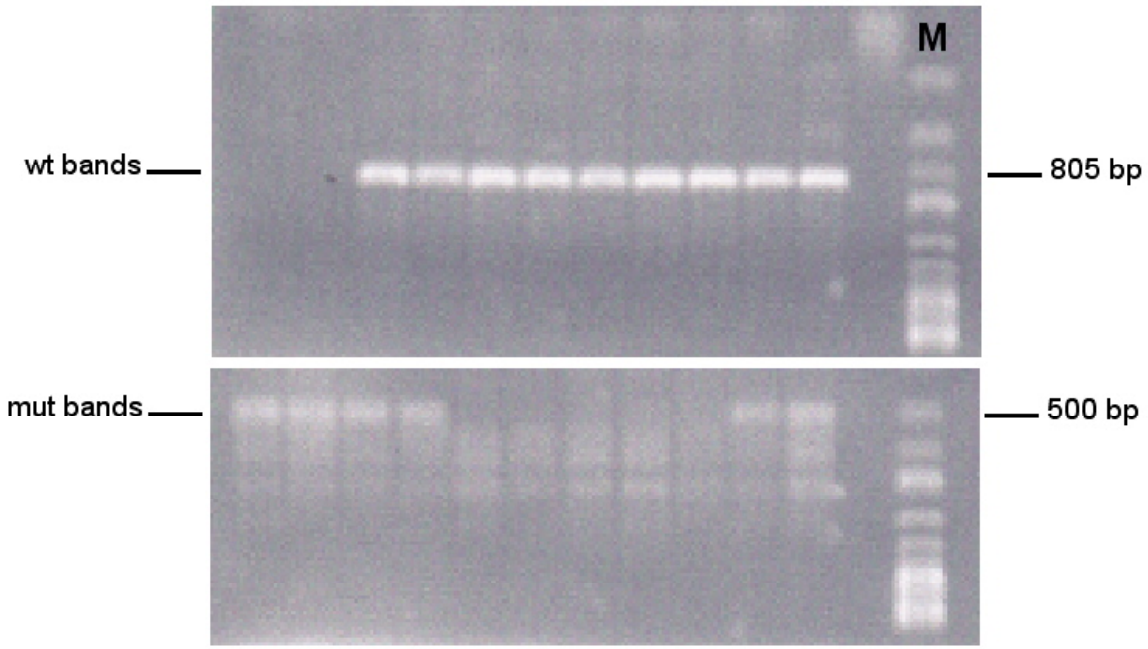

Figure 3.1:1. Electrophoretic separation on 1.5 % agarose gel and detection of $G\alpha_{i2}$ wt and mut bands by UV transilluminator. The DNA fragments were at 805 bp for the $G\alpha_{i2}$ wt and 500 bp for the $G\alpha_{i2}$ mut. M = Marker. The appearance of $G\alpha_{i2}$ wt bands at 805 bp and the lack of $G\alpha_{i2}$ mut bands at 500 bp meant $G\alpha_{i2}$ wt control mice ($G\alpha_{i2}$+/+). The appearance of both $G\alpha_{i2}$ bands demonstrated heterozygote mice ($G\alpha_{i2}$+/-). The lack of $G\alpha_{i2}$ wt bands at 805 bp and the appearance of $G\alpha_{i2}$ mut bands at 500 bp meant homozygote mice ($G\alpha_{i2}$-/-).

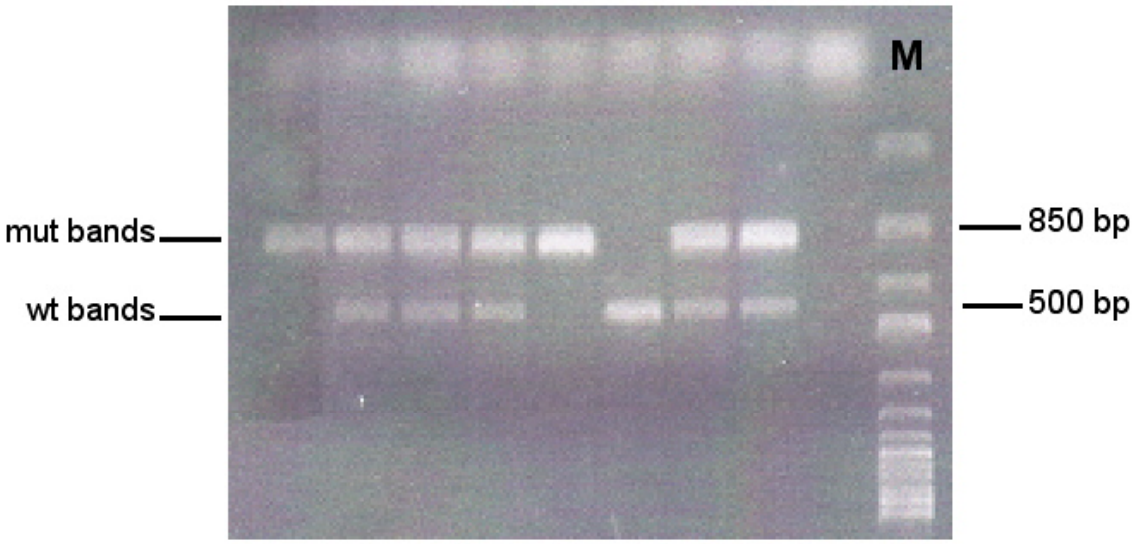

Figure 3.1:2. A 1.6 % agarose gel was used and the $G\alpha_{i3}$ wt band was detected at 500 bp and the $G\alpha_{i3}$ mutant at 850 bp. M = Marker. The appearance of $G\alpha_{i3}$ wt bands at 500 bp and the lack of $G\alpha_{i3}$ mut bands at 850 bp meant $G\alpha_{i3}$ wt control mice ($G\alpha_{i3}$+/+). The appearance of both $G\alpha_{i3}$ bands demonstrated heterozygote mice ($G\alpha_{i3}$+/-). The lack of $G\alpha_{i3}$ wt bands at 500 bp and the appearance of $G\alpha_{i3}$ mut bands at 850 bp meant homozygote mice ($G\alpha_{i3}$-/-).

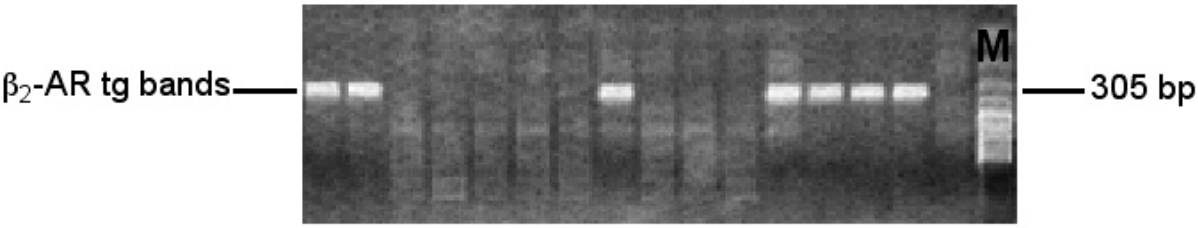

Figure 3.1:3. For β_2-AR tg band detection, a 2.0 % agarose gel was used and β_2-AR tg DNA fragments were visualized at 305 bp. M = Marker. Lack of bands at 305 bp revealed wt control mice (C57Bl6). An enzymatic restriction was induced after separation to differentiate between human and murine β_2-AR DNA fragments.

3.2 Animals

3.2.1 Offspring statistics

The following heredity scheme was determined for $G\alpha_{i2}$ breeding (Figure 3.2.1:1):

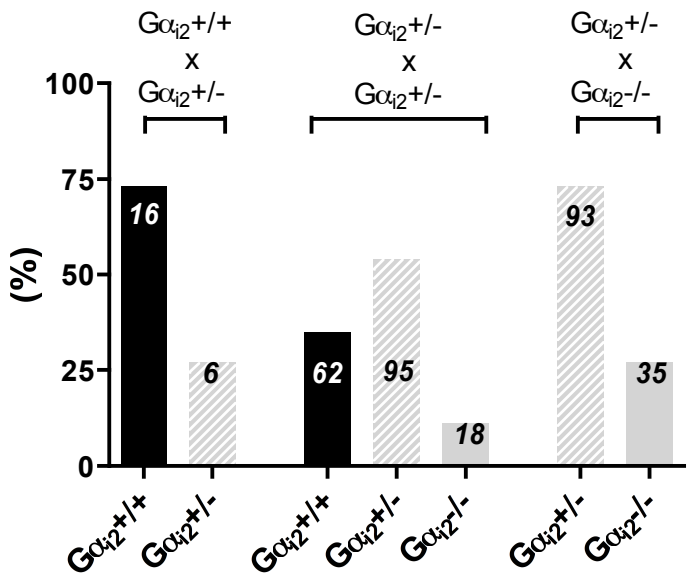

Figure 3.2.1:1. $G\alpha_{i2}$+/- mated with $G\alpha_{i2}$+/+ revealed 25 % $G\alpha_{i2}$+/- and 75 % $G\alpha_{i2}$+/+. The same behavior was demonstrated for $G\alpha_{i2}$-/- (25 %) x $G\alpha_{i2}$+/- (75 %) breeding. In $G\alpha_{i2}$+/- x $G\alpha_{i2}$+/- breeding, 54 % were heterozygous, 35 % wt and 11 % homozygous $G\alpha_{i2}$ mutants.

Compared to the illustrated theoretical Mendelian inheritance (Figure 2.3.4:1), $G\alpha_{i2}$-/- mice were born at less than expected frequency. These findings are consistent with data from previous publications [106, 112]. The distributions were in favor of the beneficial genotype in the breeding, indicating primarily loss of homozygote mutants. Thus, averages of offspring per litter were 4.0 for $G\alpha_{i2}$+/+ x $G\alpha_{i2}$+/-, 3.4 for $G\alpha_{i2}$+/- x $G\alpha_{i2}$+/- and 2.6 for $G\alpha_{i2}$+/- x $G\alpha_{i2}$-/-, underlying an offspring decrease subjected to $G\alpha_{i2}$ allelic deficiency.

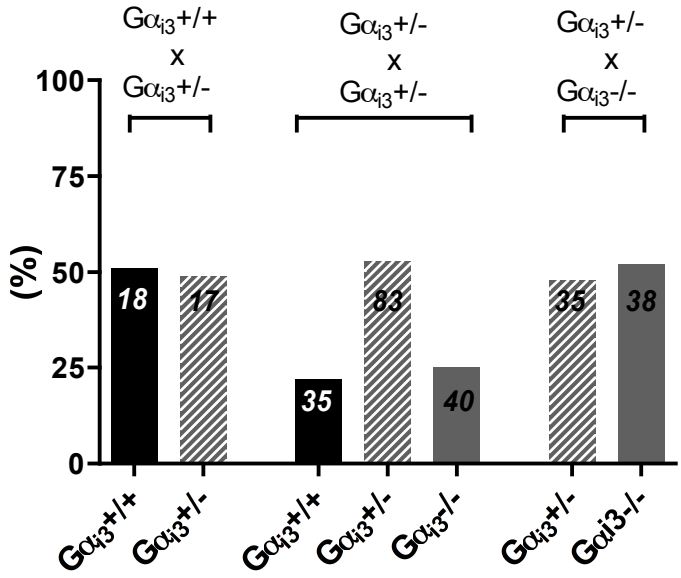

3.2.1:2. The genotypes of $G\alpha_{i3}$+/+ x $G\alpha_{i3}$+/- breeding were 51 % to 49 % and $G\alpha_{i3}$+/- x $G\alpha_{i3}$-/- breeding 48 % to 52 %. The heterozygote $G\alpha_{i3}$+/- x $G\alpha_{i3}$+/- combination yielded the expected genotypes and distribution for $G\alpha_{i3}$+/+ (22 %), $G\alpha_{i3}$+/- (53 %) and $G\alpha_{i3}$-/- (25 %).

In contrast to $G\alpha_{i2}$ breeding, $G\alpha_{i3}$ breeding tolerated the deficiency and offspring was born at the predicted Mendelian ratio (Figure 3.2.1:2). Moreover, only 6 $G\alpha_{i3}$+/- x $G\alpha_{i3}$-/- breeding were necessary for 38 $G\alpha_{i3}$-/- offspring, whereas 11 $G\alpha_{i2}$+/- x $G\alpha_{i2}$-/- breeding were required for 35 $G\alpha_{i2}$-/- offspring. However, the average of offspring per litter was lower for the deficient genotype (4.5 for $G\alpha_{i3}$+/+ x $G\alpha_{i3}$+/-, 4.7 for $G\alpha_{i3}$+/- x $G\alpha_{i3}$+/- and 3.7 for $G\alpha_{i3}$+/- x $G\alpha_{i3}$-/-).

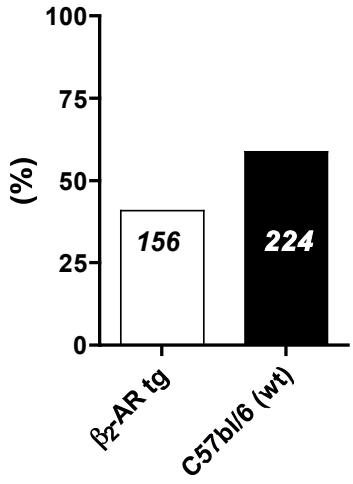

Figure 3.2.1:3. The genotypes of β_2-AR tg x C57Bl6 breeding were distributed to the amount of 41 % and 59 %, respectively.

In comparison to the theoretical Mendelain inheritance, the quantity of β_2-AR tg offspring was slightly decreased in C57Bl6 wt mice's favor.

3.2.2 Phenotype

The homozygous knockout of the $G\alpha_{i2}$ gene in mice led to a lower progeny (as shown above) and their survival time was significantly shorter than wt and $G\alpha_{i2}$+/- [109]. They lost body weight and grew more slowly compared to wt and $G\alpha_{i2}$+/- mice [106]. It was also shown that $G\alpha_{i2}$-/- mice overexpressing β_2-adrenoceptor developed a dilated heart and died within few days after birth [109].

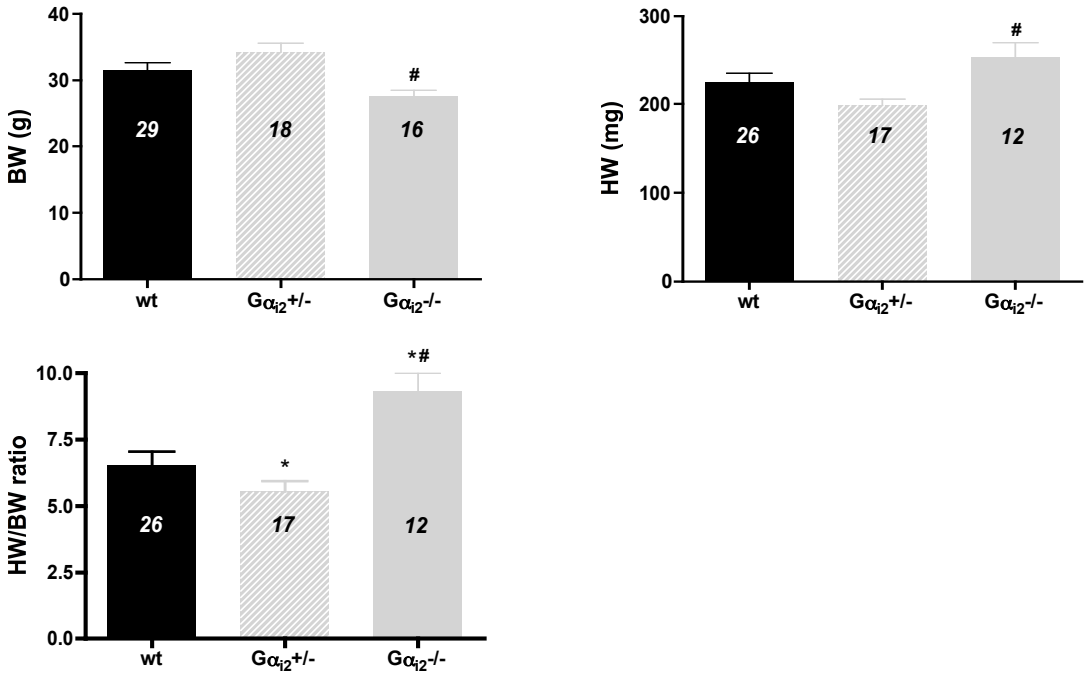

Figure 3.2.2:1. Body weight (BW) and heart weight (HW) of 3-9 months old mice were determined. BW of $G\alpha_{i2}$-/- mice on average was less (27.5±0.9 g) than of wt mice (31.5±1.2 g) and was significantly lower than of $G\alpha_{i2}$+/- mice (34.3±1.3 g). Different to the BW, the average HW was higher (254±15 mg vs. wt 225±10 mg and vs. $G\alpha_{i2}$+/- 199±6 mg), thus leading to an enhanced HW/BW ratio (9.3±0.7) compared to wt (6.5±0.4) and $G\alpha_{i2}$+/- (5.5±0.4) mice. $G\alpha_{i2}$+/- HW/BW ratio was significantly decreased in comparison to wt. *$p < 0.05$ vs. wt, #$p < 0.05$ vs. $G\alpha_{i2}$+/-.

In this work, the loss in body weight (BW) of $G\alpha_{i2}$-/- mice was confirmed. Additionally, an increased heart weight (HW) was observed (Figure 3.2.2:1). Of note, wet weight of hearts was determined, which were still aligned with their connective tissues for a quick measurement and to prevent heart injury during the isolation.

Table 3.2.2:1. Gender separation pointed out that the male $G\alpha_{i2}$-/- mice BW and HW were changed significantly compared to wt and $G\alpha_{i2}$+/- mice, unlike female $G\alpha_{i2}$-/- mice. *p < 0.05 vs. wt, #p < 0.05 vs. $G\alpha_{i2}$+/-.

	BW (g; n)	HW (mg; n)	HW/BW ratio (mg/g; n)
wt (male)	35.4 ± 1.2 (17)	245 ± 13 (15)	5.9 ± 0.4 (15)
$G\alpha_{i2}$+/- (male)	37.7 ± 1.3 (11)	211 ± 6 (11)	5.5 ± 0.3 (11)
$G\alpha_{i2}$-/- (male)	27.2 ± 1.1 (11; *#)	262 ± 18 (9; #)	9.9 ± 0.8 (9; *#)
wt (female)	26.0 ± 1.2 (12)	192 ± 11 (11)	7.6 ± 0.4 (11)
$G\alpha_{i2}$+/- (female)	29.1 ± 1.3 (7)	179 ± 7 (6)	6.5 ± 0.4 (6)
$G\alpha_{i2}$-/- (female)	28.2 ± 1.6 (5)	232 ± 27 (3)	7.6 ± 0.9 (3)

Separating the gender (Table 3.2.2:1), the observed weight differences appeared to be driven mainly by the male mice. However, the HW was increased in both male and female $G\alpha_{i2}$-/- mice, indicating maybe cardiac hypertrophy.

3.3 Cardiac $G\alpha_{i/o}$ isoforms

3.3.1 mRNA expression levels

The mRNA expression for $G\alpha_{i1}$, $G\alpha_{i2}$, $G\alpha_{i3}$, and $G\alpha_{o}$ isoforms in atrial and ventricular tissues of wt mice were determined.

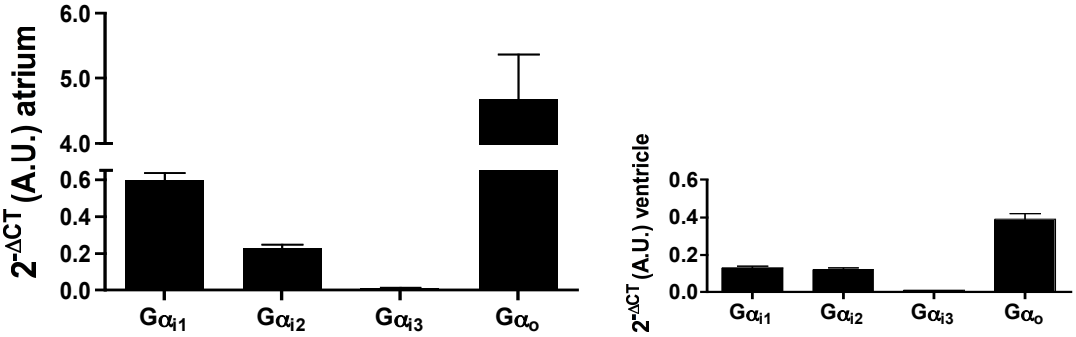

Figure 3.3.1:1. To analyze the cardiac relative expression of $G\alpha_{i/o}$ isoforms in wt (n = 3-4), $2^{-\Delta CT}$ was calculated. GAPDH was used as endogenous control. All $G\alpha_{i/o}$ isoforms were present but in different amounts and with nearly the same ratio in atrium or ventricle.

Transcripts for all $G\alpha_{i/o}$ isoforms were present at different mRNA expression levels in wt cardiac tissue. Overall expression levels were lower in the ventricle (Figure 3.3.1:1). $G\alpha_{i1}$ and $G\alpha_{i2}$ subunits are present to a similar extent in the ventricle, whereas $G\alpha_{i1}$ expression was higher in atrium than $G\alpha_{i2}$. $G\alpha_o$ was the dominant isoform in both tissues and $G\alpha_{i3}$ was the marginal existing isoform. $G\alpha_{i1}$ and $G\alpha_o$ subunits were likely transcribed in non-cardiomyocyte ventricular cells. Thus, to assess the effect of presence or absence of $G\alpha_I$ proteins mRNA expression levels were determined in atrium and ventricle from $G\alpha_{i2}$-/-, $G\alpha_{i3}$-/- and β_2-AR tg mice using wt mice as calibrator (wt expression level = set as 100 %; Figure 3.3.1:2).

As expected in $G\alpha_{i2}$-/- hearts $G\alpha_{i2}$ was absent. In $G\alpha_{i3}$-/- hearts $G\alpha_{i3}$ was barely present. Deletion of $G\alpha_{i2}$ enhanced the mRNA level of $G\alpha_{i3}$ in cardiac tissues, and vice versa. In β_2-AR tg cardiac tissue, $G\alpha_{i2}$ and $G\alpha_{i3}$ mRNA expression levels were upregulated. However, the enhancement was only significant in ventricular tissues, maybe due to the higher quantity. No significant changes in $G\alpha_o$ or $G\alpha_{i1}$ mRNA expression were detected which is in line with the assumption, that theses G proteins are not expressed in cardiomyocytes (Figure 3.3.1:2).

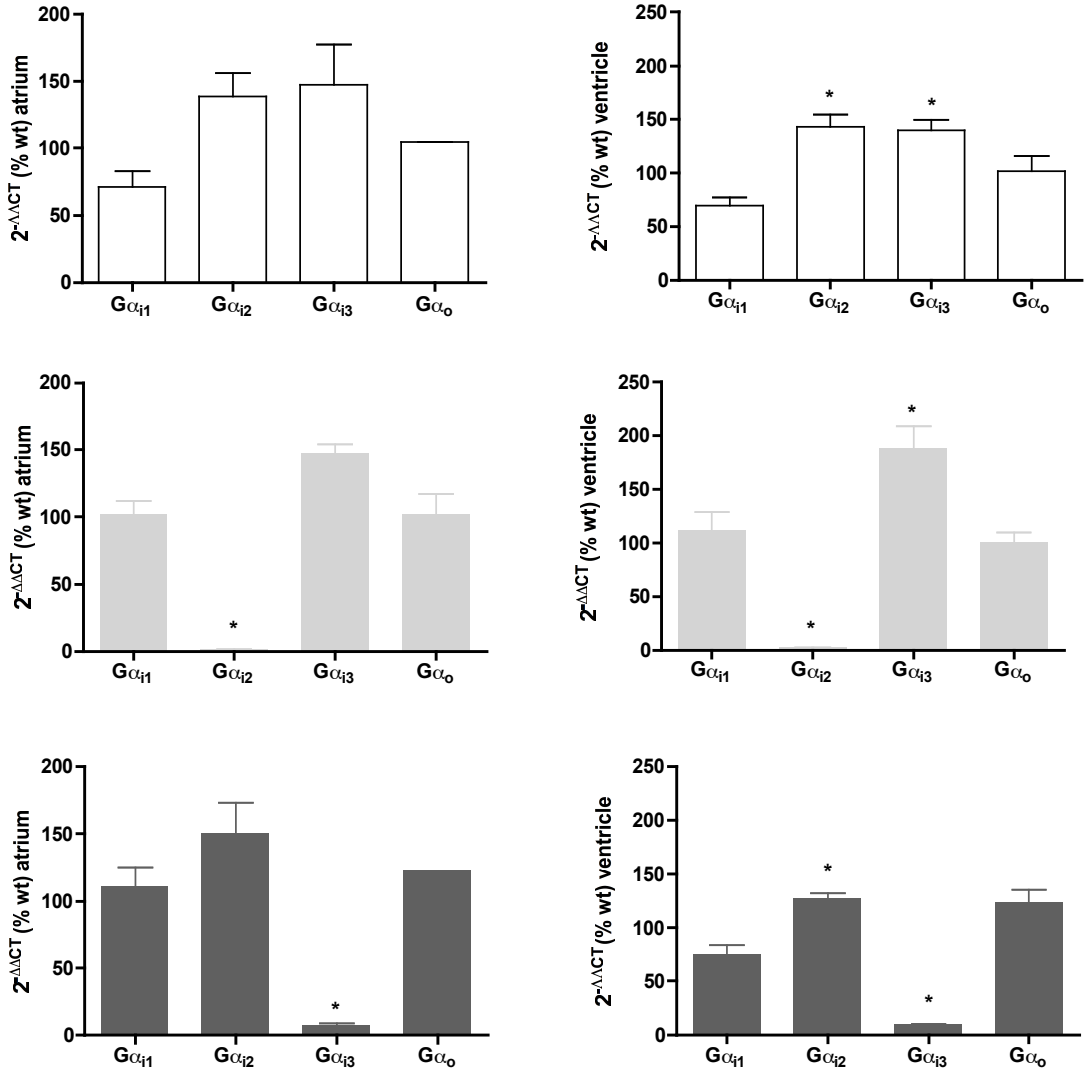

Figure 3.3.1:2. In $G\alpha_{i3}$-/- mice tissues (bottom), the relative mean expression ($2^{-\Delta\Delta CT}$) revealed an enhanced $G\alpha_{i2}$ mRNA level in atrial (left, 150±23 %, n = 1-2) and significantly in ventricular (right, 127±5 %, n = 4). $G\alpha_{i3}$ mRNA levels were upregulated to a higher extent in both atrium (right, 147±7 %, n = 2-3) and significantly in ventricle (left, 187±21 %, n = 3) of $G\alpha_{i2}$-/- mice (middle). In β_2-AR tg mice (top), both $G\alpha_{i2}$ and $G\alpha_{i3}$ expression were increased in atrium (right, 138±18 % for $G\alpha_{i2}$, 147±30 % for $G\alpha_{i3}$, n = 2-3) and significantly in ventricle (left, 143±11 % for $G\alpha_{i2}$, 140±10 % for $G\alpha_{i3}$, n = 4). $G\alpha_{i1}$ levels were not affected in all cardiac tissues, similar to $G\alpha_o$. *p < 0.05 vs. wt.

3.3.2 $G\alpha_{i2}$ and $G\alpha_{i3}$ protein expression levels

The mRNA levels and their alteration match up with protein levels. Here, the extent is shown to which specific gene deletion of one $G\alpha_i$ isoform or chronic stimulation by β_2-AR

overexpression affects protein expression level of $G\alpha_i$ isoform by analyzing cell membrane preparations obtained from wt, $G\alpha_{i2}$-/-, $G\alpha_{i3}$-/- and β_2-AR tg mice ventricles (Figure 3.3.2:1).

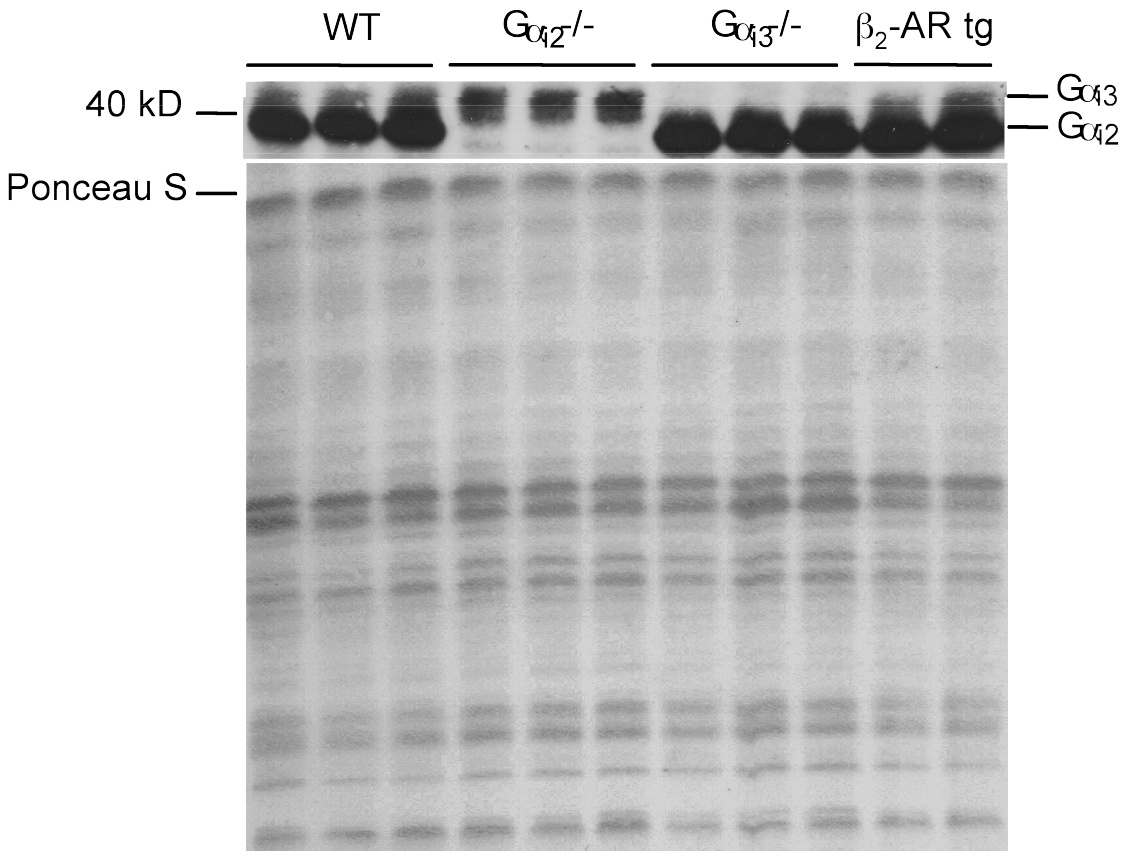

Figure 3.3.2:1. Membrane preparations of ventricular tissues of wt, $G\alpha_{i2}$-/-, $G\alpha_{i3}$-/- and β_2-AR tg mice were analyzed by immunoblotting with $G\alpha_{common}$ antibody. Equal loading was confirmed by a non-specific protein stain with Poncau S. Different film exposition times (here 30 min) were used to analyze $G\alpha_{i2}$ and $G\alpha_{i3}$ bands. In wt membrane tissue of the representative example, both bands are visual between 40 kD labeling. Both band intensities are strengthened in β_2-AR tg membrane tissue. The depletion of $G\alpha_{i2}$ (bottom band) induced upregulation of the protein levels of $G\alpha_{i3}$ (top band), and depletion of $G\alpha_{i3}$ enhanced $G\alpha_{i2}$ protein expression.

Wt mice expressed both $G\alpha_{i2}$ and $G\alpha_{i3}$ subunits, with $G\alpha_{i2}$ protein being the predominant isoform, in line with previous studies (e.g. [110]) and similar to β_2-AR tg mice. Mouse lacking the predominant isoform $G\alpha_{i2,}$ the cardiac $G\alpha_{i3}$ was increased, as expected [109, 112]. In hearts from $G\alpha_{i3}$-/- mice, only $G\alpha_{i2}$ was detectable.

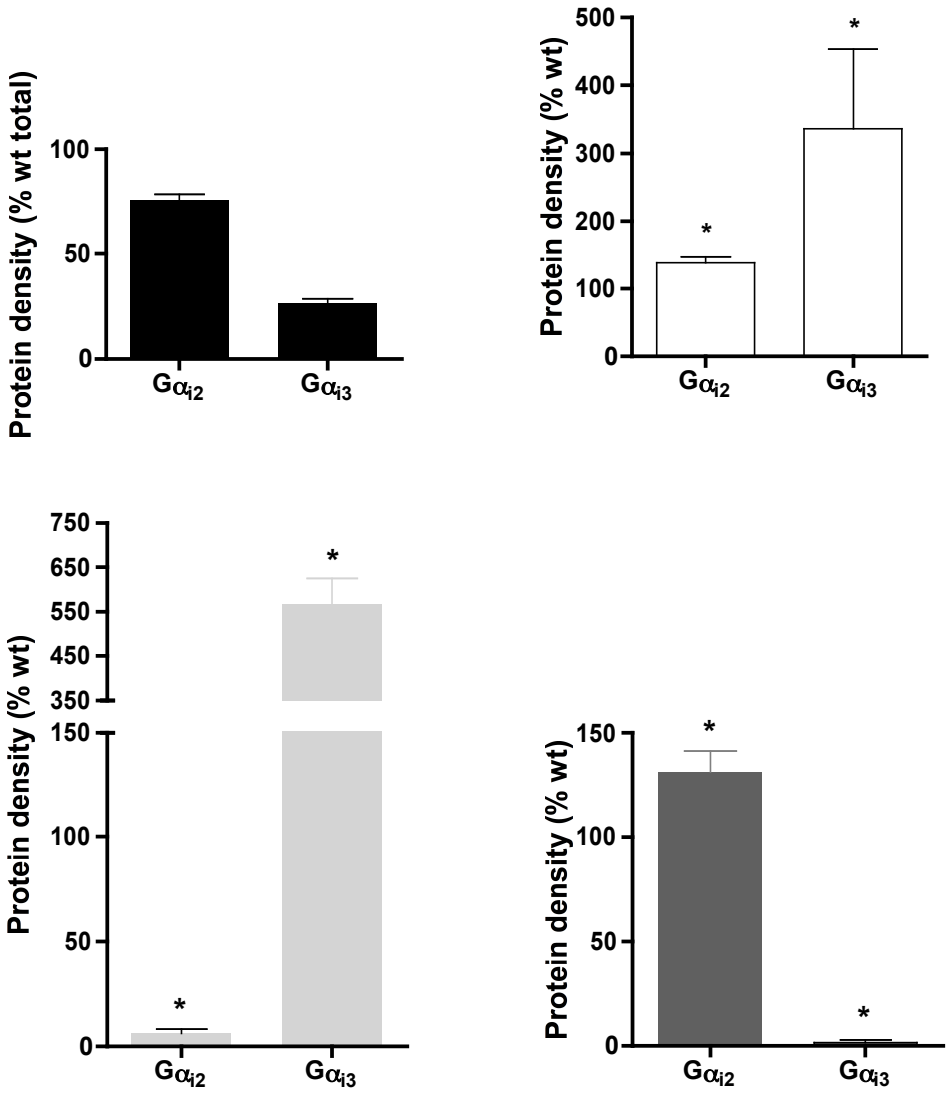

Figure 3.3.2:2. Statistical analysis of relative expression data from immunoblots show the approximate relation between $G\alpha_{i2}$ (76±3 %, n = 8) and $G\alpha_{i3}$ (26±2 %, n = 8) protein in wt cardiomyocytes (top left diagram) based on the combined total amount (100 %). Compared to each $G\alpha_i$ wt control (set as 100 %), both $G\alpha_{i2}$ (138±9 %, n = 8) and $G\alpha_{i3}$ (336±117 %, n = 8) protein expressions are significantly upregulated in β_2-AR tg mice (top right), $G\alpha_{i2}$ is significantly enhanced in ventricles obtained from $G\alpha_{i3}$-/- mice (bottom right, 131±10 %, n = 8), and $G\alpha_{i3}$ is markedly upregulated upon $G\alpha_{i2}$ deficiency (bottom left, 567±59 %, n = 8). *$p < 0.05$ vs. wt

Summarized membrane protein expression data (Figure 3.3.2:2) reveal an induced upregulation of the steady-state protein levels of $G\alpha_{i2}$ and $G\alpha_{i3}$ in β_2-AR tg mice. $G\alpha_{i3}$ protein expression level is enhanced in $G\alpha_{i2}$-/- ventricular tissue, and vice versa.

3.3.3 Specificity of the detected $G\alpha_{i2}$ and $G\alpha_{i3}$ protein bands

To confirm $G\alpha_{i2}$ and $G\alpha_{i3}$ protein bands specificity in cardiac membranes of $G\alpha_{i2}$-/-, $G\alpha_{i3}$-/-, β_2-AR tg and wt mice, modification of G_i proteins by ADP ribosylation was investigated.

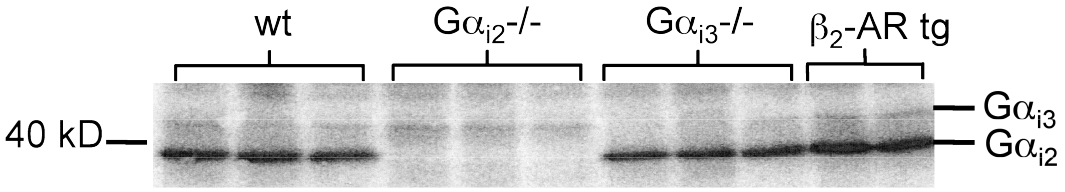

Figure 3.3.3:1. Representative autoradiograph clearly shows the presence and extent of $G\alpha_{i2}$ and $G\alpha_{i3}$ protein at 40 kD labeling in analyzed mouse models. Ponceau S was used as loading control.

Subjected ventricle tissues to PTX-catalyzed ADP-ribosylation in the presence of [^{32}P]NAD^+ revealed detected band specificity and different band intensity (Figure 3.3.3:1). In wt membrane tissue both $G\alpha_i$ isoforms were present with $G\alpha_{i2}$ being predominant. Both bands appeared intensified in cardiac tissue of β_2-AR tg mice and the $G\alpha_{i3}$ band intensity is increased in $G\alpha_{i2}$-/- mice, similar to immunoblots. In contrast to the immunoblot, the $G\alpha_{i2}$ bands seem to be unchanged in $G\alpha_{i3}$-/-.

3.3.4 Gβγ protein expression levels

To test signaling interference by the Gβγ protein-complex, expression levels of $G\beta_{1/2}$ isoforms in the same cardiac membrane tissues used for analyzing $G\alpha_{i2/3}$ proteins were also measured.

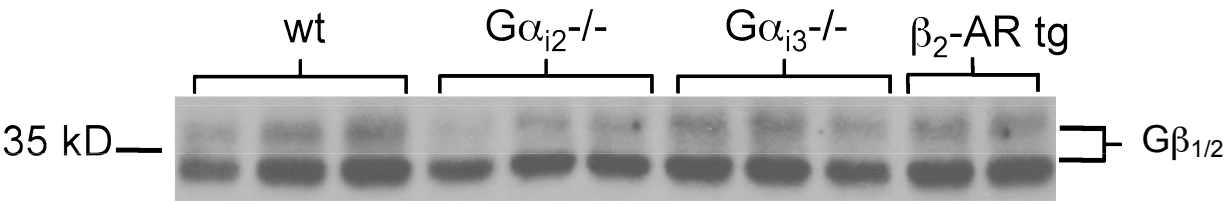

Figure 3.3.4.1. Gβγ protein complex from ventricular tissue of wt, $G\alpha_{i2}$-/-, $G\alpha_{i3}$-/- and β_2-AR tg mice detected by immunoblot with $G\beta_{common}$ antibody distinguished no major changes. The exposition time of the film was 10 min and equal loading was confirmed by staining with Ponceau S.

No changes of $G\beta_{1/2}$ isoforms were observed in examined wt, $G\alpha_{i3}$-/- and β_2-AR tg cardiac tissue preparations (Figure 3.3.4:1). Gβ expression levels in mice lacking the predominant $G\alpha_{i2}$ isoform in the heart were slightly reduced.

3.3 Cardiac L-type calcium currents of $G\alpha_{i2}$-/- and $G\alpha_{i3}$-/- mice

3.3.1 Basal whole-cell calcium current

To characterize cardiac L-type calcium channel activity, whole-cell currents in cardiomyocytes from wt, $G\alpha_{i2}$-/-, and $G\alpha_{i3}$-/- mice were measured according to the pulse protocol in Figure 2.6.6:1. Cell membrane capacitance was obtained as described in Chapter 2.6.6.

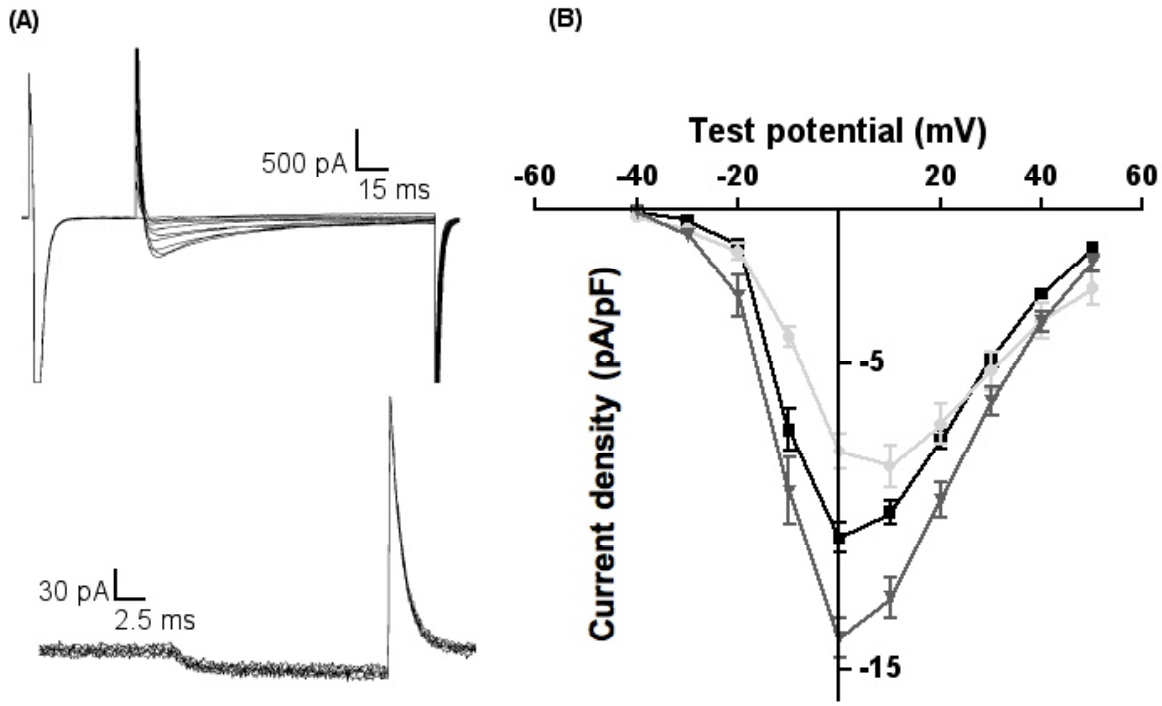

Figure 3.3.1:1. (A) Representative original L-type calcium current recording of a $G\alpha_{i2}$-/- cardiomyocyte (top) and its cell capacity recording (bottom). (B) L-type calcium current density-voltage relationship at 0 mV revealed a significant reduction in $G\alpha_{i2}$-/- (to -7.9±0.6 pA/pF, n = 11, $p < 0.05$) and a significant upregulation in $G\alpha_{i3}$-/- (to -14.0±0.6 pA/pF, [x] n = 15, $p < 0.05$) compared to wt control (-10.7±0.5 pA/pF, n = 22, [x] n = 14).

The mean cell capacity was 129±6.5 pF (n = 22) for wt, 136±13.1 pF (n = 11) for $G\alpha_{i2}$-/- and 126±7.6 pF ([x] n = 15) for $G\alpha_{i3}$-/- with no significant differences. However, current density-voltage diagrams of summarized data from currents recorded at different potentials showed changes in L-type calcium channel activity of $G\alpha_{i2}$-/- and $G\alpha_{i3}$-/- (Figure 3.3.1:1 B). The basal calcium current density at 0 mV in $G\alpha_{i2}$-/- cardiomyocytes was decreased about 25 %, whereas current density in cardiomyocytes from $G\alpha_{i3}$-/- mice was increased about 35 % as compared to wt mice. In addition, there was a slight rightward shift of peak current

[x] Unpublished data (Sonja Kaestner dissertation)

density in $G\alpha_{i2}$-/- mice. Thus, the alterations were distinct and contrasting at test potentials -10, 0 and +10 mV, the peak activity area of high voltage gated L-type calcium channel.

3.3.2 Time- and voltage-dependent inactivation

To test whether inactivation kinetics account for the differences, time- and voltage-dependent inactivation of the examined cardiomyocytes were analyzed.

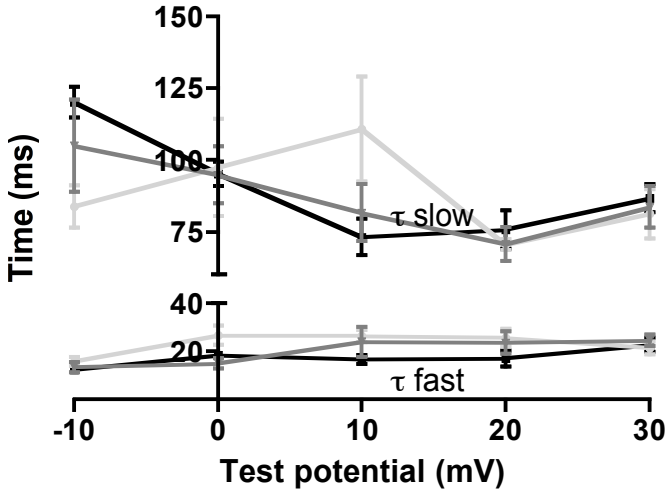

Figure 3.3.2:1. Time-dependent inactivation observed from the decay of raw current traces were at 0 mV wt = 18.4±1.0 ms [x], $G\alpha_{i2}$-/- = 26.9±4.0 ms and $G\alpha_{i3}$-/- = 15.1±2.1 ms [x] for τ_{fast} and wt = 95.3±4.2 ms [x], $G\alpha_{i2}$-/- = 97.5±17 ms and $G\alpha_{i3}$-/- = 94.9±9.9 ms [x] for τ_{slow} (n = 9-13).

Comparison of characteristics of fast and slow inactivation time constants revealed no major changes between $G\alpha_{i2}$-/-, $G\alpha_{i3}$-/- and wt mice (Figure 3.3.2:1). Hence, they are not responsible for the basal current density differences observed in 3.3.1.

[x] Unpublished data (dissertation Sonja Kaestner)

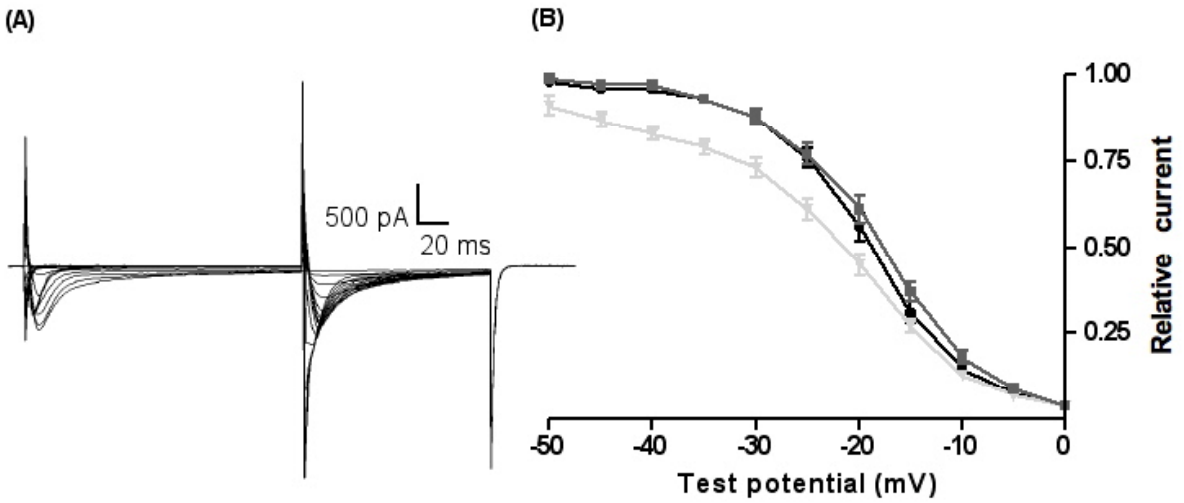

Figure 3.3.2:2. (A) A representative original trace of voltage-dependent L-type calcium channel inactivation of a $G\alpha_{i2}$-/- cardiomyocyte. Of note, sodium currents are not (fully) inactivated at very low voltage prepulses. (B) The steady-state inactivation curve analyzed by Boltzmann function showed a half-maximal response of -19.1±0.7 mV for wt cells (n = 18, [x] n = 10), -23.4±1.0 mV for $G\alpha_{i2}$-/- (n = 11) and -18.2±0.9 mV for $G\alpha_{i3}$-/- ([x] n=13).

Voltage-dependent inactivation was analyzed following the two-pulse protocol illustrated in Figure 2.6.6:2. Different to time-dependent inactivation, voltage-dependent inactivation was altered. The mean steady-state inactivation of the channel was significantly shifted towards hyperpolarized potentials in $G\alpha_{i2}$-/- with an increased slope-factor of 8.7±0.6 mV compared to $G\alpha_{i3}$-/- (slope-factor 5.4±0.2 mV, [x]) and wt (slope-factor 5.2±0.2 mV) cardiomyocytes. Voltage-dependent inactivation shift in $G\alpha_{i2}$-/- cardiomyocytes may explain the calcium current reduction shown in 3.3.1.

[x] Unpublished data (dissertation Sonja Kaestner)

3.3.3 Recovery from inactivation

To further characterize inactivation properties, recovery from inactivation was determined by a double-pulse protocol described in Figure 2.6.6:3.

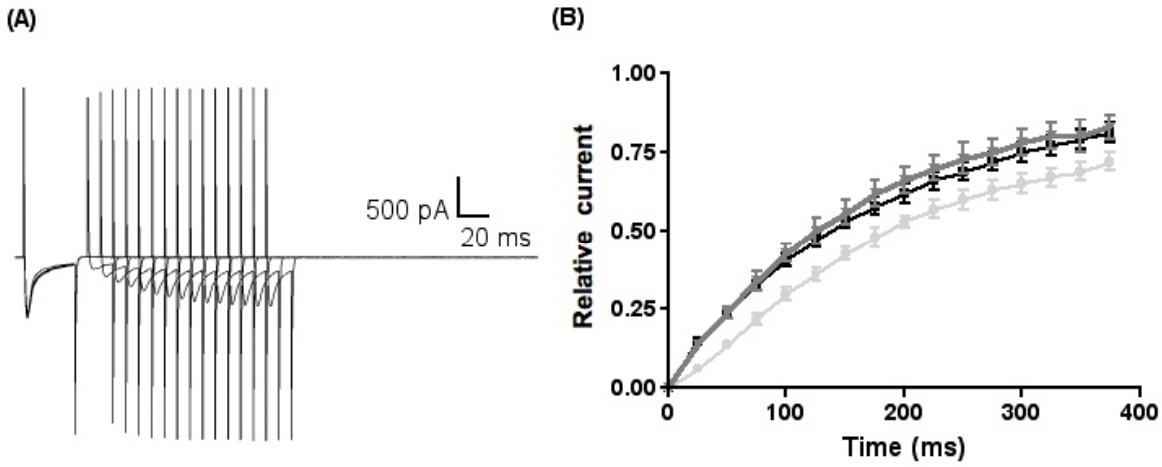

Figure 3.3.3:1. (A) A representative original trace of L-type calcium channel recovery from inactivation in a $G\alpha_{i2}$-/- cardiomyocyte. (B) The time constant of recovery, analyzed by single exponential fits was significantly slowed in cardiomyocytes from $G\alpha_{i2}$-/- mice (287±21 ms, $n = 9$, $p < 0.05$) in comparison to wt animals (215±14 ms, $n = 16$, [x] $n = 8$). The recovery in cardiomyocytes from $G\alpha_{i3}$-/- was indistinguishable from wt mice (203±24 ms, [x] $n = 9$).

A deceleration of L-type calcium channel reactivation was found in $G\alpha_{i2}$-/- with a half time of 199±15 ms compared to $G\alpha_{i3}$-/- (half time 140±17 ms, [x]) and wt control (half time 150±9.8 ms) mice. Thus, the recovery from inactivation in $G\alpha_{i2}$-/- cardiomyocytes is time dependent, providing additional evidence for altered channel kinetic properties in $G\alpha_{i2}$-/- mice.

[x] Unpublished data (dissertation Sonja Kaestner)

3.3.4 Acute inactivation of remaining $G\alpha_i$ proteins by PTX incubation

Were the effects on calcium channel properties caused by the loss of one $G\alpha_i$ protein or by the compensatory upregulation of the other? Since double-deficient ($G\alpha_{i2}$-/- / $G\alpha_{i3}$-/-) mice are not viable [110], G_i proteins were acutely inactivated by PTX treatment in wt and $G\alpha_i$-deficient mice as described in Chapter 2.6.2.

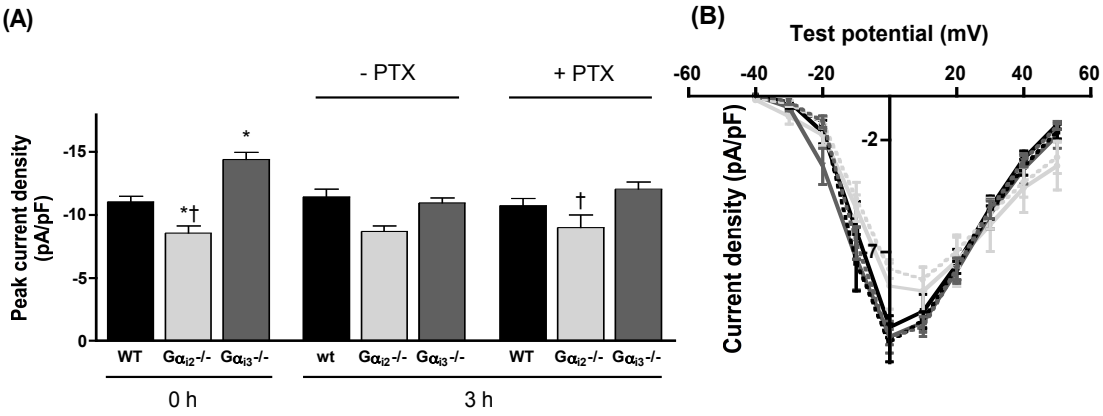

Figure 3.3.4:1. (A) The peak current density of wt control was -11.0±0.4 pA/pF (n = 22, ˣ n = 14) in freshly isolated cardiomyocytes, -11.4±0.6 pA/pF (ˣ n = 8) in incubated cells without PTX and -10.7±0.6 pA/pF (ˣ n = 9) when PTX was added for the incubation. Similar to wt, in $G\alpha_{i2}$-/- the peak current density was unaffected in the diverse pretreated cardiomyocytes (fresh cells: -8.6±0.6 pA/pF, n = 11; incubation without PTX: -8.7±0.5 pA/pF, n = 7; incubation with PTX: -9.0±1.0 pA/pF, n = 6). In $G\alpha_{i3}$-/- the peak current density was influenced already by incubation (fresh cells: -14.4±0.6 pA/pF, n = 15; incubation without PTX: -10.98±0.4 pA/pF, n = 9; incubation with PTX: -12.0±0.6 pA/pF, ˣ n = 10). (B) The current density at different test potentials revealed no changes within the genotypes when incubated cells without PTX (dashed line) were compared to incubated cells with PTX (solid line). *p < 0.05 vs. wt, †p < 0.05 vs. $G\alpha_{i3}$-/-.

ˣ Unpublished data (dissertation Sonja Kaestner)

Acute inactivation of G_i by PTX in wt control, $G\alpha_{i2}$-/- and $G\alpha_{i3}$-/- had no effect on L-type calcium channel current density compared to 3 h incubated cells without PTX (Figure 3.3.4:1 A&B). Therefore, the differences in current density among the genotypes remained the same. Of note, 3h incubation as such (without PTX) led to a decreased current density in $G\alpha_{i3}$-/- cardiomyocytes from -14.4±0.6 pA/pF in 0h freshly isolated cells to -11.0±0.4 pA/pF (Figure 3.3.4:1 A, ˣ). Thus, the significant current increase in $G\alpha_{i3}$-/- as compared to wt vanished after 3 h incubation.

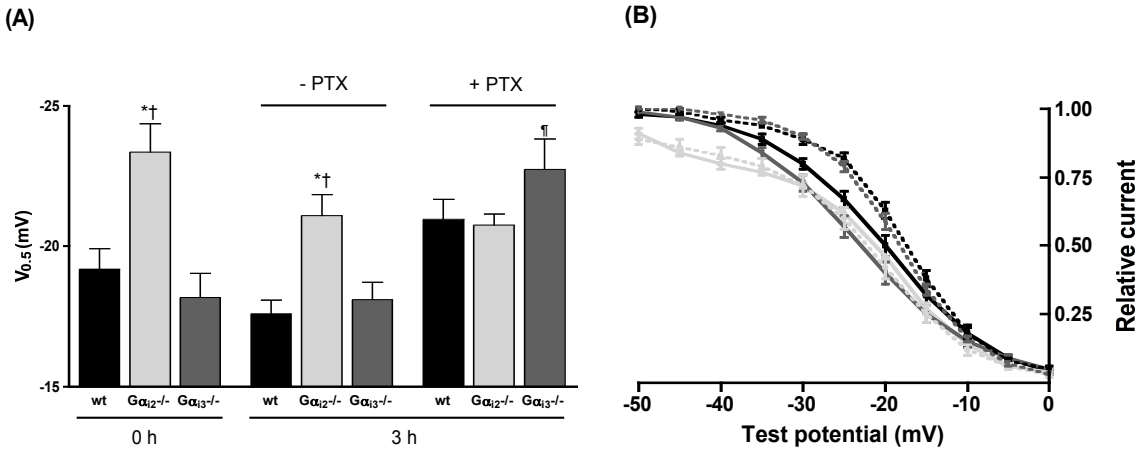

Figure 3.3.4:2. (A) The mean steady-state inactivation of L-type calcium channel in freshly isolated $G\alpha_{i2}$-/- cardiomyocytes was significantly shifted towards negative potentials (-23.4±21 mV, n = 9) compared to wt (-19.2±0.7 mV, n = 18, ˣ n = 10) and $G\alpha_{i3}$-/- (-18.2±0.9 mV, ˣ n = 13). Cell incubation for 3h at 37 °C as such did not affect the half-maximal voltage compared to 0 h cells ($G\alpha_{i2}$-/-: -21.1±0.8 mV, n = 6; wt: -17.6±0.5 mV, n = 7; $G\alpha_{i3}$-/-: -18.1±0.6 mV, n = 11, ˣ wt and $G\alpha_{i3}$-/-). PTX treatment impaired the steady-state inactivation in $G\alpha_{i3}$-/- cardiomyocytes to -22.7±1.1 mV (ˣ n = 11) compared to wt control (-21.0±0.7 mV, ˣ n = 10) and $G\alpha_{i2}$-/- (-20.8±0.4 mV, n = 7). (B) The voltage-dependent inactivation curve was deferred in $G\alpha_{i3}$-/- cardiomyocytes by adding PTX compared to incubated cells without PTX. *$p < 0.05$ vs. wt, †$p < 0.05$ vs. $G\alpha_{i3}$-/-, ¶$p<0.05$ vs. no PTX.

ˣ Unpublished data (dissertation Sonja Kaestner)

In $G\alpha_{i2}$-/- cells and wt control the half-maximal response of steady-state inactivation was resistant to time duration and treatment with PTX. Acute inactivation of $G\alpha_{i2}$ by PTX treatment in $G\alpha_{i3}$-/- myocytes induced a shift of $V_{0.5}$ to the left, similar to chronic $G\alpha_{i2}$ inactivation in $G\alpha_{i2}$-/- mouse models. Similar effects were observed concerning the recovery from inactivation (Figure 3.3.4:3).

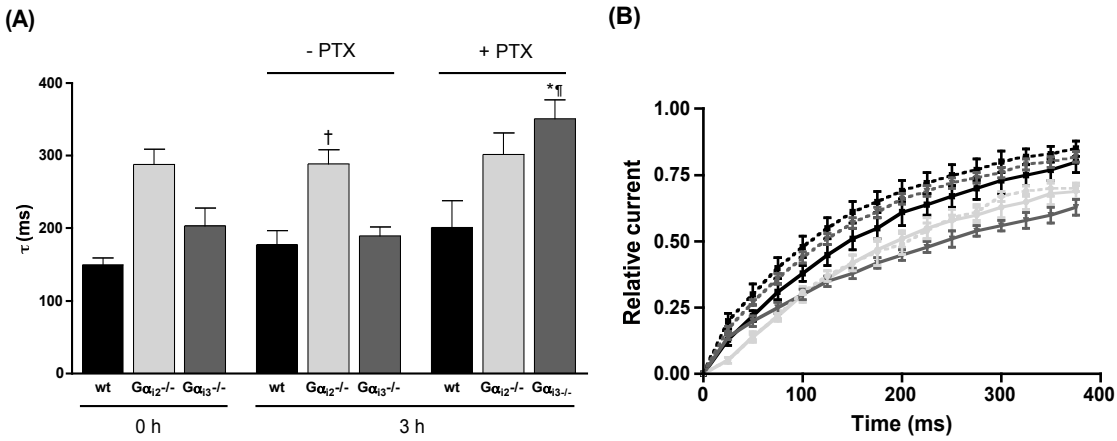

Figure 3.3.4:3. (A) The time constant of recovery of L-type calcium channel in freshly isolated $G\alpha_{i2}$-/- cardiomyocytes was slowed (287±21 ms, n = 9) compared to wt (150±9.8 ms, n = 16, ˣ n = 8) and $G\alpha_{i3}$-/- (203±24 ms, ˣ n = 9). Cells incubated for 3 h without PTX did not show any differences in recovery to 0 h cells ($G\alpha_{i2}$-/-: 288±19 ms, n = 3; wt: 177±19 ms, n = 9; $G\alpha_{i3}$-/-: 190±12 ms, n = 11, ˣ wt and $G\alpha_{i3}$-/-). PTX treatment ablated the recovery from inactivation in $G\alpha_{i3}$-/- cardiomyocytes to 350±27 ms (ˣ n = 8) compared to wt control (201±37 ms, ˣ n = 5) and $G\alpha_{i2}$-/- (301±30 ms, n = 6). (B) The recovery from inactivation curve was retarded in $G\alpha_{i3}$-/- cardiomyocytes by adding PTX compared to incubated cells without PTX and wt control. *$p < 0.05$ vs. wt, †$p < 0.05$ vs. $G\alpha_{i3}$-/-, ¶$p < 0.05$ vs. no PTX.

ˣ Unpublished data (dissertation Sonja Kaestner)

PTX treatment led to a decelerated time of recovery in $G\alpha_{i3}$-/- cells, even beyond $G\alpha_{i2}$-/-. Thus, PTX mitigates the differences between $G\alpha_{i2}$-/- and $G\alpha_{i3}$-/- by altering channel regulation in cells from $G\alpha_{i3}$-/- but not from $G\alpha_{i2}$-/- mice. Calcium channel function was not altered in wt control mice treated with PTX.

3.4 Cardiac L-type calcium channel subunits

3.4.1 mRNA expression levels

mRNA levels of the $Ca_v\alpha_1$ subunit were determined in atrium and ventricle, and of the $Ca_v\beta$ subunits $Ca_v\beta_1$, $Ca_v\beta_2$ and $Ca_v\beta_3$ in ventricles from wt, $G\alpha_{i2}$-/-, $G\alpha_{i3}$-/- and β_2-AR tg mice.

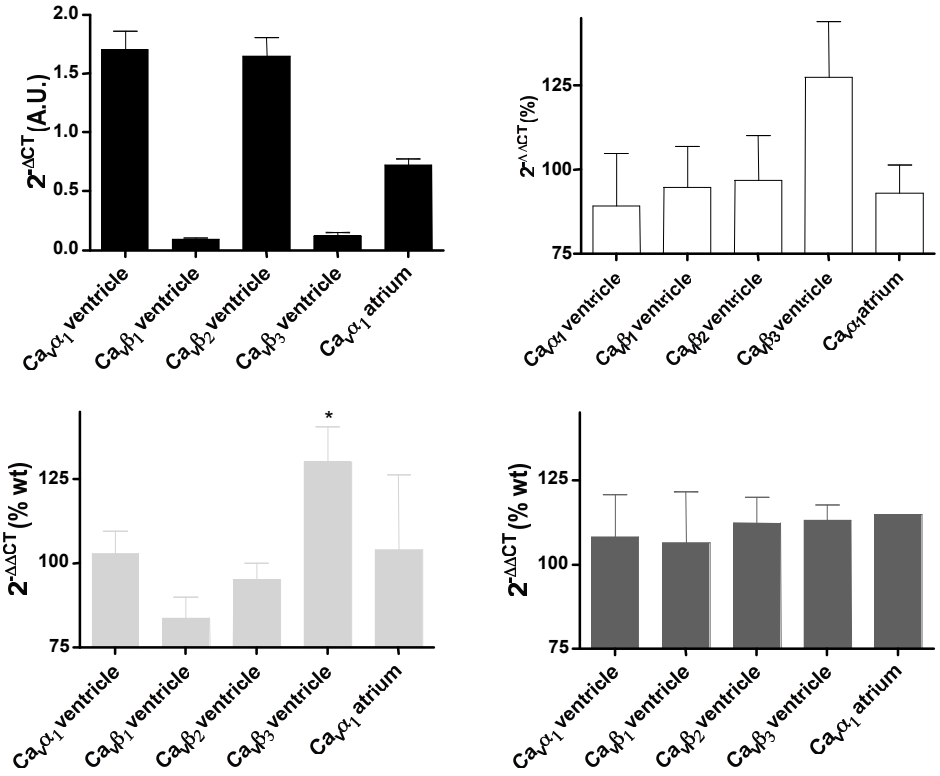

Figure 3.4.1:1. Relative mRNA calcium channel subunits expression calculated as $2^{-\Delta CT}$ in wt cells are shown (GAPDH = endogenous control), presenting dominance of $Ca_v\alpha_1$ and $Ca_v\beta_2$ in the heart (n=4; top left). Using wt mice as 100 % expression level, in β_2-AR tg cardiac tissue (top right) ventricle $Ca_v\beta_3$ mRNA level was slightly accelerated (128±17 %, n = 4). In $G\alpha_{i2}$-/- mice (bottom left) $Ca_v\beta_1$ mRNA level is decreased (84±6 %, n = 3), whereas $Ca_v\beta_3$ mRNA level is increased (130±11 %, n = 4). No substantial mRNA channel subunit alterations were observed in $G\alpha_{i3}$-/- cardiomyocytes (n = 4; bottom right). *$p < 0.05$ vs. wt.

The pore forming $Ca_v\alpha_1$ subunit mRNA level was unchanged both in atrium and in ventricle of all analyzed mouse models compared to wt control (Figure 3.4.1:1). The $Ca_v\beta$ subunit mRNA expression profile in ventricles from $G\alpha_{i2}$-/- mice is different from the wt expression profile. $Ca_v\beta_1$ subunit is reduced, $Ca_v\beta_2$ is not altered, and $Ca_v\beta_3$ is significantly enhanced. In $G\alpha_{i3}$-/- animals, the $Ca_v\beta$ subunit mRNA expressions in ventricular tissues are not affected in all genotypes.

3.4.2 $Ca_v\alpha_1$ protein expression level

The membrane protein expression levels of the pore forming $Ca_v\alpha_1$ subunit in wt, $G\alpha_{i2}$-/- and $G\alpha_{i3}$-/- ventricles exhibited no changes (Figure 3.4.1:1).

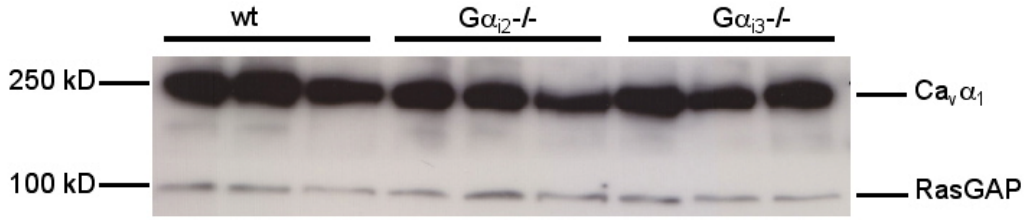

Figure 3.4.2:1. Representative example of $Ca_v\alpha_1$ protein expression in murine ventricular tissue detected at 250 kD from wt, $G\alpha_{i2}$-/- and $G\alpha_{i3}$-/- mice. RasGAP at 100 kD was used as a loading control.

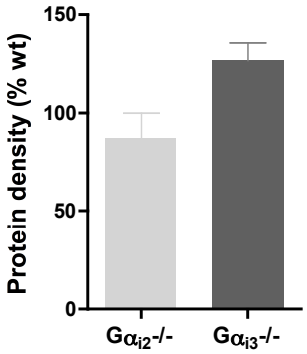

Figure 3.4.2:2. Summarized membrane protein expression data of $G\alpha_{i2}$-/- and $G\alpha_{i3}$-/- in comparison to wt control revealed 87.1±13 % and 126±9.0 % (n = 3), respectively.

Quantification of $Ca_v\alpha_1$ protein levels showed no significant change in ventricles from $G\alpha_{i2}$-/- and $G\alpha_{i3}$-/- compared to wt (Figure 3.4.2:2). These findings are in line with mRNA expression data shown in Figure 3.4.1:1.

3.5 G_i posttranslational effects induced by carbachol stimulation

3.5.1 Akt and Gsk3β phosphorylation levels

To determine posttranslational effects, functional significance of $G\alpha_i$-mediated phosphorylation of Akt and its downstream effector GSK-3α/β was examined.

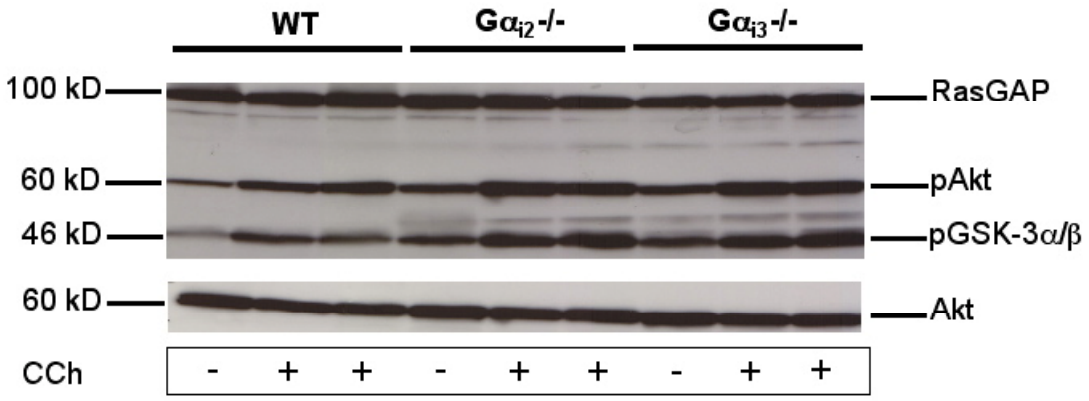

Figure 3.5.1:1 Representative western blot of cardiac tissues of animals treated either with saline or CCh. Akt phosphorylation as an event of $G\alpha_i$ signaling, and its downstream GSK-3α/β phosphorylation were higher in all genotypes tested by CCh compared to saline injection. Total amount of Akt of the same blot was controlled and unchanged. Akt and RasGAP were used as loading controls.

Akt phosphorylation and the phosphorylation of its downstream effector GSK-3α/β were increased in CCh stimulated cardiac tissue from wt, $G\alpha_{i2}$-/- and $G\alpha_{i3}$-/- mice compared to each respective basal phosphorylation by saline treatment (Figure 3.5.1:1). However, basal Akt and GSK-3α/β phosphorylation in $G\alpha_{i2}$-/- and $G\alpha_{i3}$-/- cardiac tissues were enhanced, similar to their appearance after CCh stimulation compared to wt control.

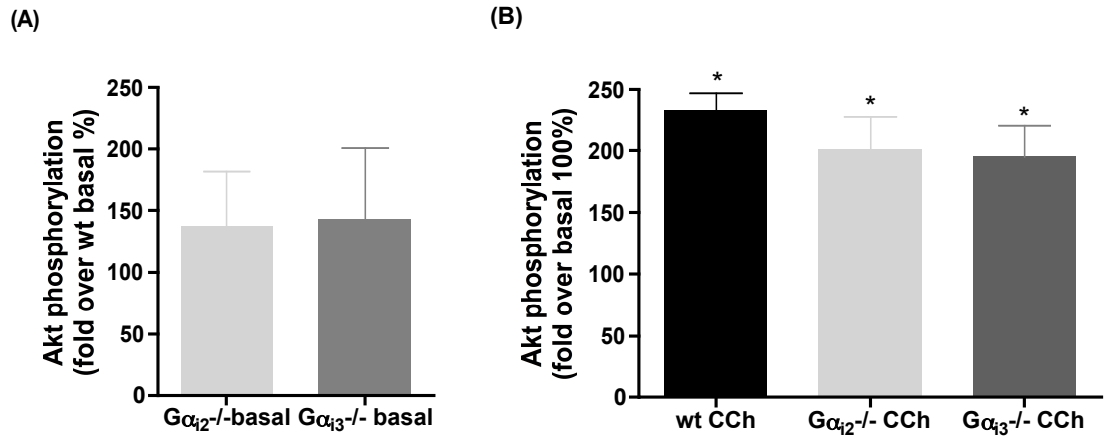

Figure 3.5.1:2. (A) Basal Akt phosphorylation in wt cardiac tissue was set as 100 %. In $G\alpha_{i2}$-/- and $G\alpha_{i3}$-/- the basal phosphorylation levels were slightly increased up to 138±44 % and 143±58 % (each n = 3), respectively. (B) The phosphorylation in stimulated cardiac tissues with CCh were 233±14 % in wt, 201±27 % in $G\alpha_{i2}$-/- and 195±25 % in $G\alpha_{i3}$-/- mice (each n = 3) referred to respective basal phosphorylation. *$p < 0.05$ vs. basal.

The basal increase of Akt phosphorylation in $G\alpha_{i2}$-/- and $G\alpha_{i3}$-/- cardiac tissue was not significant in comparison to wt basal phosphorylation (Figure 3.5.1:2 A). After CCh stimulation, Akt phosphorylation in all genotypes was significantly enhanced compared to respective basal phosphorylation (Figure 3.5.1:2 B). However, no differences in phosphorylation level could be observed between CCh stimulated wt, $G\alpha_{i2}$-/- and $G\alpha_{i3}$-/- mice. Of importance, the total amount of Akt was unchanged in all mice models.

3.5.2 ERK1/2 phosphorylation level

Next, $G\alpha_i$ involvement on ERK1/2 protein activation was investigated in cardiac tissue.

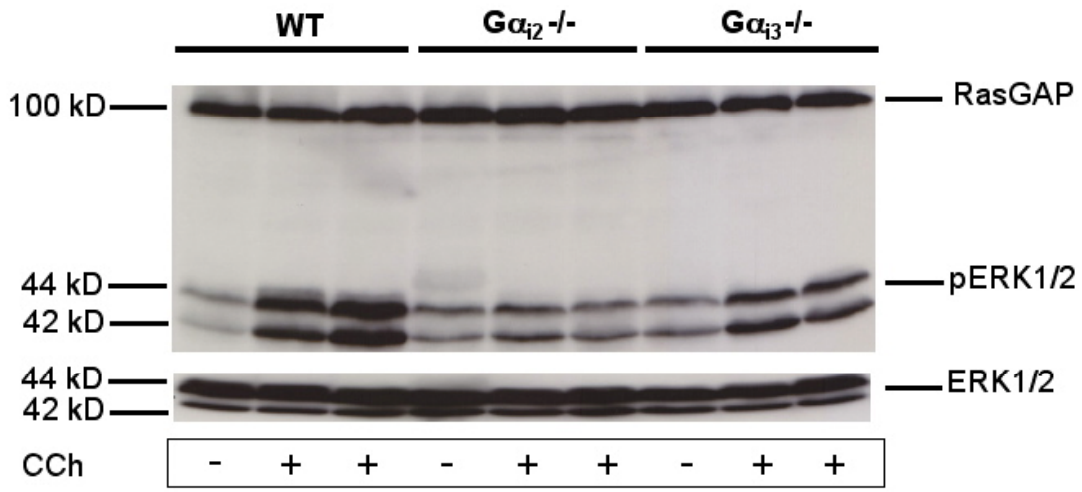

Figure 3.5.2:1. Representative western blot of cardiac tissues of animals treated either with saline or CCh. ERK1/2 phosphorylation as an event of $G\alpha_i$ signaling was enhanced in wt and $G\alpha_{i3}$-/- mice by CCh stimulation, whereas the phosphorylation in $G\alpha_{i2}$-/- cardiac tissue was unaltered compared to phosphorylation after saline injection. Total amount of ERK1/2 of the same blot was controlled and unchanged. ERK1/2 as well as RasGAP were used as loading controls.

The ERK1/2 phosphorylation was increased in CCh stimulated cardiac tissue from wt and $G\alpha_{i3}$-/- mice compared to saline treated wt and $G\alpha_{i3}$-/- mice. However, CCh stimulation did not induce ERK1/2 phosphorylation in $G\alpha_{i2}$-/- cardiac tissues (Figure 3.5.2:1).

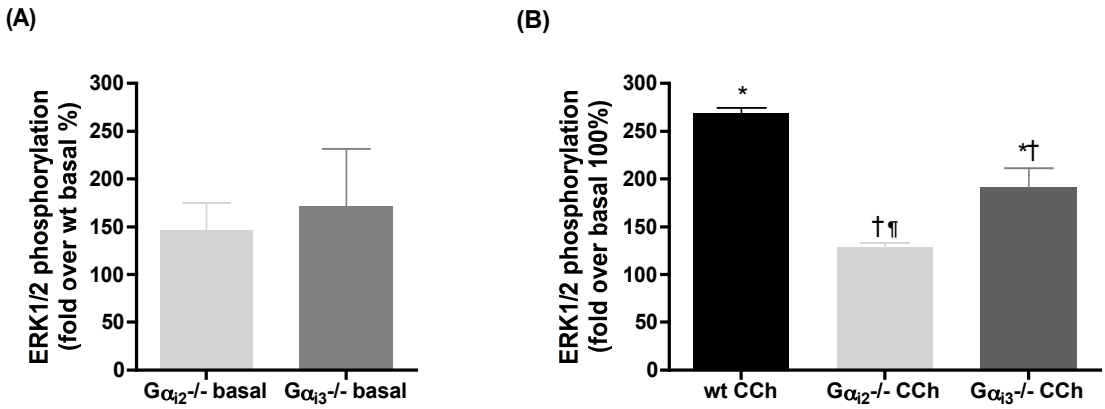

Figure 3.5.2:2. (A) In $G\alpha_{i2}$-/- and $G\alpha_{i3}$-/- cardiac tissues, the basal ERK1/2 phosphorylation levels were increased to 146±29 % and 171±60 % compared to wt basal phosphorylation (= 100 %), respectively (each = 3). (B) CCh tested mice revealed a significant increase of cardiac ERK1/2 phosphorylation in wt (269±6.1 %, n = 3) and in $G\alpha_{i3}$-/- (192±20 %, n = 3) compared to basal phosphorylation. In $G\alpha_{i2}$-/- tissues the phosphorylation was unchanged after CCh stimulation. Thus, the ERK1/2 phosphorylated amount in $G\alpha_{i2}$-/- (128±5.2 %, n = 3) mice was significantly lower than wt and $G\alpha_{i3}$-/-. *$p < 0.05$ vs. basal, †$p < 0.05$ vs. wt CCh, ¶$p < 0.05$ vs. $G\alpha_{i3}$-/- CCh.

$G\alpha_{i2}$-/- mice demonstrated a significant reduction of ERK1/2 phosphorylation in CCh-stimulated animals compared to wt and $G\alpha_{i3}$-/- cardiomyocytes (Figure 3.5.2:2). ERK1/2 phosphorylation was significantly enhanced in $G\alpha_{i3}$-/- cardiac cells after CCh stimulation compared to basal phosphorylation, but the relative increase appears to be lower compared to wt. However, total ERK1/2 expression in the heart was unchanged in all mice models and absolute ERK phosphorylation after CCh stimulation is similar in wt and $G\alpha_{i3}$-/-. These results demonstrate a specific $G\alpha_{i2}$-dependent ERK1/2 phosphorylation.

4 DISCUSSION

4.1 G_i structural and functional modification mediated by $G\alpha_{i2}$ deletion

Inhibitory G proteins play an important role in regulating and balancing cardiac functions. The two inhibitory G protein isoforms G_{i2} and G_{i3} are expressed in cardiac tissue with G_{i2} being the predominant isoform. $G\alpha_o$ was mainly described as a neuron-specific G protein [93, 139]. The data presented here underline these findings, since $G\alpha_o$ mRNA expression level is enhanced in atrium where the pacemaker tissue is located. $G\alpha_{i1}$ isoform was also present on mRNA level, but its exact function in the heart remains controversial. Jones and Reed [91] were able to detect most known G protein isoforms in myocardial tissue by Northern blotting except for $G\alpha_{i1}$. In Ras transgenic animals, the persistent cardiac downstream hypertrophic signaling activation was described as a selective $G\alpha_{i1}$ protein induction [122]. However, it is assumed that $G\alpha_{i2}$ and $G\alpha_{i3}$ protein are redundant and functionally equivalent in the heart. Previously published literature demonstrated an upregulation of both isoforms in heart failure [95-99].

The enhanced cardiac $G\alpha_{i2}$ and $G\alpha_{i3}$ expression on mRNA and membrane protein levels demonstrated in this work suggest that increased levels of $G\alpha_{i2}$ or $G\alpha_{i3}$ isoform compensate the chronic loss of the deleted other $G\alpha_i$ isoform to maintain the total amount up to the amount of wt control. β_2-AR activation dually couples to G_s and G_i and regulates PKA dependent pathways in the heart [74, 75, 118]. Moreover, L-type calcium channel regulation and G protein function by β_2-AR were described to require intact caveolae [72]. In our study, chronic β_2-AR activation significantly elevated cardiac $G\alpha_{i2}$ and $G\alpha_{i3}$ mRNA and protein levels. This could serve as a counterpart due to the higher $G\alpha_s$ stimulation and/or caveolae dysorganization. Taken together, these data emphasize that $G\alpha_{i2}$ and $G\alpha_{i3}$ are functionally redundant.

On the other hand, the Mendelian inheritance for $G\alpha_{i2}$-/- mice was markedly in favor of the "beneficial" genotype. One main reason is the severe $G\alpha_{i2}$-/- phenotype as described in Chapter 1.3 and confirmed with heart- and bodyweight data presented in this study. Of note was the high number of breeding needed for the $G\alpha_{i2}$-/- genotype. Furthermore, a previous work addressed the role of G_i proteins in normal and dysfunctional myocardium by developing a cardiac-specific G_i selective inhibitory peptide (GiCT) eliminating G_i signaling [140]. Ischemia induced GiCT transgenic mice led to an excessive upregulation of cardiac $G\alpha_{i2}$ mRNA expression level compared to sham-operated transgenic mice. This data suggests the existence of gene-specific role and isoform-specific cardiac functions.

Moreover, possible changes in associated proteins like $G\beta\gamma$ subunits might indirectly influence $G\alpha$ mediated signalling. A previous work demonstrated a decreased level of the widely distributed $G\beta_1$ subunit by siRNA silencing of $G\alpha_{i2}$ subunit in HeLa cells [141]. Indeed, using a $G\beta_{common}$ antibody [131], preliminary data suggest a decreased $G\beta_{1/2}$ expression levels in $G\alpha_{i2}$ deficient hearts, that might affect cardiac L-type calcium current [89].

In summary, despite partly $G\alpha_{i2}$ and $G\alpha_{i3}$ equivalent roles, only $G\alpha_{i2}$ protein deletion showed serious effects, maybe due its dominant presence.

4.2 Alterations of L-type calcium channel regulation by $G\alpha_{i2}$ deletion

One functionally important target affected by G_i protein signaling is the L-type calcium channel. The issue has been addressed by others for many years [111, 118, 142]. G_i proteins have been described to be responsible for the muscarinic and β_2-adrenergic L-type calcium channel inhibition [75, 117, 118]. $G\alpha_{i2}$ protein has been considered to be exclusively responsible for the cholinergic response [118, 142] and for the cardiomyopathy prevention in β_2-AR overexpression [109]. The enhanced heartweight to bodyweight ratios in $G\alpha_{i2}$-/- mice

underline this evidence. In a previous study, single channel recordings in $G\alpha_{i2}$-/- cardiomyocytes revealed a trend towards reduced L-type calcium channel currents and lower open probability. This effect was aggravated by additional β_2-AR overexpression and was reversed by PTX [109]. Hence it can be suggested that $G\alpha_{i3}$ protein plays a prominent role in the inhibition of basal L-type calcium current. Furthermore, single-channel current recordings in $G\alpha_{i3}$-/- cardiomyocytes revealed a trend towards increased peak ensemble average currents and higher open probability (×). In this study, a significant reduction or increase of basal whole cell current density in cardiomyocytes from $G\alpha_{i2}$-/- mice and $G\alpha_{i3}$-/- mice, respectively, was observed. Single channel recordings together with whole-cell experiments demonstrate contrasting functional roles of the two $G\alpha_i$ isoforms on cardiac L-type calcium channels. However, an alteration of whole-cell L-type calcium current gating was observed only in $G\alpha_{i2}$-/- cardiomyocytes. The half-maximum voltage of steady-state inactivation was shifted to more negative values and the recovery from inactivation was decelerated. Here, to discriminate between effects caused by the loss of one $G\alpha_i$ protein or by the intensified signaling exerted by the other, the remaining $G\alpha_i$ proteins were acutely inactivated by PTX pretreatment. $G\alpha_{i2}$-/- cardiomyocytes did not reveal any changes as a result of PTX treatment in L-type calcium channel current density and gating. In contrast, the peak current increase in $G\alpha_{i3}$-/- cardiomyocytes vanished with prolonged incubation times of the cardiomyoctes indicating a direct transient effect. Furthermore, the PTX pretreated $G\alpha_{i3}$-/- cardiomyocytes demonstrated same channel kinetic alterations as $G\alpha_{i2}$-/- cardiomyocytes. All these events point to a $G\alpha_{i2}$ specific regulation of L-type calcium channel gating properties.

On the other hand, Nagata *et al.* failed to detect a significant difference in L-type calcium channel modulated by wt, $G\alpha_{i2}$-/- and $G\alpha_{i3}$-/- [118]. However, Nagata *et al.* used a prepulse

× Unpublished data (dissertation Christoph Klein)

of -50 mV, while a more depolarizing prepulse (-40 mV) was used in our work to assure sodium current inactivation. The altered voltage condition may interfere with channel kinetic properties and thus lead to a reduced peak current density as in case of $G\alpha_{i2}$-/-. Recently, Zuberi *et al.* compared $G\alpha_{i2}$-/- mice with combined global genetic deleted $G\alpha_{i1}$ and $G\alpha_{i3}$ mice and found distinct effects on surface ECGs [111]. $G\alpha_{i2}$ deletion mediated ventricular arrhythmias due to QT interval prolongation and thus reduced effective refractory period. Interestingly, this study did not detect any significant abnormalities in the double knockout mice. Moreover, similar amounts of L-type calcium current density were detected for $G\alpha_{i2}$-/- cardiomyocytes, but interpreted as due to an increased effect compared to wt mice (mice were of 129SvEv background). However, the very small L-type calcium current density in cardiomyocytes of wt mice contradicts most published current density wt data [143-145]. In summary, $G\alpha_{i2}$ protein deletion showed dramatic consequences on channel regulation *in vivo* and *ex vivo*.

To obtain whether long-term or chronic $G\alpha_i$ deficiency caused any L-type calcium channel structural alterations, this study examined channel composition and abundance. As mentioned previously the cytoplasmic $Ca_v\beta$ subunit is necessary for channel trafficking and gating. It regulates the pore forming subunit by binding to the $Ca_v\alpha_1$ I-II intracellular loop. Gudzenko *et al.* [146] found profound effects on L-type calcium channel kinetics and yet ventricular action potential duration by the absence of $Ca_v\beta$ subunit. In this study, only $Ca_v\beta_3$ mRNA expression level is significantly enhanced in $G\alpha_{i2}$-/- and might have an effect on channel kinetic alterations. However, $Ca_v\beta_2$ is the predominant isoform (similar to other studies [58, 59]) and thus the change of total $Ca_v\beta$ subunit mRNA expression is very small and presumably not crucial. In addition, only $Ca_v\beta_2$ isoform phosphorylation by PKA and PI3K appear to contribute to cAMP-dependent channel regulation and channel plasma membrane trafficking, respectively [147-149]. On the other hand, the cell expression level

and location of the L-type calcium channel main $Ca_v\alpha_1$ subunit is essential for the data interpretation. However, mRNA expression level revealed no change in atrium and ventricle of all genotypes compared to wt control. To exclude the possibility that posttranslational modification led to different protein levels, membrane protein expression level of ventricular $Ca_v\alpha_1$ were examined, but no significant changes were found. These results do neither explain the $G\alpha_{i2}$ isoform-specific regulation of the channel, since the expression levels are not likely to affect the channel phenotype. It has also to be pointed out that the immunoblot data reveal total cardiac membrane channel protein levels, which does not necessarily match up the fraction of functional channels located in the sarcolemma.

4.3 Structural aspects and mechanisms underlying $G\alpha_{i2}$ requirement

Due to the L-type calcium current and kinetic alterations by $G\alpha_{i2}$ deletion, many molecular pathways come to consideration for cardiac $G\alpha_i$ regulation. The activation of stromal interaction molecule 1 (STIM1) was described to be responsible for redistribution of calcium entry between sarcoplasmic reticulum by sensing and the plasma membrane by functional presence. STIM1 overexpression or mutation resulted to an increase of calcium release-activated calcium (CRAC) activity and an altered CRAC inactivation property, respectively [150]. STIM1 regulation caused by $G\alpha_{i2}$ deficiency could explain the calcium channel phenotype in the heart. Moreover, STIM1 directly suppresses L-type calcium channel opening leading to long-term internalization of the channel from the membrane [151, 152]. On the other hand, loss of L-type calcium channels on the cell membrane by targeting to lysosomes was associated with prolonged activation of glutamate receptors via phosphatidylinositol 3-phosphate 5-kinase (PIKfyve) in neuron cells [153]. However, this study did not observe any changes of the pore forming subunit in cardiac membrane tissue, though - as mentioned before - this does not necessarily mean the fraction located in the

sacrolemma. Another candidate protein is the RGK GTPases, which belong to the Ras superfamily of monomeric G proteins. It potently inhibits L-type voltage-dependent calcium channels by binding the auxiliary $Ca_v\beta$ subunits. The slightly increased $Ca_v\beta$ subunit in $G\alpha_{i2}$ deleted cardiac tissue might suffice for calcium channel suppression. Furthermore, the RGK proteins Rad and Rem are expressed in cardiac muscle cells [154]. Rem overexpression in heart markedly decreased L-type calcium channel activity due to electrical silence on plasma membrane and reduced channel surface density [155, 156]. Mice overexpressing negative mutant Rad developed prolonged AP and displayed ventricular arrhythmias [157]. $G\alpha_{i2}$ deficiency might induce an alteration of Rem or Rad expression, modifying channel activity and AP, respectively. Little is known however about how these small GTP-binding proteins are regulated [158, 159].

The pathways mentioned above play an important role in cellular calcium homeostasis, which is essential for cardiac electrical activity and their alteration may explain our L-type calcium channel results. However, the role of G_i signaling in this context remains unclear.

Therefore, this study focused on two molecular pathways that are of high relevance for L-type calcium channel regulation and are involved in G_i protein-mediated action. First, stimulation of PKB/Akt mediated by phosphatidylinositol 3-kinase (PI3-K) induced calcium channel trafficking to the plasma membrane in excitable neuron cells [149]. Recently, Akt-mediated β-subunit phosphorylation preventing $Ca_v\alpha_1$ degradation and modulating calcium entry in cardiac cells via L-type calcium channels were shown [160]. On the other hand, G_i coupled receptor activation in the heart effectively led to Akt phosphorylation in a PI3K-dependent manner and promoted cell survival [115, 119]. The increased effect and protective action were blocked by PTX treatment [115]. This demonstrates a significant increase of Akt phosphorylation in cardiac tissue by CCh injection independent of the deleted $G\alpha_I$ isoform. Interestingly, basal Akt phosphorylation by sham injection was higher in tissue

from $G\alpha_i$ deficient animals compared to wt control. However, the total amount of Akt was similar in all genotypes. Thus, G_i subtype-specific channel regulation seems to be independent of Akt phosphorylation but might be crucial for cell survival effects.

Second, G_i coupled receptor stimulation increased mitogen-activated protein kinase / extracellular signal-regulated protein kinase (MAPK/ERK) activation subjected to RGS proteins [120]. Deactivation of G_i in turn led to a significant reduction in ERK 1/2 phosphorylation and this effect was Gs and Gq independent [115, 140]. Defects in MAPK/ERK pathway led to uncontrolled mechanisms in the cell. Recently, Smani *et al.* [161] showed a leftward shift and a marked increase in L-type calcium current density induced by urocortin involving protein kinase C (PKC) dependent activation of the MAPK-ERK1/2 pathway. In the present study, $G\alpha_{i2}$ inhibition prevents phosphorylation of ERK1/2 in CCh stimulated cardic tissue, whereas ERK1/2 phosphorylation was significantly increased in wt and $G\alpha_{i3}$-/- tissues. Again total amount of ERK1/2 was unchanged in all genotypes. Therefore, it can be suggested that activation of L-type calcium channel by ERK1/2 might be the mechanism involved in functional regulation of calcium current by $G\alpha_{i2}$ protein. Furthermore, interfering of $G\alpha_{i2}$ protein with MAPK pathway could be a potential exploration for the cardioprotection.

4.4 Conclusion and outlook

Taken together, the data reported here point to the (patho-) physiological importance of subtype-specific G_{i2} protein signaling in the heart. In particular, in terminal heart failure, $G\alpha_{i2}$ upregulation now appears as an attractive mechanism linked to structural and functional remodeling of L-type calcium channel. Furthermore, the present study demonstrates a specific $G\alpha_{i2}$-dependent ERK1/2 phosphorylation and provides new insights into potential mechanisms linking modulation of L-type calcium channel by the inhibitory G protein isoform G_{i2} in cardiomyocytes.

This work could not elucidate all effects seen in the knockout animals and require further work for the clarification. Thus, ultimately, G_{i3}'s role on L-type calcium channel regulation remains unclear. Due to the partly absent acute PTX effects, experiments in recombinant systems need to be done. This system is reasonable for observations of double deficiency and to analyze the subcellular localization of calcium channels, e.g. by Fluorescence Resonance Energy Transfer (FRET) imaging. Pretreated $G\alpha_{i2}$-/-, $G\alpha_{i3}$-/- and wt mice or cells with PTX should be retested for ERK1/2 phosphorylation by CCh addition. Moreover, the detailed signaling of G_{i2} by ERK1/2 phosphorylation and further L-type calcium channel regulation are relevant. For this, the examination of L-type calcium channel activity by directly inhibiting MAPK/ERK activity or by inhibiting PKC or PI3K pathways in cardiomyocytes of the animal models are crucial. Of further interest might be the pretreatment of the mice with zinterol instead of CCh to compare β_2-AR and thus PKA effects on ERK1/2 phosphorylation. Finally, in this work cardiac $\alpha_2\delta$ subunit expression levels in the mouse models were not analyzed. It would be relevant to address this question, since $\alpha_2\delta$ knockout mice revealed profound effects on L-type calcium channel activity and gating properties. Hence, the basal myocardial contractility and relaxation were significantly decreased indicating decreased calcium load [65]. Another aspect is the L-type calcium channel location. Differences of

whole-cell L-type calcium current density in t-tubule and surface sarcolemma were observed in failing ventricular mice [162]. Due to the dissimilar $G\alpha_i$ proteins presence in the heart, it would be interesting to assess whether there is an isoform-specific action of $G\alpha_{i2}$ or $G\alpha_{i3}$ protein on L-type calcium channel dependent on the location. Furthermore, whether the structure of the surface membrane is preserved in the genetic modified mouse models.

5 SUMMARY

Two inhibitory G protein α-subunits ($G\alpha_{i2}$ and $G\alpha_{i3}$) are expressed in cardiomyocytes and upregulated in heart failure. They are regulated by the parasympathic and sympathic nervous system via G protein couples receptors. Thus, they are responsible for many physiological and pathophysiological effects in the cell including L-type calcium channel regulation. Alterations of L-type calcium channel function are associated with cardiomyopathy and heart failure. However, the isoform-specific channel modulation and signaling pathway regulation by $G\alpha_{i2}$ or $G\alpha_{i3}$ protein remains unclear.

Previous studies of chronic human β_2-adrenoceptor overexpression in mouse hearts – but not β_1-adrenoceptor overexpression – revealed basal L-type calcium current suppression. Unlike β_1-adrenoceptors, β_2-adrenoceptors are additionally able to couple to pertussis toxin (PTX) sensitive G inhibitory proteins, inducing dual signaling effects. Furthermore, cardiac β_2-adrenoceptor overexpression mice with global $G\alpha_{i2}$ deletion developed cardiac hypertophy leading to excess mortality. Interestingly, PTX pretreatment of these cells reversed the suppressed L-type calcium channel activity. This effect was suggested to be $G\alpha_{i3}$ protein specific; $G\alpha_{i2}$ protein has been considered to be exclusively responsible for the cholinergic inhibition of the cardiac L-type calcium channel activity and for cardioprotection. So far, it was not possible to differentiate L-type calcium channel modulation in the heart by different $G\alpha_i$ protein subtypes. Therefore, to characterize $G\alpha_i$ isoform-specific modulation, the present work examined cardiomyocytes from mice lacking either $G\alpha_{i2}$ or $G\alpha_{i3}$ protein and compared to wt control.

In these cardiomyocytes, the other $G\alpha_i$ isoform is upregulated both on mRNA and protein levels, indication compensatory effect. Furthermore, in ventricular myocytes peak whole-cell basal calcium current density in $G\alpha_{i2}$-/- cardiomyocytes is significantly decreased, whereas it is significantly increased in $G\alpha_{i3}$-/- cells as compared to control animals. Kinetic changes of

suppressed whole-cell currents were observed: half-maximum voltage of steady-state inactivation was shifted to more negative values and the recovery from inactivation was delayed. $G\alpha_{i3}$-/- cardiomyocytes treated with PTX display similar channel kinetic alterations, whereas $G\alpha_{i2}$-/- and wt cardiomyocytes remain unchanged. Taken together, only genetic- or PTX-mediated ablation of $G\alpha_{i2}$ function causes calcium channel kinetic alterations. On mRNA and protein expression levels, no substantial L-type calcium channel subunit alterations were observed within the mouse models. Thus, calcium channel structural aspects are not relevant for the data reported here. Several molecular pathways come to consideration for cardiac $G\alpha_i$ regulation of L-type calcium channel. In this study, subtype-specific activation of the extracellular signal-regulated kinases 1/2 (ERK1/2) signaling cascade by $G\alpha_{i2}$ proteins was demonstrated. Thus, this study reveals the importance of $G\alpha_{i2}$ protein in L-type calcium channel regulation and in cardioprotection.

6 ZUSAMMENFASSUNG

Zwei inhibitorische Gα Proteine, $G\alpha_{i2}$ and $G\alpha_{i3}$ werden im Herzen exprimiert und bei der Herzinsuffizienz hochreguliert. Ihre Aktivierung wird durch die Stimulation der G Protein gekoppelten Rezeptoren vermittelt, welche durch das parasympatische und sympatische Nervensystem reguliert werden. Sie sind somit für viele physiologische und pathophysiologische Prozesse in der Zelle verantwortlich, unter anderem die Modulation des L-Typ Calciumkanals. Veränderungen in den Eigenschaften der L-Typ Calciumkanäle werden auch mit Kardiomyopathie und Herzinsuffizienz in Verbindung gebracht. Hierbei bleibt die spezifische Rolle der $G\alpha_{i2}$ bzw. $G\alpha_{i3}$ Isoformen bei der Signalweiterleitung und bei der Kanalmodulation ungeklärt.

Vorherige Untersuchungen haben gezeigt, dass es bei chronischer Stimulation kardialer β_2-Adrenozeptoren in der Maus, nicht aber von β_1-Adrenozeptoren, zu einer Suppression der basalen L-Typ Calciumkanalaktivität kommt. Dies ist auf die unterschiedliche Signaltransduktion von beiden Adrenozeptoren am Herzen zurückzuführen und wird durch die zusätzliche Koppelung des β_2-Adrenozeptors an Pertussistoxin (PTX) sensitive inhibitorische G Proteine erklärt. Verpaarung von β_2-Adrenozeptor transgenen Mäusen mit $G\alpha_{i2}$ k.o. Mäusen führt zu einem Phänotyp mit kardialer Hypertrophie und erhöhter Mortalität. Die Zugabe von PTX hebt die Suppression der Kanalaktivität wieder auf. Aufgrund dieser Erkenntnisse kann die Hypothese aufgestellt werden, dass β_2-Adrenozeptor den Kanal mittels $G\alpha_{i3}$ und nicht $G\alpha_{i2}$ inhibiert. Andererseits wird die cholinerge Inhibition des Kanals mittels muskarinischer Rezeptoren der Aktivierung des $G\alpha_{i2}$ Proteins zugeordnet, genauso die Kardioprotektion. Folglich ist eine genaue Abgrenzung zwischen $G\alpha_{i2}$ und $G\alpha_{i3}$ bei der Regulation des L-Typ Calciumkanals im Herzen nicht möglich. Um diesen Ansatz genauer zu betrachten und zu differenzieren, wurden in der vorliegenden Studie

Kardiomyozyten aus Mäusen mit genetisch gezielter Auslöschung der $G\alpha_{i2}$ oder $G\alpha_{i3}$ Proteine untersucht.

Die Untersuchungen in $G\alpha_{i2}$ und $G\alpha_{i3}$ k.o. Mausmodelle zeigen, dass das Fehlen an $G\alpha_{i2}$ Protein zu einer massiven Überexpression von $G\alpha_{i3}$ Protein im Herzen sowohl auf mRNA als auch Protein Ebene führt. Umgekehrt ist bei $G\alpha_{i3}$ knockout Mäusen eine Hochregulation von $G\alpha_{i2}$ Protein zu beobachten (auch wenn dieser Effekt weniger ausgeprägt ist); dies lässt einen kompensatorischen Effekt vermuten. Im Vergleich zur Kontrolle (Wildtyp) ist der basale Spitzenstrom des L-Typ Calciumkanals bei $G\alpha_{i3}$ knockout Mäusen signifikant erhöht und bei $G\alpha_{i2}$ knockout signifikant reduziert. Bei der Suppression des Calciumkanals im $G\alpha_{i2}$ knockout sind Veränderungen in der Kinetik zu vermerken: die Inaktivierung des Kanals findet bei negativeren Potentialen statt und die Erholung aus der Inaktivierung ist verlangsamt. Interessanterweise zeigen Kardiomyozyten von $G\alpha_{i3}$ k.o. Mäusen nach Inkubation mit PTX (Inaktivierung der verbleibenden G-Proteine und damit auch von $G\alpha_{i2}$) ähnliche kinetische Eigenschaften. Die Kinetik der Calciumströme in $G\alpha_{i2}$ k.o. und Wildtyp Kardiomyozyten bleibt durch die Vorbehandlung mit PTX unbeeinflusst. Zusammengefasst zeigen eine chronische (knockout) und eine akute (PTX im $G\alpha_{i3}$ knockout) Inhibition des $G\alpha_{i2}$ Proteins deutliche Effekte auf die Regulation des Calciumkanals. Die Überprüfung der Expression der Calciumkanaluntereinheiten weist keine relevanten Unterschiede auf mRNA- und Proteinebene innerhalb der Mausmodelle auf, somit spielen strukturelle Veränderungen des Kanalkomplexes hier vermutlich keine Rolle. Die Untersuchung von spezifischen Signalwegen, die von großer Bedeutung für die L-Typ Calciumkanalregulation ist und in denen G_i Proteine eine maßgebliche Rolle spielen, deuten auf eine $G\alpha_{i2}$ Protein abhängige Phosphorylierung von extrazellulären signalregulierten Kinasen (ERK1/2) hin. Dies zeigt die Wichtigkeit des $G\alpha_{i2}$ Proteins bei der Regulation des L-Typ Calciumkanals und bei Kardioprotektion.

7 BIBLIOGRAPHY

1. Jones, D.W. and J.E. Hall, *Seventh report of the Joint National Committee on Prevention, Detection, Evaluation, and Treatment of High Blood Pressure and evidence from new hypertension trials.* Hypertension, 2004. **43**(1): p. 1-3.
2. Hoppe, U.C., et al., *[Leitlinien zur Therapie der chronischen Herzinsuffizienz].* Zeitschrift für Kardiologie, 2005. **94**(8): p. 704-720.
3. Muth, C., J. Gensichen, and M. Butzlaff, *[DEGAM-Leitlinie Nr. 9: Herzinsuffizienz].* omikorn publishing / DEGAM, 2006: p. http://leitlinien.degam.de/.
4. Lowel, H. and C. Meisinger, *[Epidemiology and demographic evolution exemplified for cardiovascular diseases in Germany].* Med Klin (Munich), 2006. **101**(10): p. 804-11.
5. Zipes, D.P. and H.J. Wellens, *Sudden cardiac death.* Circulation, 1998. **98**(21): p. 2334-51.
6. Waldecker, B., et al., *[On the epidemiology of sudden cardiac death].* Notfall & Rettungsmedizin, 2003: p. 6313-317.
7. Tendera, M., *How much does Europe invest in the treatment of cardiovascular diseases?* Eur Heart J, 2006. **27**(13): p. 1521-2.
8. Levi, F., et al., *Trends in mortality from cardiovascular and cerebrovascular diseases in Europe and other areas of the world.* Heart, 2002. **88**(2): p. 119-24.
9. Fox, C.S., *Cardiovascular disease risk factors, type 2 diabetes mellitus, and the Framingham Heart Study.* Trends Cardiovasc Med, 2010. **20**(3): p. 90-5.
10. Maltsev, V.A. and E.G. Lakatta, *Dynamic interactions of an intracellular Ca2+ clock and membrane ion channel clock underlie robust initiation and regulation of cardiac pacemaker function.* Cardiovasc Res, 2008. **77**(2): p. 274-84.

11. Schram, G., et al., *Differential distribution of cardiac ion channel expression as a basis for regional specialization in electrical function.* Circ Res, 2002. **90**(9): p. 939-50.

12. DiFrancesco, D., *The role of the funny current in pacemaker activity.* Circ Res, 2010. **106**(3): p. 434-46.

13. Nerbonne, J.M. and R.S. Kass, *Molecular physiology of cardiac repolarization.* Physiol Rev, 2005. **85**(4): p. 1205-53.

14. Lakatta, E.G., V.A. Maltsev, and T.M. Vinogradova, *A coupled SYSTEM of intracellular Ca2+ clocks and surface membrane voltage clocks controls the timekeeping mechanism of the heart's pacemaker.* Circ Res, 2010. **106**(4): p. 659-73.

15. Kanno, S. and J.E. Saffitz, *The role of myocardial gap junctions in electrical conduction and arrhythmogenesis.* Cardiovasc Pathol, 2001. **10**(4): p. 169-77.

16. Koopmann, T.T., C.R. Bezzina, and A.A. Wilde, *Voltage-gated sodium channels: action players with many faces.* Ann Med, 2006. **38**(7): p. 472-82.

17. Fozzard, H.A., *Cardiac sodium and calcium channels: a history of excitatory currents.* Cardiovasc Res, 2002. **55**(1): p. 1-8.

18. Orchard, C. and F. Brette, *t-Tubules and sarcoplasmic reticulum function in cardiac ventricular myocytes.* Cardiovasc Res, 2008. **77**(2): p. 237-44.

19. Bers, D.M., *Calcium fluxes involved in control of cardiac myocyte contraction.* Circ Res, 2000. **87**(4): p. 275-81.

20. Fabiato, A., *Two kinds of calcium-induced release of calcium from the sarcoplasmic reticulum of skinned cardiac cells.* Adv Exp Med Biol, 1992. **311**: p. 245-62.

21. Bers, D.M., *Cardiac excitation-contraction coupling.* Nature, 2002. **415**(6868): p. 198-205.

22. Egger, M. and E. Niggli, *Regulatory function of Na-Ca exchange in the heart: milestones and outlook.* J Membr Biol, 1999. **168**(2): p. 107-30.

23. Maier, L.S. and D.M. Bers, *Role of Ca2+/calmodulin-dependent protein kinase (CaMK) in excitation-contraction coupling in the heart.* Cardiovasc Res, 2007. **73**(4): p. 631-40.

24. Yang, D., et al., *Ca2+/calmodulin kinase II-dependent phosphorylation of ryanodine receptors suppresses Ca2+ sparks and Ca2+ waves in cardiac myocytes.* Circ Res, 2007. **100**(3): p. 399-407.

25. Brodde, O.E. and M.C. Michel, *Adrenergic and muscarinic receptors in the human heart.* Pharmacol Rev, 1999. **51**(4): p. 651-90.

26. Herzig, S., et al., *Stimulation of protein phosphatases as a mechanism of the muscarinic-receptor-mediated inhibition of cardiac L-type Ca2+ channels.* Pflugers Arch, 1995. **429**(4): p. 531-8.

27. Fischmeister, R. and H.C. Hartzell, *Mechanism of action of acetylcholine on calcium current in single cells from frog ventricle.* J Physiol, 1986. **376**: p. 183-202.

28. Bylund, D.B., et al., *International Union of Pharmacology nomenclature of adrenoceptors.* Pharmacol Rev, 1994. **46**(2): p. 121-36.

29. Kaumann, A.J. and P. Molenaar, *Modulation of human cardiac function through 4 beta-adrenoceptor populations.* Naunyn Schmiedebergs Arch Pharmacol, 1997. **355**(6): p. 667-81.

30. Tomaselli, G.F. and E. Marban, *Electrophysiological remodeling in hypertrophy and heart failure.* Cardiovasc Res, 1999. **42**(2): p. 270-83.

31. Tomaselli, G.F., et al., *Sudden cardiac death in heart failure. The role of abnormal repolarization.* Circulation, 1994. **90**(5): p. 2534-9.

32. Aiba, T. and G.F. Tomaselli, *Electrical remodeling in the failing heart.* Curr Opin Cardiol, 2010. **25**(1): p. 29-36.

33. Jin, H., A.R. Lyon, and F.G. Akar, *Arrhythmia mechanisms in the failing heart.* Pacing Clin Electrophysiol, 2008. **31**(8): p. 1048-56.

34. Catterall, W.A., *Structure and regulation of voltage-gated Ca2+ channels.* Annu Rev Cell Dev Biol, 2000. **16**: p. 521-55.

35. Ertel, E.A., et al., *Nomenclature of voltage-gated calcium channels.* Neuron, 2000. **25**(3): p. 533-5.

36. Perez-Reyes, E., *Molecular physiology of low-voltage-activated t-type calcium channels.* Physiol Rev, 2003. **83**(1): p. 117-61.

37. Kinoshita, H., et al., *T-type Ca2+ channel blockade prevents sudden death in mice with heart failure.* Circulation, 2009. **120**(9): p. 743-52.

38. Chiang, C.S., et al., *The Ca(v)3.2 T-type Ca(2+) channel is required for pressure overload-induced cardiac hypertrophy in mice.* Circ Res, 2009. **104**(4): p. 522-30.

39. Le Quang, K., et al., *Role of T-type calcium channel subunits in post-myocardial infarction remodelling probed with genetically engineered mice.* Cardiovasc Res, 2011.

40. Vacher, H., D.P. Mohapatra, and J.S. Trimmer, *Localization and targeting of voltage-dependent ion channels in mammalian central neurons.* Physiol Rev, 2008. **88**(4): p. 1407-47.

41. Schroder, E.A., Y. Wei, and J. Satin, *The developing cardiac myocyte: maturation of excitability and excitation-contraction coupling.* Ann N Y Acad Sci, 2006. **1080**: p. 63-75.

42. Striessnig, J., *Pharmacology, structure and function of cardiac L-type Ca(2+) channels.* Cell Physiol Biochem, 1999. **9**(4-5): p. 242-69.

43. Benitah, J.P., J.L. Alvarez, and A.M. Gomez, *L-type Ca(2+) current in ventricular cardiomyocytes.* J Mol Cell Cardiol, 2010. **48**(1): p. 26-36.

44. Black, D.J., et al., *Calmodulin interactions with IQ peptides from voltage-dependent calcium channels.* Am J Physiol Cell Physiol, 2005. **288**(3): p. C669-76.

45. Dick, I.E., et al., *A modular switch for spatial Ca2+ selectivity in the calmodulin regulation of CaV channels.* Nature, 2008. **451**(7180): p. 830-4.

46. Hudmon, A., et al., *A mechanism for Ca2+/calmodulin-dependent protein kinase II clustering at synaptic and nonsynaptic sites based on self-association.* J Neurosci, 2005. **25**(30): p. 6971-83.

47. Fink, M.A., et al., *AKAP-mediated targeting of protein kinase a regulates contractility in cardiac myocytes.* Circ Res, 2001. **88**(3): p. 291-7.

48. Davare, M.A., M.C. Horne, and J.W. Hell, *Protein phosphatase 2A is associated with class C L-type calcium channels (Cav1.2) and antagonizes channel phosphorylation by cAMP-dependent protein kinase.* J Biol Chem, 2000. **275**(50): p. 39710-7.

49. Kobayashi, T., et al., *Regulation of Cav1.2 current: interaction with intracellular molecules.* J Pharmacol Sci, 2007. **103**(4): p. 347-53.

50. Abernethy, D.R. and J.B. Schwartz, *Calcium-antagonist drugs.* N Engl J Med, 1999. **341**(19): p. 1447-57.

51. Xu, X. and H.M. Colecraft, *Engineering proteins for custom inhibition of Ca(V) channels.* Physiology (Bethesda), 2009. **24**: p. 210-8.

52. Bodi, I., et al., *The L-type calcium channel in the heart: the beat goes on.* J Clin Invest, 2005. **115**(12): p. 3306-17.

53. Dolphin, A.C., *B subunits of voltage-gated calcium channels.* J Bioenerg Biomembr, 2003. **35**(6): p. 599-620.

54. Foell, J.D., et al., *Molecular heterogeneity of calcium channel beta-subunits in canine and human heart: evidence for differential subcellular localization.* Physiol Genomics, 2004. **17**(2): p. 183-200.

55. Pragnell, M., et al., *Calcium channel beta-subunit binds to a conserved motif in the I-II cytoplasmic linker of the alpha 1-subunit.* Nature, 1994. **368**(6466): p. 67-70.

56. Buraei, Z. and J. Yang, *The ss subunit of voltage-gated Ca2+ channels.* Physiol Rev, 2010. **90**(4): p. 1461-506.

57. Colecraft, H.M., et al., *Novel functional properties of Ca^{2+} channel β subunits revealed by their expression in adult rat heart cells.* J Physiol, 2002. **541**(Pt 2): p. 435-52.

58. Hullin, R., et al., *Increased expression of the auxiliary β_2-subunit of ventricular L-type Ca^{2+} channels leads to single-channel activity characteristic of heart failure.* PLoS One, 2007. **2**(3): p. e292.

59. Link, S., et al., *Diversity and developmental expression of L-type calcium channel β_2 proteins and their influence on calcium current in murine heart.* J Biol Chem, 2009. **284**(44): p. 30129-37.

60. Gonzalez-Gutierrez, G., et al., *The guanylate kinase domain of the β-subunit of voltage-gated calcium channels suffices to modulate gating.* Proc Natl Acad Sci U S A, 2008. **105**(37): p. 14198-203.

61. Hullin, R., et al., *Cardiac L-type calcium channel β-subunits expressed in human heart have differential effects on single channel characteristics.* J Biol Chem, 2003. **278**(24): p. 21623-30.

62. Kobrinsky, E., et al., *Differential role of the alpha1C subunit tails in regulation of the Cav1.2 channel by membrane potential, beta subunits, and Ca2+ ions.* J Biol Chem, 2005. **280**(13): p. 12474-85.

63. Platano, D., et al., *Expression of the alpha(2)delta subunit interferes with prepulse facilitation in cardiac L-type calcium channels.* Biophys J, 2000. **78**(6): p. 2959-72.

64. Klugbauer, N., et al., *Molecular diversity of the calcium channel alpha2delta subunit.* J Neurosci, 1999. **19**(2): p. 684-91.

65. Fuller-Bicer, G.A., et al., *Targeted disruption of the voltage-dependent calcium channel alpha2/delta-1-subunit.* Am J Physiol Heart Circ Physiol, 2009. **297**(1): p. H117-24.

66. Davies, A., et al., *The alpha2delta subunits of voltage-gated calcium channels form GPI-anchored proteins, a posttranslational modification essential for function.* Proc Natl Acad Sci U S A, 2010. **107**(4): p. 1654-9.

67. Schroder, F., et al., *Increased availability and open probability of single L-type calcium channels from failing compared with nonfailing human ventricle.* Circulation, 1998. **98**(10): p. 969-76.

68. Pitt, G.S., W. Dun, and P.A. Boyden, *Remodeled cardiac calcium channels.* J Mol Cell Cardiol, 2006. **41**(3): p. 373-88.

69. Burashnikov, E., et al., *Mutations in the cardiac L-type calcium channel associated with inherited J-wave syndromes and sudden cardiac death.* Heart Rhythm, 2010. **7**(12): p. 1872-82.

70. Lohse, M.J., S. Engelhardt, and T. Eschenhagen, *What is the role of β-adrenergic signaling in heart failure?* Circ Res, 2003. **93**(10): p. 896-906.

71. Xiao, R.P. and E.G. Lakatta, *Beta 1-adrenoceptor stimulation and beta 2-adrenoceptor stimulation differ in their effects on contraction, cytosolic Ca2+, and Ca2+ current in single rat ventricular cells.* Circ Res, 1993. **73**(2): p. 286-300.

72. Balijepalli, R.C., et al., *Localization of cardiac L-type Ca(2+) channels to a caveolar macromolecular signaling complex is required for beta(2)-adrenergic regulation.* Proc Natl Acad Sci U S A, 2006. **103**(19): p. 7500-5.

73. Kuschel, M., et al., *G(i) protein-mediated functional compartmentalization of cardiac beta(2)-adrenergic signaling.* J Biol Chem, 1999. **274**(31): p. 22048-52.

74. Xiao, R.P., *Beta-adrenergic signaling in the heart: dual coupling of the beta2-adrenergic receptor to G(s) and G(i) proteins.* Sci STKE, 2001. **2001**(104): p. re15.

75. Xiao, R.P., et al., *Coupling of β_2-adrenoceptor to G_i proteins and its physiological relevance in murine cardiac myocytes.* Circ Res, 1999. **84**(1): p. 43-52.

76. Simon, M.I., M.P. Strathmann, and N. Gautam, *Diversity of G proteins in signal transduction.* Science, 1991. **252**(5007): p. 802-8.

77. Kjeldgaard, M., J. Nyborg, and B.F. Clark, *The GTP binding motif: variations on a theme.* Faseb J, 1996. **10**(12): p. 1347-68.

78. Clapham, D.E. and E.J. Neer, *G protein beta gamma subunits.* Annu Rev Pharmacol Toxicol, 1997. **37**: p. 167-203.

79. Liggett, S.B., et al., *Coupling of a mutated form of the human beta 2-adrenergic receptor to Gi and Gs. Requirement for multiple cytoplasmic domains in the coupling process.* J Biol Chem, 1991. **266**(8): p. 4816-21.

80. Hein, P., et al., *Dynamics of receptor/G protein coupling in living cells.* EMBO J, 2005. **24**(23): p. 4106-14.

81. Oldham, W.M. and H.E. Hamm, *Structural basis of function in heterotrimeric G proteins.* Q Rev Biophys, 2006. **39**(2): p. 117-66.

82. Hamm, H.E., *The many faces of G protein signaling.* J Biol Chem, 1998. **273**(2): p. 669-72.

83. Rockman, H.A., W.J. Koch, and R.J. Lefkowitz, *Seven-transmembrane-spanning receptors and heart function.* Nature, 2002. **415**(6868): p. 206-12.

84. Hata, J.A. and W.J. Koch, *Phosphorylation of G protein-coupled receptors: GPCR kinases in heart disease.* Mol Interv, 2003. **3**(5): p. 264-72.

85. Ross, E.M. and T.M. Wilkie, *GTPase-activating proteins for heterotrimeric G proteins: regulators of G protein signaling (RGS) and RGS-like proteins.* Annu Rev Biochem, 2000. **69**: p. 795-827.

86. Wieland, T. and S. Herzig, *Specificity and diversity in Gi/o-mediated signaling: how the heart operates the RGS brake pedal.* Circ Res, 2006. **98**(5): p. 585-6.

87. Zamponi, G.W. and T.P. Snutch, *Decay of prepulse facilitation of N type calcium channels during G protein inhibition is consistent with binding of a single Gbeta subunit.* Proc Natl Acad Sci U S A, 1998. **95**(7): p. 4035-9.

88. Dascal, N., *Ion-channel regulation by G proteins.* Trends Endocrinol Metab, 2001. **12**(9): p. 391-8.

89. Volkers, M., et al., *The inotropic peptide betaARKct improves betaAR responsiveness in normal and failing cardiomyocytes through G(betagamma)-mediated L-type calcium current disinhibition.* Circ Res, 2011. **108**(1): p. 27-39.

90. Eschenhagen, T., *G proteins and the heart.* Cell Biol Int, 1993. **17**(8): p. 723-49.

91. Jones, D.T. and R.R. Reed, *Molecular cloning of five GTP-binding protein cDNA species from rat olfactory neuroepithelium.* J Biol Chem, 1987. **262**(29): p. 14241-9.

92. Wettschureck, N. and S. Offermanns, *Mammalian G proteins and their cell type specific functions.* Physiol Rev, 2005. **85**(4): p. 1159-204.

93. Asano, T., et al., *Ontogeny of the GTP-binding protein G_o in rat brain and heart.* J Neurochem, 1988. **51**(6): p. 1711-6.

94. Zolk, O., et al., *Heterotrimeric G proteins in heart disease.* Can J Physiol Pharmacol, 2000. **78**(3): p. 187-98.

95. Bohm, M., et al., *Desensitization of adenylate cyclase and increase of $G_i\alpha$ in cardiac hypertrophy due to acquired hypertension.* Hypertension, 1992. **20**(1): p. 103-12.

96. Eschenhagen, T., et al., *Increased messenger RNA level of the inhibitory G protein alpha subunit Gi alpha-2 in human end-stage heart failure.* Circ Res, 1992. **70**(4): p. 688-96.

97. Feldman, A.M., et al., *Increase of the 40,000-mol wt pertussis toxin substrate (G protein) in the failing human heart.* J Clin Invest, 1988. **82**(1): p. 189-97.

98. Mittmann, C., et al., *Differential coupling of m-cholinoceptors to G_i/G_o-proteins in failing human myocardium.* J Mol Cell Cardiol, 2003. **35**(10): p. 1241-9.

99. Neumann, J., et al., *Increase in myocardial G_i-proteins in heart failure.* Lancet, 1988. **2**(8617): p. 936-7.

100. Nerbonne, J.M., *Studying cardiac arrhythmias in the mouse--a reasonable model for probing mechanisms?* Trends Cardiovasc Med, 2004. **14**(3): p. 83-93.

101. Xu, H., W. Guo, and J.M. Nerbonne, *Four kinetically distinct depolarization-activated K+ currents in adult mouse ventricular myocytes.* J Gen Physiol, 1999. **113**(5): p. 661-78.

102. Kobilka, B.K., et al., *An intronless gene encoding a potential member of the family of receptors coupled to guanine nucleotide regulatory proteins.* Nature, 1987. **329**(6134): p. 75-9.

103. Milano, C.A., et al., *Enhanced myocardial function in transgenic mice overexpressing the beta 2-adrenergic receptor.* Science, 1994. **264**(5158): p. 582-6.

104. Liggett, S.B., et al., *Early and delayed consequences of beta(2)-adrenergic receptor overexpression in mouse hearts: critical role for expression level.* Circulation, 2000. **101**(14): p. 1707-14.

105. Jiang, M., et al., *Mouse gene knockout and knockin strategies in application to α subunits of G_i/G_o family of G proteins.* Methods Enzymol, 2002. **344**: p. 277-98.

106. Rudolph, U., et al., *Ulcerative colitis and adenocarcinoma of the colon in $G\alpha_{i2}$-deficient mice.* Nat Genet, 1995. **10**(2): p. 143-50.

107. Hornquist, C.E., et al., *G(alpha)i2-deficient mice with colitis exhibit a local increase in memory CD4+ T cells and proinflammatory Th1-type cytokines.* J Immunol, 1997. **158**(3): p. 1068-77.

108. Skokowa, J., et al., *Macrophages induce the inflammatory response in the pulmonary Arthus reaction through $G\alpha_{i2}$ activation that controls C5aR and Fc receptor cooperation.* J Immunol, 2005. **174**(5): p. 3041-50.

109. Foerster, K., et al., *Cardioprotection specific for the G protein G_{i2} in chronic adrenergic signaling through β_2-adrenoceptors.* Proc Natl Acad Sci U S A, 2003. **100**(24): p. 14475-80.

110. Gohla, A., et al., *An obligatory requirement for the heterotrimeric G protein Gi3 in the antiautophagic action of insulin in the liver.* Proc Natl Acad Sci U S A, 2007. **104**(8): p. 3003-8.

111. Zuberi, Z., et al., *Absence of the Inhibitory G-protein, $G\alpha_{i2}$, Predisposes to Ventricular Cardiac Arrhythmia.* Circ Arrhythm Electrophysiol, 2010: p. in press; doi:10.1161/CIRCEP.109.894329.

112. Gohla, A., K. Klement, and B. Nurnberg, *The heterotrimeric G protein G(i3) regulates hepatic autophagy downstream of the insulin receptor.* Autophagy, 2007. **3**(4): p. 393-5.

113. Engelhardt, S., et al., *Progressive hypertrophy and heart failure in beta1-adrenergic receptor transgenic mice.* Proc Natl Acad Sci U S A, 1999. **96**(12): p. 7059-64.

114. Lohse, M.J., et al., *Mechanisms of beta-adrenergic receptor desensitization: from molecular biology to heart failure.* Basic Res Cardiol, 1996. **91 Suppl 2**: p. 29-34.

115. Chesley, A., et al., *The β_2-adrenergic receptor delivers an antiapoptotic signal to cardiac myocytes through G_i-dependent coupling to phosphatidylinositol 3'-kinase.* Circ Res, 2000. **87**(12): p. 1172-9.

116. Foerster, K., et al., *Calcium channel function and regulation in beta 1- and beta 2-adrenoceptor transgenic mice.* Naunyn Schmiedebergs Arch Pharmacol, 2004. **369**(5): p. 490-5.

117. Heubach, J.F., et al., *Murine ventricular L-type Ca^{2+} current is enhanced by zinterol via β_1-adrenoceptors, and is reduced in TG4 mice overexpressing the human β_2-adrenoceptor.* Br J Pharmacol, 2001. **133**(1): p. 73-82.

118. Nagata, K., et al., *$G\alpha_{i2}$ but not $G\alpha_{i3}$ is required for muscarinic inhibition of contractility and calcium currents in adult cardiomyocytes.* Circ Res, 2000. **87**(10): p. 903-9.

119. Murga, C., et al., *Activation of Akt/protein kinase B by G protein-coupled receptors. A role for alpha and beta gamma subunits of heterotrimeric G proteins acting through phosphatidylinositol-3-OH kinasegamma.* J Biol Chem, 1998. **273**(30): p. 19080-5.

120. Anger, T., et al., *RGS protein specificity towards Gq- and Gi/o-mediated ERK 1/2 and Akt activation, in vitro.* J Biochem Mol Biol, 2007. **40**(6): p. 899-910.

121. Beetz, N., et al., *Transgenic simulation of human heart failure-like L-type Ca^{2+}-channels: implications for fibrosis and heart rate in mice.* Cardiovasc Res, 2009. **84**(3): p. 396-406.

122. Ruan, H., et al., *G_i α_1-mediated cardiac electrophysiological remodeling and arrhythmia in hypertrophic cardiomyopathy.* Circulation, 2007. **116**(6): p. 596-605.

123. Livak, K.J. and T.D. Schmittgen, *Analysis of relative gene expression data using real-time quantitative PCR and the 2(-Delta Delta C(T)) Method.* Methods, 2001. **25**(4): p. 402-8.

124. Schmittgen, T.D. and K.J. Livak, *Analyzing real-time PCR data by the comparative C(T) method.* Nat Protoc, 2008. **3**(6): p. 1101-8.

125. Lowry, O.H., et al., *Protein measurement with the Folin phenol reagent.* J Biol Chem, 1951. **193**(1): p. 265-75.

126. Peterson, G.L., *A simplification of the protein assay method of Lowry et al. which is more generally applicable.* Anal Biochem, 1977. **83**(2): p. 346-56.

127. Gehrmann, J., et al., *Impaired parasympathetic heart rate control in mice with a reduction of functional G protein betagamma-subunits.* Am J Physiol Heart Circ Physiol, 2002. **282**(2): p. H445-56.

128. Bradford, M.M., *A rapid and sensitive method for the quantitation of microgram quantities of protein utilizing the principle of protein-dye binding.* Anal Biochem, 1976. **72**: p. 248-54.

129. Laemmli, U.K., *Cleavage of structural proteins during the assembly of the head of bacteriophage T4.* Nature, 1970. **227**(5259): p. 680-5.

130. Qin, N., et al., *Direct interaction of gbetagamma with a C-terminal gbetagamma-binding domain of the Ca2+ channel alpha1 subunit is responsible for channel inhibition by G protein-coupled receptors.* Proc Natl Acad Sci U S A, 1997. **94**(16): p. 8866-71.

131. Leopoldt, D., et al., *Gbetagamma stimulates phosphoinositide 3-kinase-gamma by direct interaction with two domains of the catalytic p110 subunit.* J Biol Chem, 1998. **273**(12): p. 7024-9.

132. Ikuno, Y., F.L. Leong, and A. Kazlauskas, *Attenuation of experimental proliferative vitreoretinopathy by inhibiting the platelet-derived growth factor receptor.* Invest Ophthalmol Vis Sci, 2000. **41**(10): p. 3107-16.

133. Exner, T., et al., *Posttranslational modification of $G\alpha_{o1}$ generates $G\alpha_{o3}$, an abundant G protein in brain.* Proc Natl Acad Sci U S A, 1999. **96**(4): p. 1327-32.

134. Nurnberg, B., T. Gudermann, and G. Schultz, *Receptors and G proteins as primary components of transmembrane signal transduction. Part 2. G proteins: structure and function.* J Mol Med, 1995. **73**(3): p. 123-32.

135. Xiao, R.P., X. Ji, and E.G. Lakatta, *Functional coupling of the beta 2-adrenoceptor to a pertussis toxin-sensitive G protein in cardiac myocytes.* Mol Pharmacol, 1995. **47**(2): p. 322-9.

136. Hamill, O.P., et al., *Improved patch-clamp techniques for high-resolution current recording from cells and cell-free membrane patches.* Pflugers Arch, 1981. **391**(2): p. 85-100.

137. Hodgkin, A.L. and A.F. Huxley, *A quantitative description of membrane current and its application to conduction and excitation in nerve.* J Physiol, 1952. **117**(4): p. 500-44.

138. Meszaros, J., et al., *L-type calcium current in catecholamine-induced cardiac hypertrophy in the rat.* Exp Physiol, 1997. **82**(1): p. 71-83.

139. Offermanns, S., *In vivo functions of heterotrimeric G-proteins: studies in Galpha-deficient mice.* Oncogene, 2001. **20**(13): p. 1635-42.

140. DeGeorge, B.R., Jr., et al., *Targeted inhibition of cardiomyocyte Gi signaling enhances susceptibility to apoptotic cell death in response to ischemic stress.* Circulation, 2008. **117**(11): p. 1378-87.

141. Krumins, A.M. and A.G. Gilman, *Targeted knockdown of G protein subunits selectively prevents receptor-mediated modulation of effectors and reveals complex changes in non-targeted signaling proteins.* J Biol Chem, 2006. **281**(15): p. 10250-62.

142. Chen, F., et al., *Lack of muscarinic regulation of Ca^{2+} channels in $G_{i2}\alpha$ gene knockout mouse hearts.* Am J Physiol Heart Circ Physiol, 2001. **280**(5): p. H1989-95.

143. Lu, Z., et al., *Decreased L-type Ca2+ current in cardiac myocytes of type 1 diabetic Akita mice due to reduced phosphatidylinositol 3-kinase signaling.* Diabetes, 2007. **56**(11): p. 2780-9.

144. Pereira, L., et al., *Mechanisms of [Ca2+]i transient decrease in cardiomyopathy of db/db type 2 diabetic mice.* Diabetes, 2006. **55**(3): p. 608-15.

145. Perrier, R., et al., *A direct relationship between plasma aldosterone and cardiac L-type Ca2+ current in mice.* J Physiol, 2005. **569**(Pt 1): p. 153-62.

146. Gudzenko, V., et al., *Influence of channel subunit composition on L-type Ca2+ current kinetics and cardiac wave stability.* Am J Physiol Heart Circ Physiol, 2007. **293**(3): p. H1805-15.

147. Bunemann, M., et al., *Functional regulation of L-type calcium channels via protein kinase A-mediated phosphorylation of the beta(2) subunit.* J Biol Chem, 1999. **274**(48): p. 33851-4.

148. Miriyala, J., et al., *Role of CaVbeta subunits, and lack of functional reserve, in protein kinase A modulation of cardiac CaV1.2 channels.* Circ Res, 2008. **102**(7): p. e54-64.

149. Viard, P., et al., *PI3K promotes voltage-dependent calcium channel trafficking to the plasma membrane.* Nat Neurosci, 2004. **7**(9): p. 939-46.

150. Spassova, M.A., et al., *STIM1 has a plasma membrane role in the activation of store-operated Ca(2+) channels.* Proc Natl Acad Sci U S A, 2006. **103**(11): p. 4040-5.

151. Park, C.Y., S. A, and R.E. Dolmetsch, *Stim1 Binds to and Inhibits $Ca_V1.2$ Voltage Gated Calcium Channels.* Biophys J, 2010. **98**(3(Suppl. 1)): p. 691a.

152. Park, C.Y., A. Shcheglovitov, and R. Dolmetsch, *The CRAC channel activator STIM1 binds and inhibits L-type voltage-gated calcium channels.* Science, 2010. **330**(6000): p. 101-5.

153. Tsuruta, F., et al., *PIKfyve regulates $Ca_v1.2$ degradation and prevents excitotoxic cell death.* J Cell Biol, 2009. **187**(2): p. 279-94.

154. Finlin, B.S., et al., *Regulation of voltage-gated calcium channel activity by the Rem and Rad GTPases.* Proc Natl Acad Sci U S A, 2003. **100**(24): p. 14469-74.

155. Xu, X., S.O. Marx, and H.M. Colecraft, *Molecular mechanisms, and selective pharmacological rescue, of Rem-inhibited CaV1.2 channels in heart.* Circ Res, 2010. **107**(5): p. 620-30.

156. Yang, T., et al., *Rem, a member of the RGK GTPases, inhibits recombinant CaV1.2 channels using multiple mechanisms that require distinct conformations of the GTPase.* J Physiol, 2010. **588**(Pt 10): p. 1665-81.

157. Yada, H., et al., *Dominant negative suppression of Rad leads to QT prolongation and causes ventricular arrhythmias via modulation of L-type Ca2+ channels in the heart.* Circ Res, 2007. **101**(1): p. 69-77.

158. Correll, R.N., et al., *Plasma membrane targeting is essential for Rem-mediated Ca^{2+} channel inhibition.* J Biol Chem, 2007. **282**(39): p. 28431-40.

159. Reynet, C. and C.R. Kahn, *Rad: a member of the Ras family overexpressed in muscle of type II diabetic humans.* Science, 1993. **262**(5138): p. 1441-4.

160. Catalucci, D., et al., *Akt regulates L-type Ca^{2+} channel activity by modulating $Ca_v\alpha_1$ protein stability.* J Cell Biol, 2009. **184**(6): p. 923-33.

161. Smani, T., et al., *Mechanisms underlying the activation of L-type calcium channels by urocortin in rat ventricular myocytes.* Cardiovasc Res, 2010. **87**(3): p. 459-66.

162. Horiuchi-Hirose, M., et al., *Decrease in the density of t-tubular L-type Ca2+ channel currents in failing ventricular myocytes.* Am J Physiol Heart Circ Physiol, 2011. **300**(3): p. H978-88.

8 PUBLICATIONS

Dizayee S, Kaestner S, Kuck F, Hein P, Klein C, Piekorz RP, Meszaros J, Matthes J, Nürnberg B, Herzig S, *$G\alpha_{i2}$- and $G\alpha_{i3}$-specific regulation of voltage-dependent L-type calcium channels in cardiomyocytes.* PLoS ONE, 2011 Sep;6(9):e24979.

Hübner M, **Dizayee S**, Matthes J, Seifert R, Herzig S, *Effect of MANT-nucleotides on basal L-type calcium currents in murine cardiomyocytes.* Naunyn-Schmiedeberg's Arch. Pharmacol., 2011 Jun; 383(6):573-83.

Abstracts

Dizayee S, Kaestner S, Kuck F, Piekorz RP, Hein P, Matthes J, Nürnberg B, Herzig S, *$G\alpha_{i2}$-specific regulation of voltage-dependent L-type calcium channels (L-VDCC) in heart.* Cardiovascular Research, 2010. 87 (Suppl 1):364-104.

Hübner M, **Dizayee S**, Matthes J, Herzig S, Seifert R, *Effect of MANT-nucleotides on basal L-type calcium currents in murine cardiomyocytes.* Naunyn-Schmiedeberg's Archives of Pharmacology, 2010. 381 (Suppl 1):110-29.

Dizayee S, Kaestner S, Felda O, Piekorz RP, Fabisch C, Meszaros J, Matthes J, Nürnberg B, Herzig S, *Differential modulation of cardiac L-type calcium currents by $G\alpha_{i2}$ and $G\alpha i_3$.* Biophysical Journal, 2009. 96(3)pp. 187a.

Dizayee S, Kaestner S, Piekorz RP, Matthes J, Meszaros J, Nürnberg B, Herzig S, *Subtype-specific inhibition of cardiac L-type calcium channels by $G\alpha_{i3}$.* Naunyn-Schmiedeberg's Archives of Pharmacology, 2009. 379 (Suppl 1):139-32.